DESIGN OF A 150kw SOLAR POWER PLANT IN CIHANBEYLI

by

ALİ SÜRMEN

B.Sc. in Mechanical Engineering

Boğaziçi University, 1978

Submitted to the Mechanical Engineering Department

in Partial Fulfillments of the Requirements for the

Degree of

MASTER OF SCIENCE

in

MECHANICAL ENGINEERING

Boğaziçi University

April, 1981

TABLE OF CONTENTS

Chapter		Page

ACKNOWLEDGEMENT

ABSTRACT

This study is devoted to the modeling of the performance of solar concentrators for central receiver power plants.A continuum field representation of ideal heliostat arrays is adopted in the formulation of the modeling.This representation accounts for two governing factors: the law of reflection of light rays imposes steering constraints on mirror orientations; the proximity of mirrors creates shadow effects by blocking the incident and/or reflected solar radiation.The results of a steering analysis which develops the space-time characteristics of heliostats and of a shadow analysis which determines the local effectiveness of mirrors in reflecting solar energy to a central point are combined to obtain in closed analytical form the global characteristics of circular concentrators.These charasteristics appear as time profiles for mirror orientations and for effective concentrator areas.A 150kw actual solar power plant is designed for Cihanbeyli by introduction of suitable derating factors by moving from the upper limits of performance establiished by these characteristics.

ÖZ

Bu çalışma merkezî alıcılı güneş enerji santrallerinde kullanılan heliostatların modellendirilmesine tahsis edilmiştir. Modelin formüllendirilmesinde ideal heliostat dizilerinin kesintisiz (continious) olduğu şeklinde bir temsil tarzı benimsendi. Böyle bir yaklaşım iki ana noktanın önemine işaret eder; birincisi ayna pozisyonuna sınırlama koyan yansıma kanunları, diğeri ise gelen ve yansıyan güneş enerjisini perdeleyerek gölgelemeye sebep olan ayna yakınlığı meselesi. Heliostatların zaman-mekan karakterini ortaya koyan yönelim analizi ile aynaların güneş enerjisini merkezî bir noktaya yansıtmaktaki muvaffakiyetini tesbit eden gölgeleme analizinin sonuçları birleştirilerek dairesel konsantratörlerin global karakterleri kapalı analitik formda elde edildi. Bu karakterler ayna pozisyonlarının ve etkili konsantratör alanının zaman yörüngelerinin çizimiyle ortaya kondu. Karakterlerin ortaya koyduğu en üst performans sınırlarından hareketle ve uygun eksiltme faktörlerini de ilâve ederek Cihanbeyli (Konya) için 150kw'lık bir güneş enerji santralinin dizaynı yapıldı.

LIST OF SYMBOLS

A_c	receiver area
A_i	actual concentrator area
A_r	effective concentrator area
a_i	$= A_i/\Pi H^2$, per-unit actual concentrator or per-unit required ground area
a_r	$= A_r/\Pi H^2$, per-unit effective concentrator area
D (length)	per-unit distance between two parallel mirrors (referred to mirror width)
D (angle)	declination
D_p	$= D\cos(\beta_n - \beta_d)$, profile distance in side view
H (length)	tower height
H (angle)	hour angle
I	solar radiation constant
I_o	maximum solar radiation constant
k	resultant steering-shadow or mirror area coverage factor
k_d	$= k \cdot k_r$, derating factor
k_g	$= 1/D_p$, ground area utilization factor
k_i	$= \bar{n} \cdot \bar{s} = \bar{n} \cdot \bar{t} = \cos\emptyset = |\bar{N}|/2$, incidence fector
k_m	mirror area utilization factor
k_o	$= k_g \cdot k_m$, overall area utilization factor
k_r	mirror reflectivity
k_s	$= \cos\Theta_s$, sun shading factor
k_t	$= \cos\Theta_t$, tower screening factor
L (length)	per-unit length of mirror
L (angle)	latitude

L_i	image per-unit length of mirror at receiver
1_R	length of receiver (height)
N	North
P (point)	any location (site) on the earth
P (power)	solar power at receiver
q	$= \cos\Theta_s / \cos\Theta_t$, parameter
R	distance of mirror to tower base
r_R	receiver lower radius (considering a straight cross-cut conic one)
S	South
T (length)	distance of mirror to receiver
T (period)	time interval between integration limits
t	time
W	per-unit width of mirror
W_i	(image) per-unit width of mirror at receiver
X	top exposure
X_m	shadow length (perpendicular to mirror horizontal edge)
Y	side exposure
Y_m	shadow scew length (parallel to mirror edge)
$\propto$	$= 90° - \Theta_s$, sun's altitude angle
β_d	azimuth orientation of seperation distance
β_n	azimuth orientation of mirror
β_r	azimuth orientation of side exposed end of mirror
β_s	azimuth orientation of the sun
β_t	azimuth orientation of mirror location with respect to tower

γ azimuthal displacement from XYZ coordinate system to xyz coordinate system

Θ_n mirror tilt angle (from horizontal)

Θ_s $= 90^\circ - \alpha$, sun's zenith angle

Θ_t mirror-tower distance angle

ϕ mirror inclination angle

$\mathcal{M}$ receiver surface inclination angle

η $= A_r/A_i$, concentrator efficiency

Subscribts

f   mirror front view

h   horizontal

i   actual concentrator (in A_i)

i   image

i
j   unit triads
k

M   maximum (rim)

m   minimum

m   mirror (in X_m and Y_m)

n   mirror's normal

p   mirror profile view

R   receiver

r   effective concentrator

s   sun

t   tower

x   (general subscribt standing for either 's' or 't'

Vectors

$\bar{i}$
$\bar{j}$ unit vectors pointing towards East, North and
$\bar{k}$ local vertical respectively

$\bar{N}$ $= \bar{s} + \bar{t}$, resultant vector

$\bar{n}$ unit normal vector (outward normal)

$\bar{s}$ unit sun vector (toward sun)

$\bar{t}$ unit tower vector (toward receiver)

Tensors

$\underline{\underline{T}}$

LIST OF ABBREVIATIONS

A.	appendix
am	before noon
avg.	avarage
cos	cosine
cot	cotangent
Dec.	December
Feb.	February
hr.	hour
J	joule
kw	kilowatts
Mar.	March
MJ	megajoule
max	maximum
min	minimum
min	minutes

pm	after noon
pp	between the pages
Sept.	September
SETP	sun effective time period
SR	solar radiation
SROA	solar radiation outside the atmosphere
s.	second
sin	sine
tan	tangent
W	watts

LIST OF FIGURES

[x] Page numbers.

. . . .

LIST OF TABLES

Chapter I

INTRODUCTION

As the energy problem predominates over the other problems of the human being,people attempted to find new energy sources in recent years.One of such sources,which is being interested in,is the sun.

Solar energy utilization techniques for high level of power are being are being studied in a great extend since,as input,equivalent of obtained energy is nothing.Although no technique was suggested to be practically preferable because of its first cost or some technical dificulties which have not been avoided yet,it is a great possibility that these techniques will be the equally preferred ones in near future.

Two such techniques,for conversion of solar energy into electrical energy,are:direct method;utilization of photo-voltaic cells,and solar-thermal power systems;employing concentrating mirrors to raise the temperature of working fluid operating a heat engine.In this thesis we attempted to develop some basic physical and theorethical performance characterics underlying solar-thermal power systems.Particular interest,however,is focused on the system of utilization which is referred to as Central Tower-Receiver System.This system consists of a large field of heliostats (flat mirrors) which collects the solar radiation,concentrates it on a receiver (located at the top of a central tower.) Receiver,acting as a boiler,raises a fluid to high temperatures and pressures compatible with modern power generating plants.The analysis postulates an ideal model

for the heliostat arrays which assumes that mirrors are
perfectly flat,perfectly steered to redirect sunlight to the
central receiver and may be placed in any desired field config-
uration around the central tower.A continuum field approach is
adopted to describe the ideal heliostat arrays as a function of
location and time of the day.As a consequence of this approach,
adjacent mirrors (front-back) considered to be parallel and no
side exposure factor is considered to exist.Continuum field
approach will be discussed in detail in Chapter III.

Two fundamental considerations govern the space-time char-
acteristics of the mirror field:

a) The steering relations needed to satisfy the constraint
of the reflection law of light rays,that is the equality of
incidence and reflection angles.

b) The presence, of neighboring mirrors which creates the
possibility of blocking the incident and/or reflected sun rays.
Steering and shadowing analyses are therefore performed to
determine the local properties of the mirror field.The contin-
uum field approach which considers the heliostat field as a
concentrator, made it possible to get simple analytic expres-
sions of useful heliostat area and efficiency as functions
of system angles by evaluation of some governing integrals.

The principal results are presented as time profiles for
mirror steering angles,for effective concentrator areas and
for efficiency of the system.The ideal characteristics of
circular concentrators establish theoretical upper limits of
performance against which actual or realistic systems can be

evaluated with the introduction of suitable derating factors

to account for such effects as steering errors,mirror size and

reflectivity,area coverage and geometry,and solar radiation.

Special interest is devoted to the assignment of solar radia-

tion considering the site under study,i.e.,Cihanbeyli. A

criteria is suggested to stand against the problems arising

from theorethical or other possible variations in solar radia-

ation and effective concentrator area.This is primarily impor-

tant for the reason that the principal results and main dimen-

sions of the system elements (such as mirror and receiver dimen-

sions,tower height exc.) should be as much realistic as pos-

sible and also the assigned power should be attainable most of

the time in the characteristic period.We also tried to find a

compromise point to decide for the receiver size and mirror

dimensions depending on the relation between them.

Chapter II

LITERATURE SURVEY

2.1 History of the Solar Tower Concept:

The concentration of the direct beam component of sunlight
with heliostats was first attributed to Archimedes who
instructed soldiers to reflect the sun rays onto the sail of an
enemy vessel by carefully orienting their burnished shields
(heliostats).Their efforts were succesful,for the vessel was
set afire.It was not until several thousand years later that
Trombe and his co-workers added hydrolically controlled servo-
mechanism to an array of large heliostats to produce an auto-
matically controlled 1-megawatt (thermal) solar collector.
Interested in producing high temperatures to melt materials,
Trombe added a large,fixed concentrator consisting of a para-
bolic dish and achieved a temperature of 4100 K. Baum et al.
investigated a tracking array consisting of heliostats   on
moving railroad cars,aimed at an elevated cavity receiver-
boiler.The cavity was to be rotated to face the heliostats
throughout the day to achieve improved performance.

Francia developed an intricate clock-driven field of 271
heliostats and was able to produce steam at a rate equivalent
to 150 kilowatts.This concept is not suited for large-scale
utilization of solar energy on a megawatt (electric) basis,
because it is impractical to connect many thousands of helio-
stats into a single clockwork device with sufficient precision.
Moreover,the mechanism is not well suited to the large mirrors
required for an economical system design.

A reinvention involving a large number of heliostats took place in 1970-1971 at the University of Houston.This work was supported by the,what is called,RANN program of the National Science Foundation,NSF,beginning in 1973,and in 1975 it was transferred to ERDA (Energy Research and Development Administration.) Long term studies in science and engineering made it apparent that the outlook for energy sources beyond fossil fuels was hopeful but uncertain.Clearly,solar energy could be utilized.Since some investigations of the possibilities had already been carried out,we consider only the most promising options.Photovoltaic cells were considered first but,because of their large cost and low efficiency at that time,were rejected in favor of potentially efficient thermal conversion cycles compatible with the utility grids.Steam-electric conversion cycles producing 100 to 300 megawatts (electric) are well developed by the utilities,which also have a large-scale distribution system.It seemed advisable to utilize available transmission methods.

Aspects of the Central Tower-Receiver System;external or cavity receiver,flat or focusing heliostats,and methods of storage are under study by four-team ERDA effort to result in a preliminary design for a 10-megawatt (electric) pilot plant by June 1977. (x) Barstow,California,has been selected as the site for the pilot plant.It is anticipated that the first step in bringing costs for commercial plants into the range experienced for the construction and fueling of nuclear plants will be to increase plant size to at least 100-megawatts (electric) at a

_____

(x) Unfortunately,we are unaware of studies have been carried out since 1978.

single site to achieve better collector and turbine efficiency.
Fig.2.1. describes the concept for a 100-megawatt (electric)
demonstration plant.

Other solar developments include plot plants planned by
the Electric Power Research Institute in U.S.A. as well as the
French and Japanese governments. An ERDA-funded Solar Thermal
Test Facility (STTF) is under construction at Sandia Laboratory
Albuquerque, New Mexico, and is scheduled for completion in 1978.
The STTF is a small 5-megawatt (thermal) solar tower collector
for testing the 10-megawatt (electric) pilot plant prototype
components and performing related solar energy research [1].
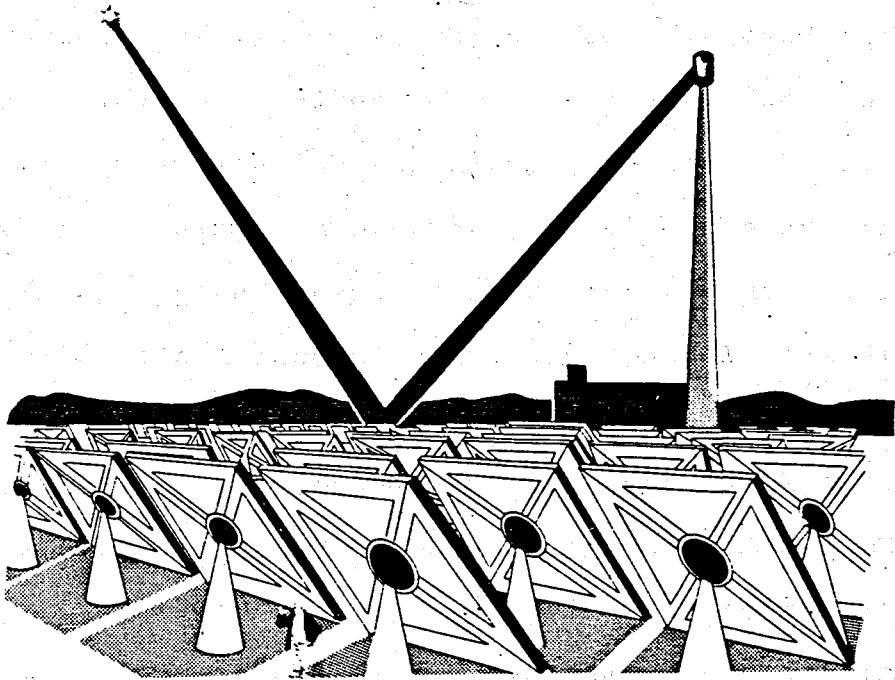
Fig.2.1 The 100-megawatt(electric) heliostat power plant con-
cept. The tower(260m.high) near the center of the field has a
boiler on top. About 20.000 heliostats(6.4 by 6.4 meters) would
be required, spread over an area of about 3.5 square kilometers.
A 10-Mw.(electric) pilot plant is under development by ERDA.

2.2 Available Sources About the Technique of Solar-Thermal Power Plants:

There are many books,papers or other puplications in the literature of solar energy dealing with the defined and derived earth-sun angles and angles related to reflecting or absorbing materials of various special configurations with respect to a coordinate system on the earth's surface.The identifications for some relati vely important ones are given [2,3, 4.] We tried,however,to utilize these materials during our study in such a fashion that anybody shell not be in need of having them otherwise strictly required.

Information about the studies of aspects of Central Tower-Receiver System,namely the ones which were mentioned before; additionally detailed receiver design considerations,automatic control mechanism,available temperature and power limits,advantages of system of single unit over thet of doble and triple units (i.e.,single plant composed up of two or three different heliostat arrays field each with its own central tower),area, mirror and receiver size requirements,tower height,maximum allowable angular oberrations and mirror type is also obtainable in literature [1,5,6,7,8,9.] A few of these are studied in this thesis while the other many are not considered to be subject to our study.References [5] and [10] especially constitute the major part of the help to our study.

All the theory is adopted to the local properties of Cihanbeyli,Konya.

ANALYSIS OF THE HELIOSTAT ARRAYS FIELD

3.1 Mirror Steering Analysis:

3.1.1 Fundamental Steering Relations:

Fig.3.1 illustrates the geometrical configuration of a flat-faced mirror at a given location and instant of the day with respect to the tower .It is well-known by Euclid's Law that angle of incidence and reflection of light rays are equal.This law imposes a constraint for the positions of the sun,tower and mirrors.Since the position and dimensions of the tower are considered to be fixed,assuming an arbitrary configuration for a mirror,this constraint leads us to determine the position of the sun at a given instant of the day.

By Fig.3.1,any normal to the mirror and its magnitude are given by the expressions

$$\bar{N} = \bar{s} + \bar{t}$$

and

$$|\bar{N}| = |\bar{s} + \bar{t}|$$

respectively.Then the unit normal $\bar{n}$ is expressed by

$$\bar{n} = \frac{\bar{N}}{|\bar{N}|} = \frac{(\bar{s} + \bar{t})}{|\bar{s} + \bar{t}|} \tag{3.1}$$

If $\bar{n}$ is a unit normal (which is the case) Eq.(3.1) is a requirement for Euclid's Law,namely that

$$\bar{n}.\bar{s} = \bar{n}.\bar{t} = \cos\emptyset \tag{3.2}$$

where $\emptyset$ is the incidence angle,which is expressed in various forms by Eqs.(A.2.1)-(A.2.5) in Appendix-2.

Since the vector $\bar{t}$ is a fixed one and the vector $\bar{s}$
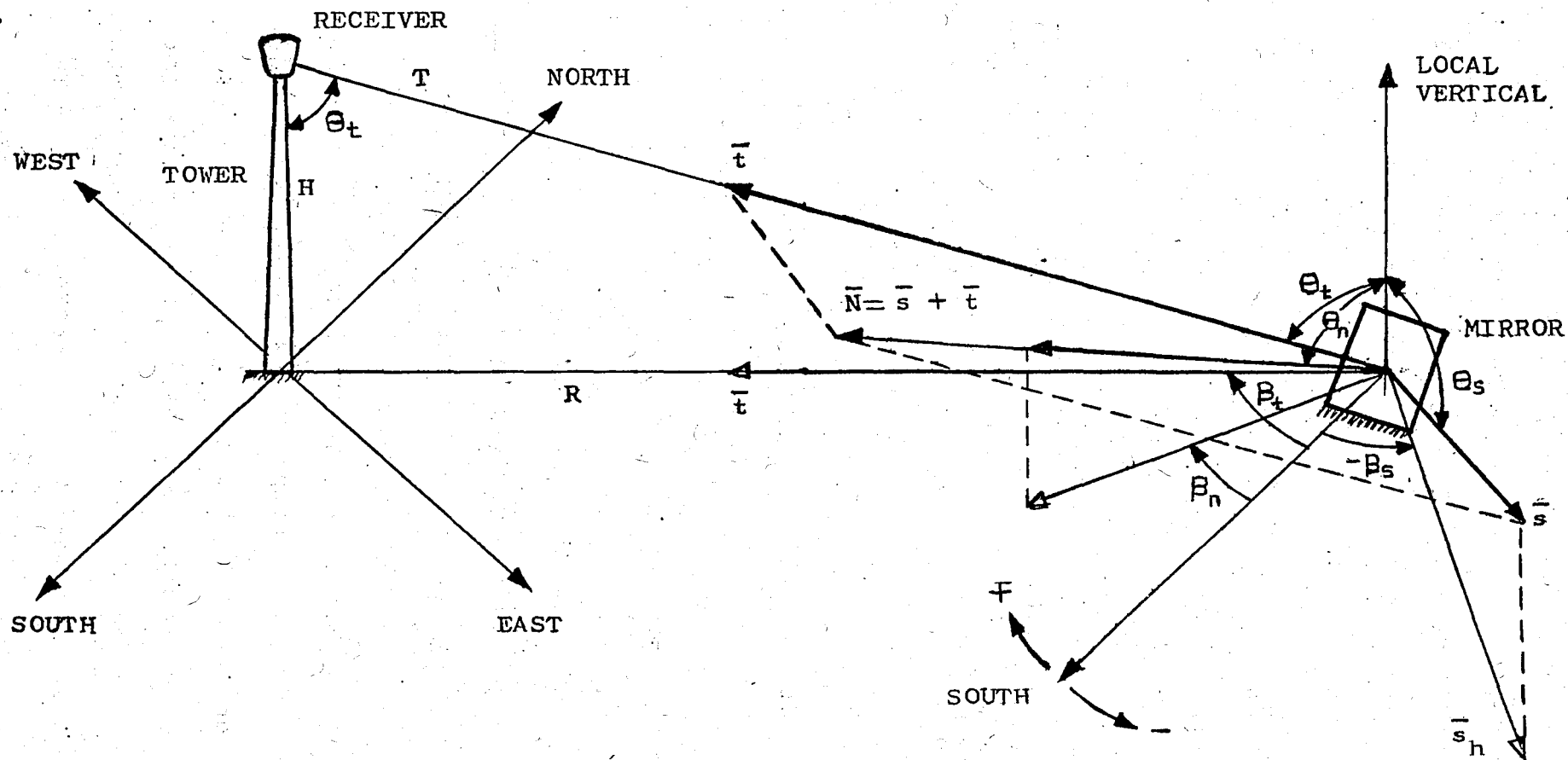
Fig. 3.1 Geometrical configuration of unit vectors associated with sun tower and mirror.

represents the sun's time-varying position, Eq.(3.1) is the basic steering relation for a mirror and it defines mirror orientations as a function of time. As it is obvious from this explanation the position of the mirror, with respect to the top of the tower with a height H from the ground, is specified by the unit vector $\bar{t}$ as shown in Fig.3.1. The unit vectors $\bar{s}, \bar{t}$ and $\bar{n}$ can be described by two kinds of angle components; the zenith angles θ_s, θ_t (corresponding to a radial distance R, $R = H\tan\theta_t$) and θ_n, and the azimuth angles β_s, β_t and β_n respectively. It follows from Fig.3.1. that the components of these three unit vectors are:

Mirror:

$$n_i = -\sin\theta_n \sin\beta_n$$
$$n_j = -\sin\theta_n \cos\beta_n$$
$$n_k = \cos\theta_n$$

Tower:

$$t_i = -\sin\theta_t \sin\beta_t$$
$$t_j = -\sin\theta_t \cos\beta_t \qquad\qquad (3.3)$$
$$t_k = \cos\theta_t$$

Sun:

$$s_i = \sin\theta_s \sin\beta_s$$
$$s_j = -\sin\theta_s \cos\beta_s$$
$$s_k = \cos\theta_s$$

where i, j and k are subscribts related to the triad of unit vectors $\bar{i}, \bar{j}$ and $\bar{k}$, pointing towards East, North and the local vertical, respectively. Then the vector $\bar{N} = \bar{s} + \bar{t}$ can be expressed

by

$$\bar{N} = (\sin\theta_s \sin\beta_s - \sin\theta_t \sin\beta_t)\bar{i} + (-\sin\theta_s \cos\beta_s - \sin\theta_t \cos\beta_t)\bar{j}$$
$$+ (\cos\theta_s + \cos\theta_t)\bar{k}$$

and its magnitude $|\bar{N}|$ by

$$|\bar{N}| = \sqrt{2}\left[1 + \cos\theta_s \cos\theta_t + \sin\theta_s \sin\theta_t \cos(\beta_t - \beta_s)\right]^{1/2} \quad (3.4)$$

The orientation of any mirror is expressed by Eq.(3.1) or equivalently by angles θ_n and β_n. By Cosine Law

$$\cos\theta_n = \bar{n}.\bar{k}$$

Substituting Eq.(3.1) for $\bar{k}$, previous equation takes the form

$$\cos\theta_n = \frac{1}{|\bar{N}|}(\bar{s}.\bar{k} + \bar{t}.\bar{k})$$

But $\bar{s}.\bar{k} = \cos\theta_s$ and $\bar{t}.\bar{k} = \cos\theta_t$

Therefore

$$\cos\theta_n = \frac{1}{|\bar{N}|}(\cos\theta_s + \cos\theta_t) \quad (3.5)$$

We can also develop an equation for $\sin\theta_n$, since it is the magnitude of a unit vector normal to the plane formed by the unit vectors $\bar{n}$ and $\bar{k}$, i.e.,

$$\sin\theta_n = |\bar{n}x\bar{k}| = \frac{1}{|\bar{N}|}|(\bar{s}x\bar{k} + \bar{t}x\bar{k})|$$

Inserting the expressions for the vectors $\bar{s}, \bar{t}$ and $\bar{k}$ into the equation above and carrying out some required calculations, the expression for $\sin\theta_n$ is found to be

$$\sin\theta_n = \frac{1}{|\bar{N}|}\left[\sin^2\theta_s + \sin^2\theta_t - 2\sin\theta_s \sin\theta_t \cos(\beta_t - \beta_s)\right]^{1/2}$$
$$(3.6)$$

(See Appendix-3). Consequently, the equivalence of Eq. (3.5) and/or Eq. (3.6) is

$$\tan\theta_n = \frac{\left[\sin^2\theta_s + \sin^2\theta_t + 2\sin\theta_s\sin\theta_t\cos(\beta_t-\beta_s)\right]^{1/2}}{(\cos\theta_s + \cos\theta_t)} \qquad (3.7)$$

The derivation of the expression for β_n is analogous to that of θ_n and it is found to be

$$\tan\beta_n = \frac{(\sin\theta_s\sin\beta_s + \sin\theta_t\sin\beta_t)}{(\sin\theta_s\cos\beta_s + \sin\theta_t\cos\beta_t)} \qquad (3.8)$$

(See Appendix-4), or identically

$$\frac{\sin(\beta_n-\beta_t)}{\sin(\beta_n-\beta_s)} = -\frac{\sin\theta_s}{\sin\theta_t} \qquad (3.9)$$

Another important concept in solar energy calculations is the incidence factor, denoted by k_i and defined as the normal component of the incident sun rays. Thus

$$k_i = \bar{n}.\bar{s} \qquad (3.10)$$

By Eq. (3.2)

$$\bar{n}.\bar{s} = \bar{n}.\bar{t}$$

then

$$2(\bar{n}.\bar{s}) = \bar{n}.\bar{s} + \bar{n}.\bar{t} = \bar{n}.(\bar{s} + \bar{t})$$

but

$$\bar{n}.(\bar{s} + \bar{t}) = \frac{(\bar{s} + \bar{t})}{|\bar{s} + \bar{t}|} \cdot (\bar{s} + \bar{t}) = \frac{|\bar{N}|^2}{|\bar{N}|} = |\bar{N}|$$

hence

$$\bar{n}.\bar{s} = \bar{n}.\bar{t} = \frac{|\bar{N}|}{2} \qquad (3.11)$$

Consequently

$$k_i = \frac{|\overline{N}|}{2} \tag{3.12}$$

in which $|\overline{N}|$ has a value computed by Eq.(3.4).

Eqs.(3.1)-(3.12) are basic relations dictating the motion of any mirror depending on time-varying position of the sun and these equations will serve us through all calculations and derivations defining the properties of the heliostat field completely. The time-varying evaluation of a mirror, at a fixed position specified by Θ_t and β_t, was expressed as functions of the sun angles Θ_s and β_s up to here. The following sections will make us capable of expressing this evaluation as a function of time.

3.1.2 Fixed-Time Mapping of Mirror Orientations:

At a fixed time of the day the sun vector $\overline{s}$ is specified by its zenith angle Θ_s and azimuth angle β_s as it is indicated earlier. For a fixed location of the central tower, mirror orientations in the field may be characterized by two sets of local property:

a) Loci of constant azimuthal orientations (constant β_n lines).

b) Loci of constant tilt (constant Θ_n lines)

Taking Θ_s and β_s as parameters, and, Θ_t and β_t as our variables, we can plot constant Θ_n and β_n lines. Fig. 3.2. shows a typical set of polar plots of these constant lines in the $\Theta_t - B_t$ plane. Some other sets are given in Appendix-7. It is extremely work-saving to use relative azimuth angles $B_{ts} = B_t - B_s$ and $B_{ns} =$
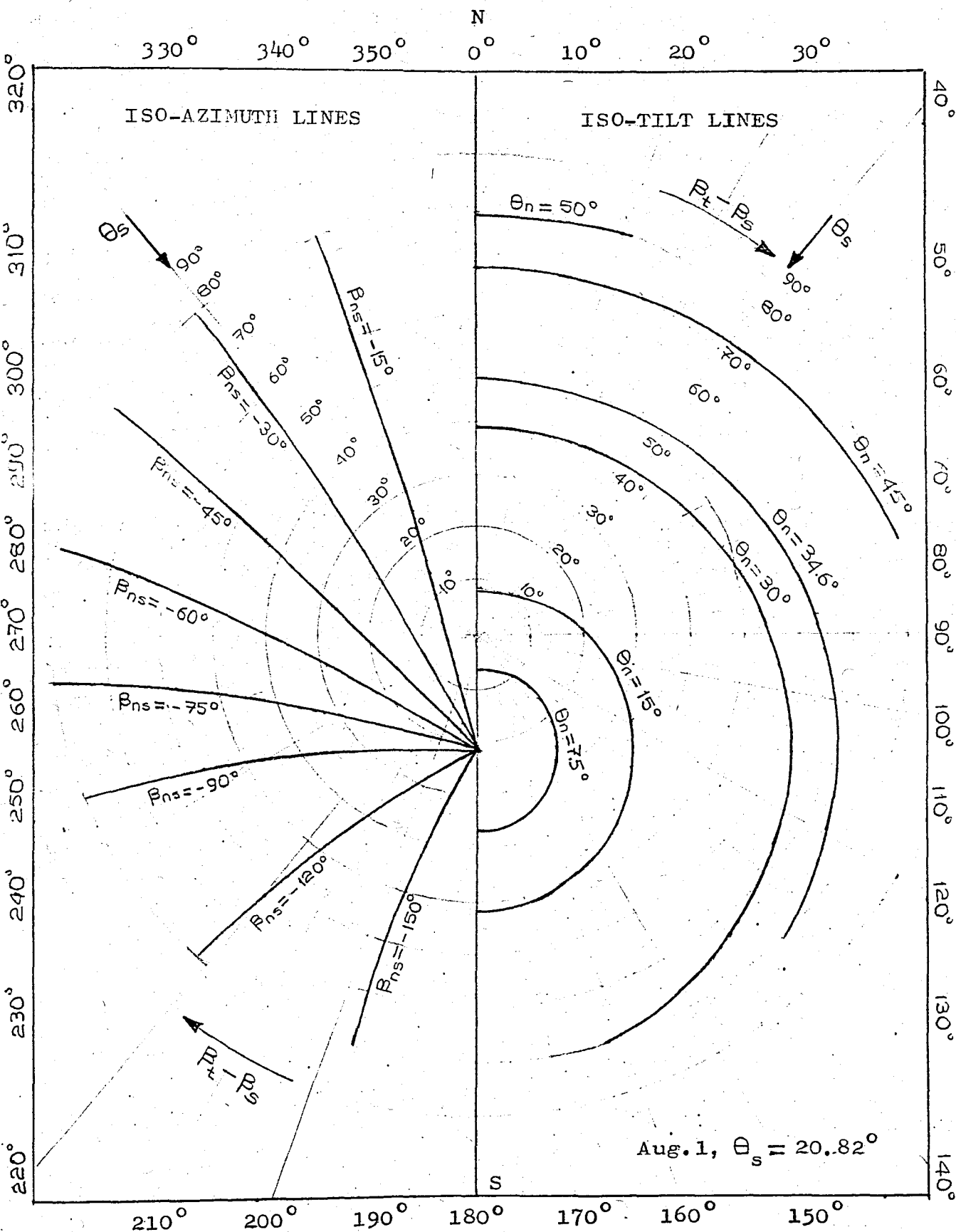
Fig. 3.2 Mirror field distribution

for Cihanbeyli ($L = 38.67°$), $\beta_s = 0°$.

$\beta_n - \beta_s$ instead of β_t and β_n respectively in plotting since this leaves us with only one parameter, Θ_s. Certainly this operation has no physical meaning at solar noon at which $\beta_s = 0$ or 180. For Cihanbeyli latitude angle L (L $=$ 38.67) is always greater than maximum absolute declination angle (D $= \pm$ 23.45). Therefore at solar noon $\beta_s = 180$ in Cihanbeyli. Figs. A.14 to A.18 are however, for $\beta_s = 0$. When it is desired to see the situation for absolute azimuth angles, plots are simply rotated by the specified sun azimuth angle β_s. Then for $\beta_s = 180$, for example, it is sufficient to turn the graphs for $\beta_s = 0$ upside down. For $\beta_s = -30$ the situation is illustrated in Fig. A.19 by some sample plots at $\Theta_s = 38.47$ (for L $=$ 38.67 on Mar. 22 and Sept. 22) As an obvious conclusion, from the physics of the system, we can state that the plots are symmetric about a line parallel to horizontal component of sun's vector $\bar{s}$ (i.e. in the direction of $\bar{s}_h$) and passing through the central tower.

Eqs. (3.7) and (3.9) make it clear that the simplest mapping occurs when the sun's zenith angle is zero. By Eq. (3.7) substituting $\Theta_s = 0$

$$\tan\Theta_n = \frac{\sin\Theta_t}{1 + \cos\Theta_t} \quad .$$

By using trigonometric identity $\tan\Theta_n = \sin\Theta_n / \cos\Theta_n$ and rearranging we result in

$$\sin(\Theta_t - \Theta_n) = \sin\Theta_n$$

It follows that for $\Theta_s = 0$

$$\Theta_n = \frac{\Theta_t}{2} \tag{3.13}$$

Likewise, by Eq. (3.9), $\beta_n = \beta_t$ for $\theta_s = 0$. Of course for any location other than latitude angle $L = 0$, θ_s can never become zero. This special case is illustrated by Fig. A.14 in which constant azimuthal configurations of mirrors are shown by constant azimuthal, and constant tilts by half of the constant radial orientations.

As θ_s takes values greater than zero, iso-tilt lines become distorted, looking like a south-faced growing bud and iso-azimuth lines take the shape of concentric hyperbolas. This kind of a mapping, however, possess interesting properties. For instance iso-tilt lines are quadratic curves which form closed paths for some values of θ_n. These curves, forming closed paths, cross the $\beta_{ts} = 0$ -180 line at two points. This fact leads us to get a conclusion about the characteristics of these iso-tilt lines.

For $\beta_{ts} = 0$ Eq. (3.7) becomes

$$\tan\theta_n = \frac{(\sin^2\theta_s + \sin^2\theta_t + 2\sin\theta_s \sin\theta_t)^{1/2}}{(\cos\theta_s + \cos\theta_t)}$$

$$= \frac{\sin\theta_s + \sin\theta_t}{\cos\theta_s + \cos\theta_t}$$

Substituting the trigonometric identity $\tan\theta_n = \sin\theta_n / \cos\theta_n$ and rearranging we result with

$$\theta_n = \frac{1}{2}(\theta_t - \theta_s)$$

But θ_t is taking the values in the range $0° < \theta_t < 90°$, therefore $\theta_n = 45 - (\theta_s/2)$. If we perform the calculations for $\beta_{ts} = 180°$ we come out with the same result. This means that iso-tilt lines

form closed paths for values of Θ_n, $\Theta_n < 45° - (\Theta_s/2)$.

Iso-azimuth lines, on the other hand, are made up of portions of hyperbolas intersecting at a singular point at which $\Theta_t = \Theta_s$ and $\beta_{ts} = 180$. This particular point, referred to as 'NODE' of the mapping, is also the point at which closed paths converges to a point. At the node $\Theta_n = 0$, physically means that the mirror at the node is horizontal. Since the node has a time-varying position and it is characterizing the mirror field distribution at a given time, the time-variation of the distribution can be visualized by observing the motion of this node. The complete distribution can be obtained by superimposing the pertinent mapping (for a given Θ_s) in Figs. A.4. and A.5. such that node and sun's position coincide.

3.1.3 Fixed-Location Profiles of Mirrors:

Once the location of any mirror is specified (by Θ_t and β_t), the motion of the mirror can be expressed in terms of the hour angle H. This is done by simply introducing the time-dependent expressions of sun angles Θ_s and β_s (i.e. Eqs. (A.1.1) and (A.1.4) respectively) into Eqs. (3.4), (3.5) and (3.8). Then we obtain

$$\cos\Theta_n = \frac{1}{|\bar{N}|} (\cos\Theta_t + \sinL\sinD + \cosL\cosD\cosH) \qquad (3.14)$$

in which

$$|\bar{N}| = \sqrt{2}\Big[1 + \cos\Theta_t(\sinL\sinD + \cosL\cosD\cosH)$$
$$+ \sin\Theta_t\sin\beta_t\cosD\cosH + \sin\Theta_t\cos\beta_t$$
$$\cdot(\sinL\cosD\cosH - \cosL\sinD)\Big]^{1/2}$$
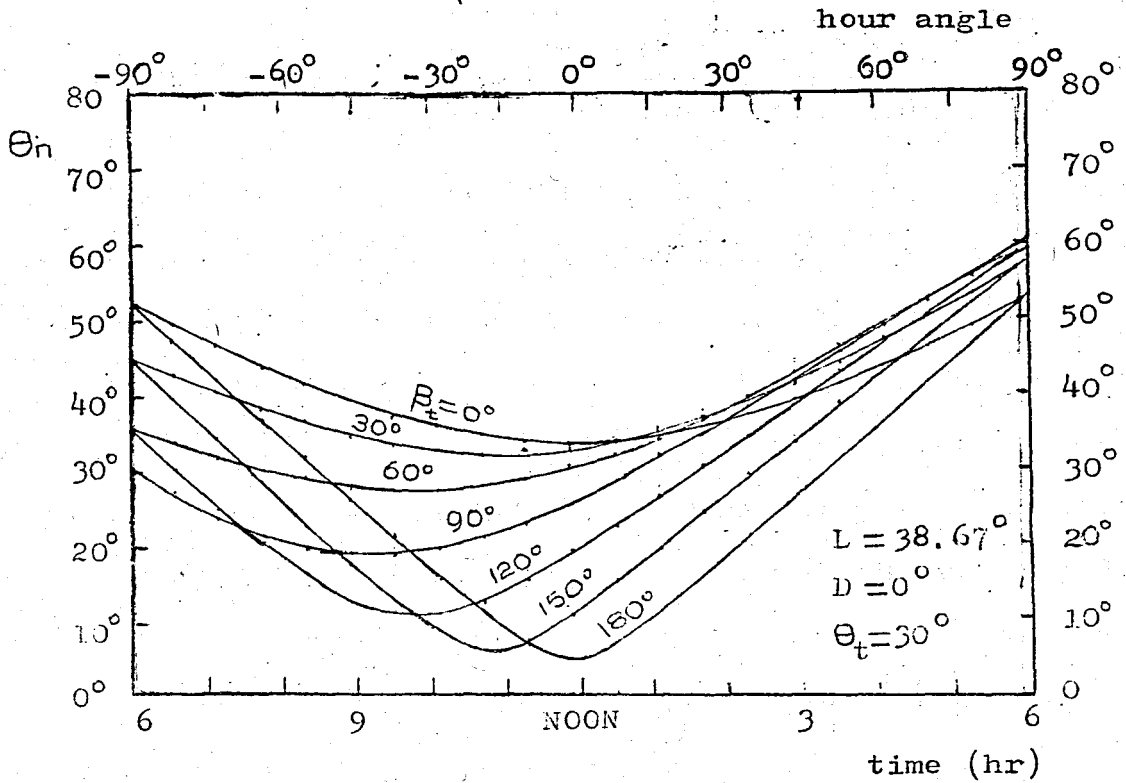
Fig. 3.3 Time profiles of mirror tilt angle
(above) and mirror azimuth angle (below).
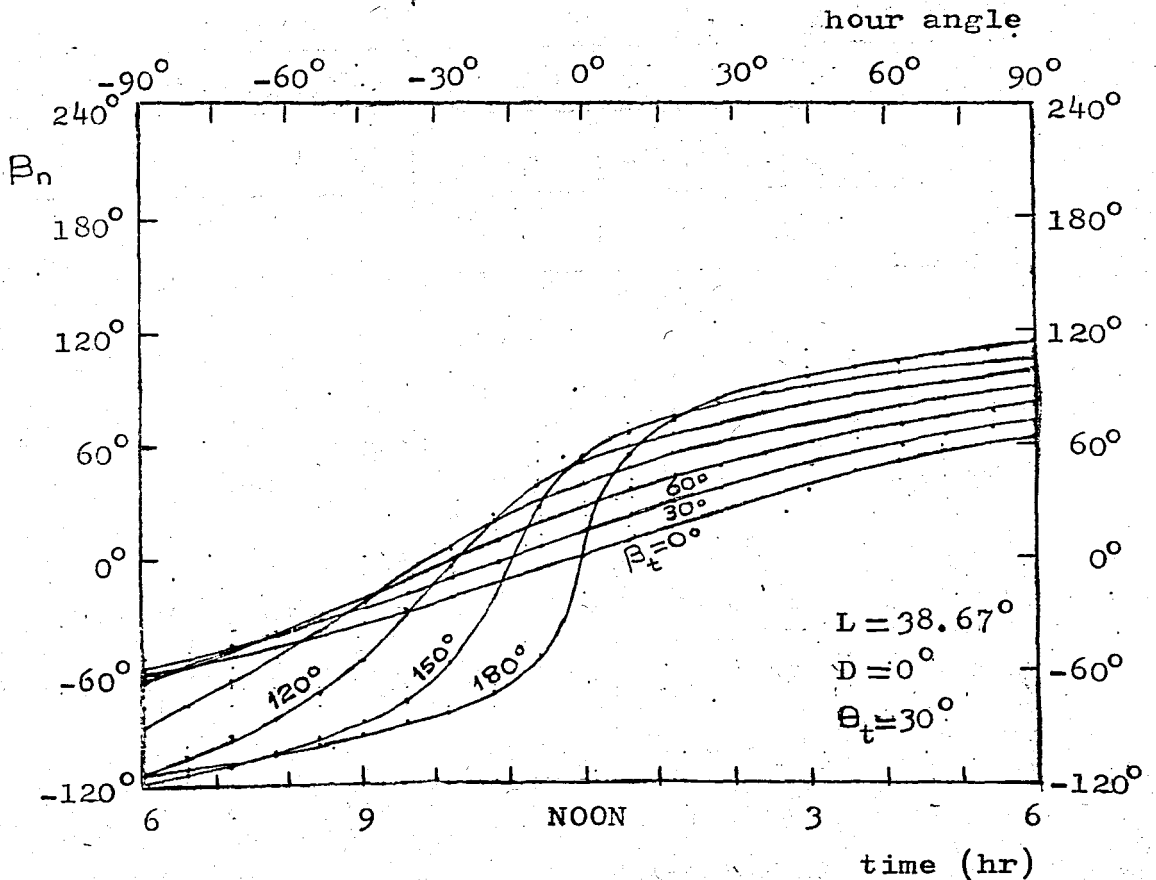
and also

$$\tan\beta_n = \frac{\sin\theta_t\sin\beta_t + \cos D\sin H}{\sin\theta_t\cos\theta_t + \sin L\cos D\cos H - \cos L\sin D} \qquad (3.15)$$

Fig. 3.3 shows time profiles of the mirror angles θ_n and β_n for a mirror of radial orientation $\theta_t = 30^\circ$. Seven different mirrors oriented at azimuthal locations of 30° apart (starting from $\beta_t = 0^\circ$) are considered. Eastern quadrants are sufficient for representation of the whole field because of the symmetry. The latitude angle for Cihanbeyli is considered, and, March 22 and September 22 are taken as the days for which profiles are formed. The time profiles for some other combinations of day and location are given in Appendix-8. It is worth noting that the mirror closest to the node of the field at a certain time and azimuthal orientation exhibits the largest time rate of

	$D = -23.45^\circ$		$D = 0^\circ$		$D = 23.45^\circ$	
	$\theta_t = 30^\circ$	$\theta_t = 75^\circ$	$\theta_t = 30^\circ$	$\theta_t = 75^\circ$	$\theta_t = 30^\circ$	$\theta_t = 75^\circ$
H	undef.(x)	-44.89°	undef.	-70.64	-30.47	-89.19
β_t						

Table 3.1

change of angular velocity at that time. The hour angles of nodal points and corresponding azimuthal orientations for two radial orientations and three characteristic days of the year are given in Table 3.1. It is not difficult to see that once nodal time is calculated from Eq. (A.1.1) by introducing $\theta_t = \theta_s$

(x) The mirror at the corresponding orientation can never become horizontal. This means the point cannot become a node.

we can calculate corresponding azimuthal orientation by Eq. (3.14) since $\Theta_n = 0$ at the node.

Eqs. (3.14) and (3.15) make us capable of deriving time profiles of angular velocities and accelerations which are very important for the control and torque requiremens during the steering action.

3.2 Shadowing Effects on Mirrors:

There are two major effects governing the performance of ideal heliostat arrays: shading and screening. Shading, for any mirror , is blocking of incident rays by any of the adjacent mirrors, and screening is blocking of reflected rays which are not exposed to shading.

At a given instant of time any two mirrors in their true positions in the field are not parallel. If they are parallel however, all the vectors related to these mirrors are equal respectively. Fig. 3.4 illustrates such an ideal case of two parallel mirrors in the field which will be base to our study.

Let the dimensions of the mirrors under consideration be W(width) and L(length), and let both of these lengths be equal to unity as a specification. The shaded area portions of the back mirror is the portion under blocking effects. Specifically the portion which is exposed to shading is shown by the shaded area limited by the incident sun rays, and the other which is exposed to screening by that of limited by the reflected sun rays. Be sure that there may exist a portion which is exposed to both shading and screening at the same time. Such a portion is shown by cross-shaded area in Fig. 3.4.

N

W

E(x')

S(y')

a) PLAN VIEW

SUN
SHADE

$\bar{t}_1$

$\bar{s}_1$

$\bar{t}_2$

x

y

Y_{ms}

Y_{mt}

TOWER
SCREEN

MIRROR
PROJECTION

side
exposure

$\bar{s}_2$

$\cos\theta_n$

X_t

D_p X_{mt} X_{ms}

b) SIDE VIEW

c) FRONT VIEW

θ_{sp}

θ_{tp}

X_t
X_s
top
exposure

$\sin\theta_n$

θ_n

Seperation

Tower Shadow

Sun Shadow

D_p

X_{mt}

X_{ms}

θ_{sf} θ_{tf}

Y_{ms} Y_{mt}

L
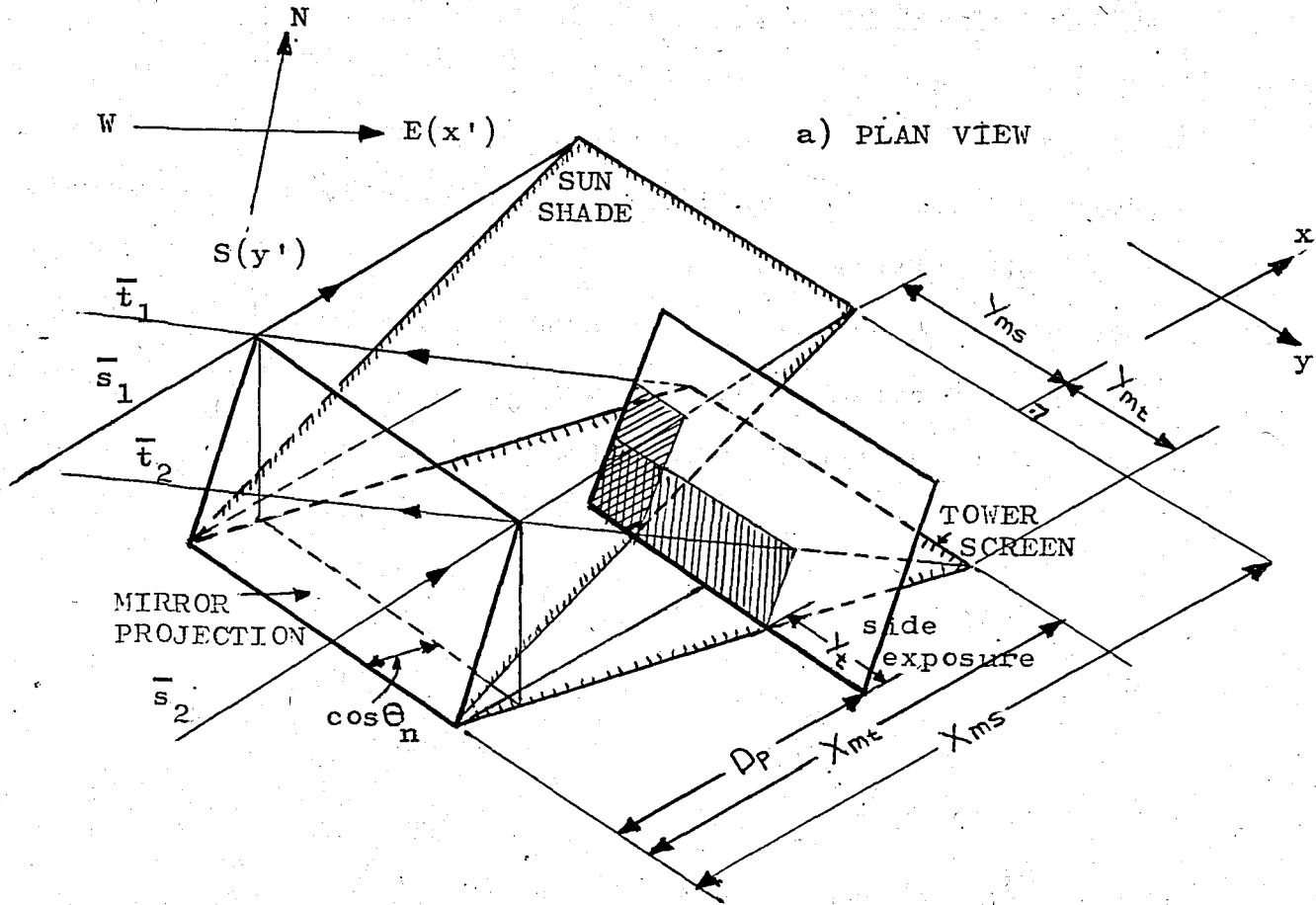
Fig. 3.4 Relative positions of neighboring heliostats in the
field.

3.2.1 Mirror Shadows on Ground (Mirror "Footprints"):

To analyze the shadowing effects of neighboring mirrors, the shadows produced by a single mirror on the horizontal surface are first examined as a function of space and time; such horizontal shadows can be viewed as defining the "footprints" of a mirror. Again be sure that the analysis is confined to rectangular (or square) shaped mirrors having an edge (i.e., two corners) placed on the ground which is assumed to be horizontal.

Fig. 3.5 Mirror projection angles.

Before starting with their derivations, it is helpful to define some new angles. Fig. 3.5 above shows these angles, θ_{sp} and θ_{sf}, in relation to the mirror's normal plane and the vertical plane formed by incident sun rays. (Both planes are intersecting along the local vertical.) The projection of the sun's zenith angle θ_s in the mirror's normal plane denoted by

θ_{sp}, and the angle which appears to be coincident with the sun's zenith angle in the front view is denoted by θ_{sf}. Similar definitions can be made for the angles θ_{tp} and θ_{tf} by simply interchanging the vectors $\bar{s}$ and $\bar{t}$, and the subscripts s and t.

From geometry of Fig. 3.5,

$$\tan\theta_{sp} = \frac{OC}{BC} = \frac{OC}{AD} = \frac{OD}{AD} \cdot \frac{OC}{OD} \quad , \text{and} \quad \tan\theta_{sf} = \frac{CD}{AD} = \frac{CD}{OD} \cdot \frac{OD}{AD} \quad ,$$

but,

$$\frac{OD}{AD} = \tan\theta_s \quad , \quad \frac{OC}{OD} = \cos(\beta_n - \beta_s) \quad , \quad \frac{CD}{OD} = \sin(\beta_n - \beta_s)$$

thus,

$$\tan\theta_{sp} = \tan\theta_s \cos(\beta_n - \beta_s) \qquad (3.16)$$

and

$$\tan\theta_{sf} = \tan\theta_s \sin(\beta_n - \beta_s) \qquad (3.17)$$

Now we can start with the analysis of the two shadowing effects. The parallelograms of the two types of shadows are shown in Fig. 3.4(a). Knowing that 's' and 't' are subscribts related to sun shade and tower screen, X_{ms} and X_{mt} are defined as the distances between the horizontal edge of the mirror and the farest side of the corresponding parallelogram in the frame of reference of the mirror, xy. The notations Y_{ms} and Y_{mt}, on the other hand, stands for the scew lengths or lateral distances between the corners of the corresponding parallelogram and parallel to the mirror edge.

From Fig. 3.4(b)

$$X_{ms} = \cos\theta_n + \sin\theta_n \tan\theta_{sp} \qquad (3.18)$$

Substitution of Eq. (3.16) into Eq. (3.18) gives

$$X_{ms} = \cos\theta_n + \sin\theta_n \tan\theta_s \cos(\beta_n - \beta_s) \qquad (3.19a)$$

or multiplying and dividing Eq.(3.18) by $\cos_{sp}$ we obtain

$$X_{ms} = \frac{\cos(\theta_n - \theta_{sp})}{\cos\theta_{sp}} \qquad (3.19b)$$

From Fig.3.4(c) Y_{ms} is found to be

$$Y_{ms} = \sin\theta_n \tan\theta_{sf} \qquad (3.20)$$

Substituting Eq.(3.17) in Eq.(3.20) we result in

$$Y_{ms} = \sin\theta_n \tan\theta_s \sin(\beta_n - \beta_s) \qquad (3.21)$$

Since the xy-coordinate system depends on location of the mirrors, there are as many coordinate systems as number of the mirrors. Thus it would be desired to express the distances X_{ms} and Y_{ms} of the sun shade in a fixed coordinate system in the horizontal plane defined by the coordinate axes 'x' and 'y', directed toward East and South respectively. The components X'_{ms} and Y'_{ms} of the corners along these new axes can be derived from the components X_{ms} and Y_{ms} in the mirror's frame by performing a rotation of axes involving the mirror azimuth angle β_n. Thus,

$$X'_{ms} = \cos\theta_n \sin\beta_n + \sin\theta_n \tan\theta_s \sin\beta_s \qquad (3.22a)$$

$$Y'_{ms} = \cos\theta_n \cos\beta_n + \sin\theta_n \tan\theta_s \cos\beta_s \qquad (3.22b)$$

(See Appendix-5.)

We can analogously obtain the expressions for the components related to the tower screen. By simply interchanging the subscripts s and t we can obtain the following results:

$$X_{mt} = \cos\Theta_n + \sin\Theta_n \tan\Theta_t \cos(\beta_n - \beta_t) \qquad (3.23a)$$

$$X_{mt} = \frac{\cos(\Theta_n - \Theta_{tp})}{\cos\Theta_{tp}} \qquad (3.23b)$$

$$Y_{mt} = \sin\Theta_n \tan\Theta_n \sin(\beta_n - \beta_t) \qquad (3.24)$$

$$X'_{mt} = \cos\Theta_n \sin\beta_n + \sin\Theta_n \tan\Theta_t \sin\beta_t \qquad (3.25a)$$

$$Y'_{mt} = \cos\Theta_n \cos\beta_n + \sin\Theta_n \tan\Theta_t \cos\beta_t \qquad (3.25b)$$

Eqs.(3.18)-(3.25) express the components of the sun shade and tower screen which are established by the unit vectors $\bar{s}$ and $\bar{t}$. But these vectors are related in turn by the steering equations so that the relative components of the "footprints" are not independant. Therefore we are expecting to find some relations between these components. Specifically, from Eq.(3.3)

$$\bar{n}.\bar{s} = \cos\Theta_s \cos\Theta_n + \sin\Theta_s \sin\Theta_n \cos(\beta_n - \beta_s)$$
$$= \cos\Theta_s . X_{ms} = \frac{|\bar{N}|}{2} \qquad (3.26a)$$

$$\bar{n}.\bar{t} = \cos\Theta_t \cos\Theta_n + \sin\Theta_t \sin\Theta_n \cos(\beta_n - \beta_t)$$
$$= \cos\Theta_t . X_{mt} = \frac{|\bar{N}|}{2} \qquad (3.26b)$$

so that

$$\frac{X_{mt}}{X_{ms}} = \frac{\cos\Theta_s}{\cos\Theta_t} = q \qquad (3.27)$$

Furthermore, using Eq.(3.9)

$$\frac{Y_{mt}}{Y_{ms}} = -\frac{\cos\Theta_s}{\cos\Theta_s} = -q \qquad (3.28)$$

A unit vector, along any side of the sun shade which is not parallel to the horizontal edge of the mirror, can be expressed by

$$\bar{s}_s = \frac{(X'_{ms})\bar{i} + (Y'_{ms})\bar{j}}{\sqrt{(X'_{ms})^2 + (Y'_{ms})^2}} \qquad (3.29)$$

which is obviously a function of angles Θ_n, Θ_s, β_n, β_s. However a unit vector along the horizontal projection of the sun vector is expressed by

$$\bar{s}_h = \sin\beta_s \bar{i} + \cos\beta_s \bar{j} \qquad (3.30)$$

which is a function of β_s only. This means that the horizontal projection of the sun vector and the longitudinal sides of the sun shade are not coincident. (They are coincident for only the special case $\Theta_n = 90°$ and $\Theta_s = 45°$ which is physically impossible.) The physical situation is illustrated in Fig. 3.6 below.
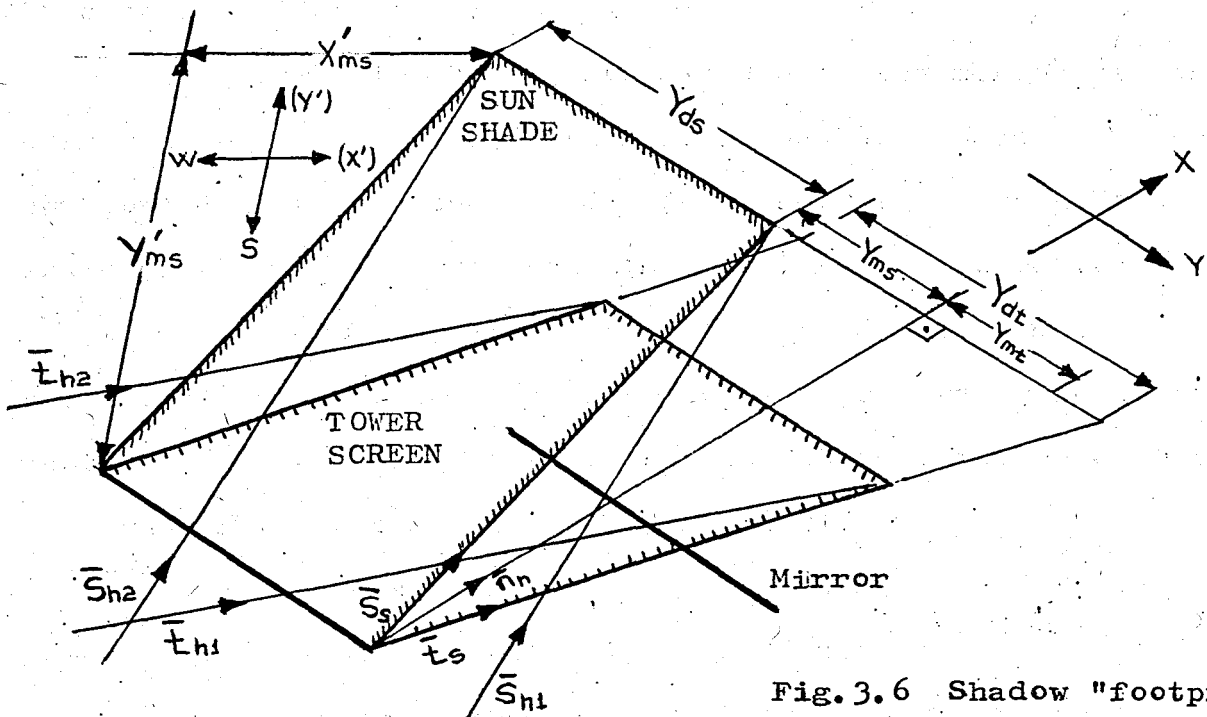

Fig. 3.6 Shadow "footprints" of a rectangular mirror.

The same results can be stated for the tower screen. Furthermore from Eqs. (3.27) and (3.28)

$$\left|\frac{Y_{ms}}{X_{ms}}\right| = \left|\frac{Y_{mt}}{X_{mt}}\right|$$

which requires that

$$\bar{n}_h \cdot \bar{s}_s = \bar{n}_h \cdot \bar{t}_s \qquad (3.31)$$

Under the illimunation of the explanations above, and Figs. 3.4 and 3.6, the following short results interperet the shadow foctprint analysis:

a) The quotient $\cos\Theta_s / \cos\Theta_t$ is practically significant and worth being named by a parameter q. This paremeter uniquely characterizes the relative extend of shadows for the sun shade and tower screen: when $q < 1$, (i.e., $\Theta_t < \Theta_s$) the sun shade is larger than the tower screen; if $q > 1$, (i.e., $\Theta_t > \Theta_s$) the reverse situation holds.

b) The normal to the horizontal edge of the mirror at its corner bisects the sun and tower line shadows produced in the horizontal plane by the tilted side edge of the mirror. Thus while the horizontal projections of the three basic vectors $(\bar{n}_h, \bar{t}_h$ and $\bar{s}_h)$ do not satisfy the equality of incidence and reflection angles (see Appendix-6), this equality property is recovered in the edge shadows. The proof of this interpretation is given in the steps resulted in Eq. (3.31).

c) The skewed side lengths of the sun shade and tower screen, Y_{ds} and Y_{dt} respectively, are identical.

d) The skewing of the two parallelograms occurs in

opposite directions which are determined by the sign of the relative angles $\beta_n - \beta_s$ or $\beta_n - \beta_t$.

e) Shadow computations need be performed for only one type of shadow, the other being derived from it by simply scaling with the parameter q.

3.2.2 Shadowing Effects on Adjacent Mirrors:

After the analysis of the shadow footprints of a single mirror comes the analysis of the shadowing effects in a system of adjacent mirrors. Fig. 3.7 (which is nothing than a portion of Figs. 3.4 and 3.6) shows a representative view of such a system composed of two parallel mirrors located at a distance D. This distance can be characterized by an azimuth angle β_d, measured from South, as usual.
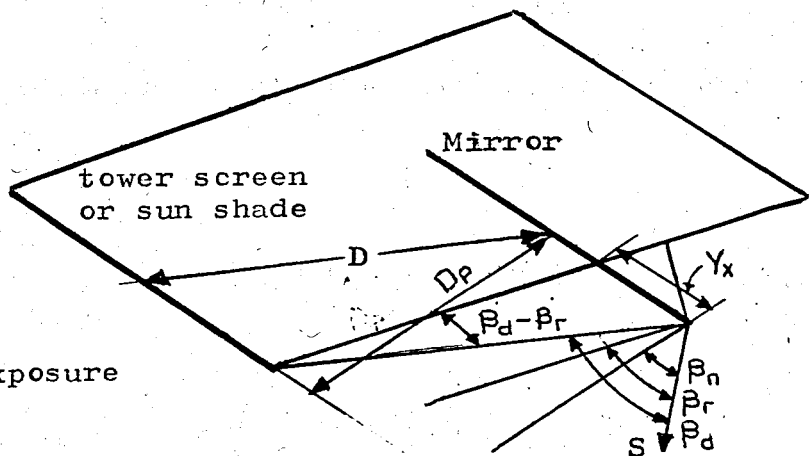

Fig. 3.7 Side exposure angles.

In a side view, as shown in Fig. 3.4(b), the mirrors appear to be seperated by the profile distance

$$D_p = D\cos(\beta_n - \beta_d).$$

When the sun shade is larger (i.e., q 1), from geometry of Fig. 3.4(b) we obtain

$$\frac{1}{X_{ms}} = \frac{1 - X_s}{X_{ms} - D_p}$$

or, solving for the exposed top distance X_s

$$X_s = \frac{D_p}{X_{ms}} \tag{3.32}$$

Obviously when D_p is greater than X_{ms} there is no shading on the back mirror such that, Eq. (3.32) can be written as

$$X_s = \begin{cases} D_p/X_{ms} & \text{for } D_p < X_{ms} \\ 1 & \text{for } D_p \geqslant X_{ms} \end{cases} \tag{3.33}$$

Likewise, in the case of the tower screen's being larger

$$X_t = \begin{cases} D_p/X_{mt} & \text{for } D_p < qX_{ms} \quad (\text{or } D_p < X_{mt}) \\ 1 & \text{for } D_p \geqslant qX_{ms} \quad (\text{or } D_p \geqslant X_{mt}) \end{cases} \tag{3.34}$$

The side exposure distance (for either sun or tower) can be obtained also as

$$Y_x = D \frac{\sin(\beta_d - \beta_r)}{\cos(\beta_n - \beta_r)} \qquad \text{for } |Y_x| \leqslant L \text{ and } X_x < 1 \tag{3.35}$$

in which $\beta_r = \tan^{-1}(X_{mx}/Y_{mx})$ and subscribt 'x' stands for 's' or 't' depending on the sun shading or tower screening's being effective respectively. Certainly, if either $|Y_x| \geqslant L$ or $X_x \geqslant 1$ the mirror is fully exposed.

These two mirror area utilization effects are conceptual complements of the incidence factor k_i such that the final effective area is simply the available or exposed area times k_i.

3.2.3 Area Utilization Factors:

Before starting with the analysis of the area utilization factors it is worth mentioning about the continium field approach in more detail which is briefly mentioned about in "Introduction".To get the basic idea lying under this approach it is helpful to consider first a circular orientation of heliostats in the field,as shown in Fig.3.8(a).Secondly,assume that the heliostats are not flat and there is no opening between them such that they form concentric circles,Fig.3.8(b).Then we can visualize a field which is composed of continious circular
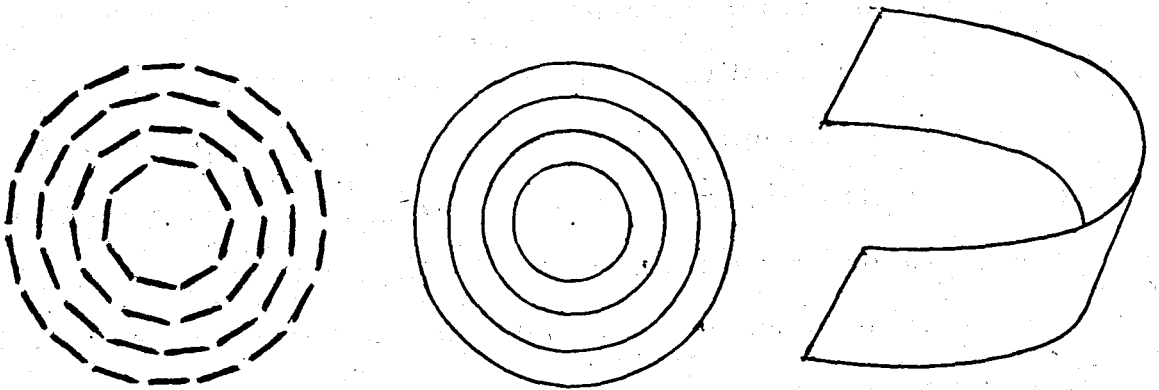
a) top view (actual)   b) top view (ideal)   c) Plan view (ideal)

Fig.3.8   Illustration of ideal heliostat arrays concept.

strips (i.e.,heliostat arrays) of width identical to that of mirrors.The situation is tried to be illustrated in Fig.3.8(c). Of course,such a situation is not realistic and the system is motionless.However,this assumption simplifies the area utilization analysis extremely with possibly not much error in return.

The explanation above may be interpreted by two important results:

1) Since the heliostat arrays are assumed as continious circular strips,there is no side exposure distance Y.(The subscribt 'x' is dropped due to the generality)

2)The area portion of any mirror below the smallest of the two top exposure distances,X_s and X_t,is completely ineffective.

Consequently,going back to Fig.3.4,we should say that the mirror area swept by distances Y_t and X_t-X_s is ineffective (i.e.,shaded) when the whole field is considered in the analysis.(Obviously, this area is effective if any pair of adjacent mirrors (front-back) is isolated,which is the situation shown in Fig.3.4)

At this point we can ask a question:How small is the error arising from the idealization introduced above? Of course an exact answer cannot be given to this question otherwise a full analytic study of the system is made.Therefore we will be contended by only indicating the basic sources of error.This is done best by comparing the physics of an ideal and actual or a realistic system.

First of all,in an ideal system the heliostat arrays are parallel while in a realistic system adjacent mirrors (front-back) are flat and they are not parallel to assure that both redirect the sun rays to the same target.However the radia of the circular paths along which the mirrors are oriented should be so large compared to the mirror dimensions that these assumptions will not result in serious errors.Therefore this assumption can still be kept valid.Secondly,as it was indicated before,ideal heliostat arrays are thought to be of continious

concentric strips;but they cannot be so,and there should exist openings between the mirrors for free motion of them.This means that the adjacent sides of the neighboring mirrors derive out of the ideal arrangement.Such a situation causes the sun rays' escape through these openings and results in small changes in effective or ineffective area portions of the shaded mirror by relative changes in theconfiguations of the neighboring mirrors.

We can go back now,to the analysis of the area utilization factors.Under the illimunation of the assumptions and idea idealizations above,the performance of the field may be characterized by the following factors:

a) Ground area utilization factor k_g:It is simply defined as $1/D_p$, D_p being the per-unit seperation distance.Thus $D_p < 1$ means overlaping of mirrors in the horizontal position and $D_p = 1$ means mirrors are just touching.

b) Mirror area utilization factor k_m:This is the least of the top exposed per-unit lengths,X_s or X_t.Thus the factor

$$k_m = \begin{cases} D_p/X_m & \text{for } D_p < X_m \\ 1 & \text{for } D_p \geqslant X_m \end{cases} \qquad (3.36)$$

c) Overall area utilization factor k_o:This is just the product of the two factors above,i.e.,

$$k_o = k_g \cdot k_m = \begin{cases} 1/X_m & \text{for } D_p < X_m \\ 1/D_p & \text{for } D_p \geqslant X_m \end{cases} \qquad (3.37)$$

d) Incidence factor k_i:By Eqs.(3.2),(3.11),(3.26a) and (3.26b)

$$k_i = \bar{n}.\bar{s} = \bar{n}.\bar{t} = \cos\theta_s . X_{ms} = \cos\theta_t . X_{mt} = |\bar{N}|/2 \qquad (3.38)$$

e) Resultant steering-shadow factor k:This factor is the product of all the others encountered is a measure of a mirror in reflecting the sun rays to a central point.Thus three possible cases are examined for this product:

1) Any mirror which is not exposed to any shadowing effect,screening or shading,has a resultant area utilization factor equal to incidence factor k_i.

2) In the case of sun shading,the maximum utilization factor is given by the shading factor

$$k_s = \frac{1}{X_{ms}} (\bar{n}.\bar{s}) = \frac{1}{X_{ms}} (\cos\theta_s . X_{ms})$$

$$= \cos\theta_s \qquad (3.39)$$

3) In the case of tower screening the maximum utilization factor is given by the screening factor

$$k_t = \frac{1}{X_{mt}} (\bar{n}.\bar{t}) = \frac{1}{X_{mt}} (\cos\theta_t . X_{mt})$$

$$= \cos\theta_t \qquad (3.40)$$

These simple and fine-looking results are very significant and indicate the following fact;for an ideal heliostat field,in the presence of either shading or screening the resultant area efficiency factor is a functionof only the cosine of the appropriate zenith angle θ_s or θ_t but not of azimuth angles.(See Discussion-1.c)For an isolated mirror however,the utilization factor is incidence factor,k_i which is a function of the azimuth angles β_s and β_t as well as θ_s and θ_t.

3.3 Concentrator Area and Efficiency:

In order to talk about the total area requirement and performance limits of an ideal field of heliostat arrays, we should additionally note the following assumptions:

a) At any instant of time the mirrors are arranged such that they all satisfy the steering equations and achieve maximum possible exposure compatible with minimum shading and screening effects.
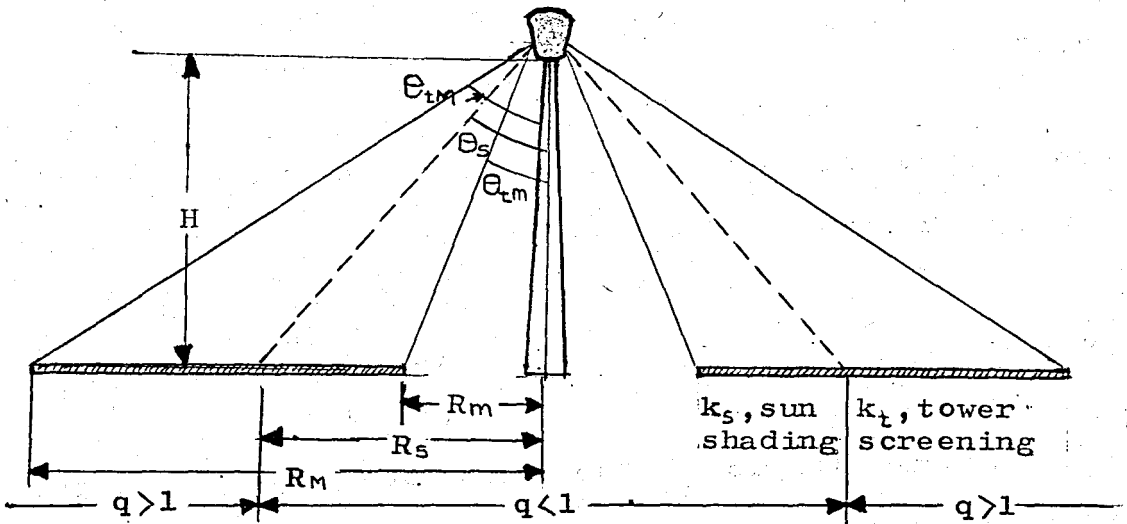

Fig.3.9 Distribution of mirror utilization factors in a circular ring concentrator.

b) The field is considered to be covered by a single concentrator having a shape of circular ring and composed of horizontal heliostats with no seperation distance in between. As illustrated in Fig.3.9 the outer radius is $R_M = Htan\Theta_{tM}$, where Θ_{tM} is the rim angle of the concentrator. The inner radius is $R_m = Htan\Theta_{tm}$.

c) The land is taken to be horizontal with no obstructions anywhere in the field. In particular, the blocking effects of the central tower are considered to be negligible.

3.3.1 Mathematical Model of Concentrator:

Some conceptual considerations and the area utilization factors were explained in previous sections such that we can get some mathematical results for the total area requirement and the efficiency of the heliostat arrays field.

Considering a ring element area, total integral area equation of the concentrator is expressed by

$$A_c = \int 2\Pi R \cdot dR = \int 2\Pi R \cdot \frac{\sin\theta_t}{\cos^3\theta_t} \, d\theta_t \qquad (3.41)$$

Introduction of the resultant steering-shadow factor k gives us its total effective area A_r in the most general form. Thus,

$$A_r = \int 2\Pi R \cdot k \cdot \frac{\sin\theta_t}{\cos^3\theta_t} \, d\theta_t \qquad (3.42)$$

Since shading and screening effects are differentiated by the value of the parameter q, it is appropriate as shown in Fig. 3.9 to divide the concentrator field into two regions separated by a circle of radius $R_s = H\cos\theta_s$ which passes through the node (at the azimuth angle β_s): inside this circle $(q < 1)$ sun shading dominates, while outside it $(q > 1)$ tower screening is the governing feature. If the node occurs inside the circular hole $(\theta_s < \theta_{tm})$, the whole concentrator experiences tower screening effects; on the other hand, with the node outside $(\theta_s > \theta_{tM})$, the concentrator is influenced by sun shading. The total effective concentrator area A_r which intercepts at a given time (i.e. given node location) the maximum solar flux and redirects it to the central receiver without shadowing effects can now be

obtained in closed form by carrying out the integral given by Eq.(3.42) which is the reduced form of Eq.(3.41) by the factor $k; k_s$ if located in shading zone or k_t in the screening zone. Thus depending upon the location of the node with respect to the concentrator, due to three possibilities above, three expressions for its total effective area A_r can be obtained by integration:

a) Node ON concentrator $(\Theta_{tm} < \Theta_s < \Theta_{tM})$:

$$A_r = 2\Pi H^2 \left[\int_{\Theta_{tm}}^{\Theta_s} \left(\frac{\sin\Theta_t}{\cos^3\Theta_t}\right).\cos\Theta_s.d\Theta_t + \int_{\Theta_s}^{\Theta_{tM}} \left(\frac{\sin\Theta_t}{\cos^3\Theta_t}\right).\cos\Theta_t.d\Theta_t \right.$$

$$A_r = \Pi H^2 \left(\frac{2}{\cos\Theta_{tM}} - \frac{\cos\Theta_s}{\cos^2\Theta_{tm}} - \frac{1}{\cos\Theta_s}\right) \qquad (3.43a)$$

b) Node INSIDE concentrator $(\Theta_s \leq \Theta_{tm})$:

$$A_r = 2\Pi H^2 \int_{\Theta_{tm}}^{\Theta_{tM}} \left(\frac{\sin\Theta_t}{\cos^3\Theta_t}\right).\cos\Theta_t.d\Theta_t$$

$$A_r = 2\Pi H^2 \left(\frac{1'}{\cos\Theta_{tM}} - \frac{1}{\cos\Theta_{tm}}\right) \qquad (3.43b)$$

c) Node OUTSIDE concentrator $(\Theta_s \geq \Theta_{tM})$:

$$A_r = 2\Pi H^2 \int_{\Theta_{tm}}^{\Theta_{tM}} \left(\frac{\sin\Theta_t}{\cos^3\Theta_t}\right).\cos\Theta_s.d\Theta_t$$

$$A_r = \Pi H^2 (\tan^2\Theta_{tM} - \tan^2\Theta_{tm}).\cos\Theta_s \qquad (3.43c)$$

We can define an area efficiency $\eta = A_r/A_i$ knowing that total concentrator area $A_i = \Pi H^2 (\tan^2\Theta_{tM} - \tan^2\Theta_{tm})$. Hence,

$$\eta = \begin{cases} 2\left(\dfrac{1}{\cos\theta_{tM}} + \dfrac{1}{\cos\theta_{tm}}\right)^{-1} & \text{for } (\theta_s \leq \theta_{tm}) \qquad (3.44a) \\[2em] \dfrac{\dfrac{2}{\cos\theta_{tM}} - \dfrac{\cos\theta_s}{\cos^2\theta_{tm}} - \dfrac{1}{\cos\theta_s}}{\dfrac{1}{\cos^2\theta_{tM}} - \dfrac{1}{\cos^2\theta_{tm}}} & \text{for } (\theta_{tm} < \theta_s < \theta_{tM}) \qquad (3.44b) \\[3em] \cos\theta_s & \text{for } (\theta_s \geqslant \theta_{tM}) \qquad (3.44c) \end{cases}$$

For convenience and generality, it is desirable to express the concentrator effective area in a per-unit dimensionless form by using as normalizing base area ΠH^2 of a circle of radius equal to the tower height. In this per-unit system, equations 3.44 become

$$a_r = \begin{cases} 2\left(\dfrac{1}{\cos\theta_{tM}} - \dfrac{1}{\cos\theta_{tm}}\right) & \text{for } (\theta_s \leq \theta_{tm}) \qquad (3.45a) \\[2em] \dfrac{2}{\cos\theta_{tM}} - \dfrac{\cos\theta_s}{\cos^2\theta_{tm}} - \dfrac{1}{\cos\theta_s} & \text{for } (\theta_{tm} < \theta_s < \theta_{tM}) \qquad (3.45b) \\[1.5em] (\tan^2\theta_{tM} - \tan^2\theta_{tm}) \cdot \cos\theta_s & \text{for } (\theta_s \geqslant \theta_{tM}) \qquad (3.45c) \end{cases}$$

3.3.2 Graphical View of Field Performance:

Clearly, from Eqs. (3.44) and (3.45), effective concentrator area and area utilization efficiency are not functions of any of the azimuth angles but are functions of only the radial

distances corresponding the angles Θ_{tm} and Θ_{tM}, as expected. Because the shading and screening factors are not functions of azimuth angles. Thus we can demonstrate the per-unit area a_r and efficiency η graphically. Fig.3.10 shows plots of the
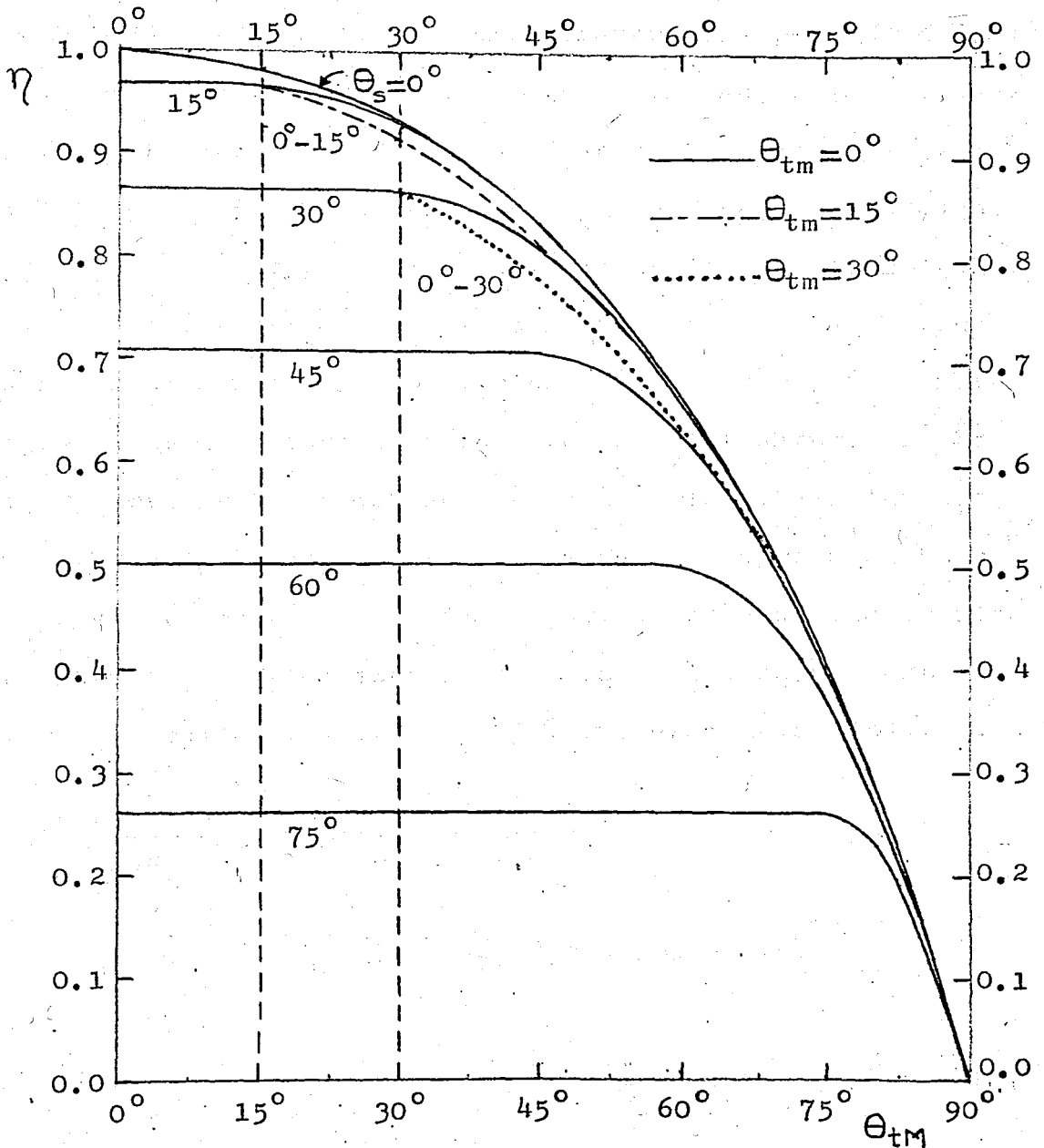
Fig.3.10 Concentrator area efficiency characteristics.

(x) The plots for $\Theta_s > \Theta_{tm}$ coincide with the ones for $\Theta_s = 0°$.

ideal concentrator area effeciency as a function of various values of sun zenith angle .Three possibilities are encountered due to the three different values of Θ_{tm}.

For $\Theta_s \leqslant \Theta_{tm}$ efficiency is not a function of the sun's zenith angle Θ_s. That is only tower screening occurs in this range. When the node is on the concentrator (i.e., $\Theta_{tm} < \Theta_s < \Theta_{tM}$) both effects, sun shading and tower screening act together, and, the effect of variation of Θ_{tm} on efficiency is negligibly small. As long as Θ_s is greater than Θ_{tM} we observe a straight line since efficiency, in this range, is a function of Θ_s only.

Plots of effective per-unit concentrator area a_r versus the sun's zenith angle Θ_s for various field size Θ_{tM} are given in Fig. 3.11. It is interesting to note the flat nature of the effective area over a wide range of sun angles; this flatness is due to the combined effects of shading and screening when $\Theta_s \leqslant \Theta_{tM}$. In fact in that region all curves are essentially dis- placed from one another, exhibiting identical absolute drops. This drop is calculated for $\Theta_{tm} = 30^\circ$, for example, as follows:

$$a_r = \frac{2}{\cos\Theta_{tM}} - 1.333\cos\Theta_s - \frac{1}{\cos\Theta_s}$$

But for $\Theta_s = 0^\circ$, $(a_r)_{\Theta_s=0^\circ} = (2/\cos\Theta_{tM}) - 2.333$. Then,

$$a_r|_{\Theta_s=0^\circ} - a_r|_{\Theta_s} = 1.333\cos\Theta_s - \frac{1}{\cos\Theta_s} - 2.333 \quad (\Theta_s \leqslant \Theta_{tM})$$

As it is obvious from the above calculation, the absolute drop is a function of Θ_s only.
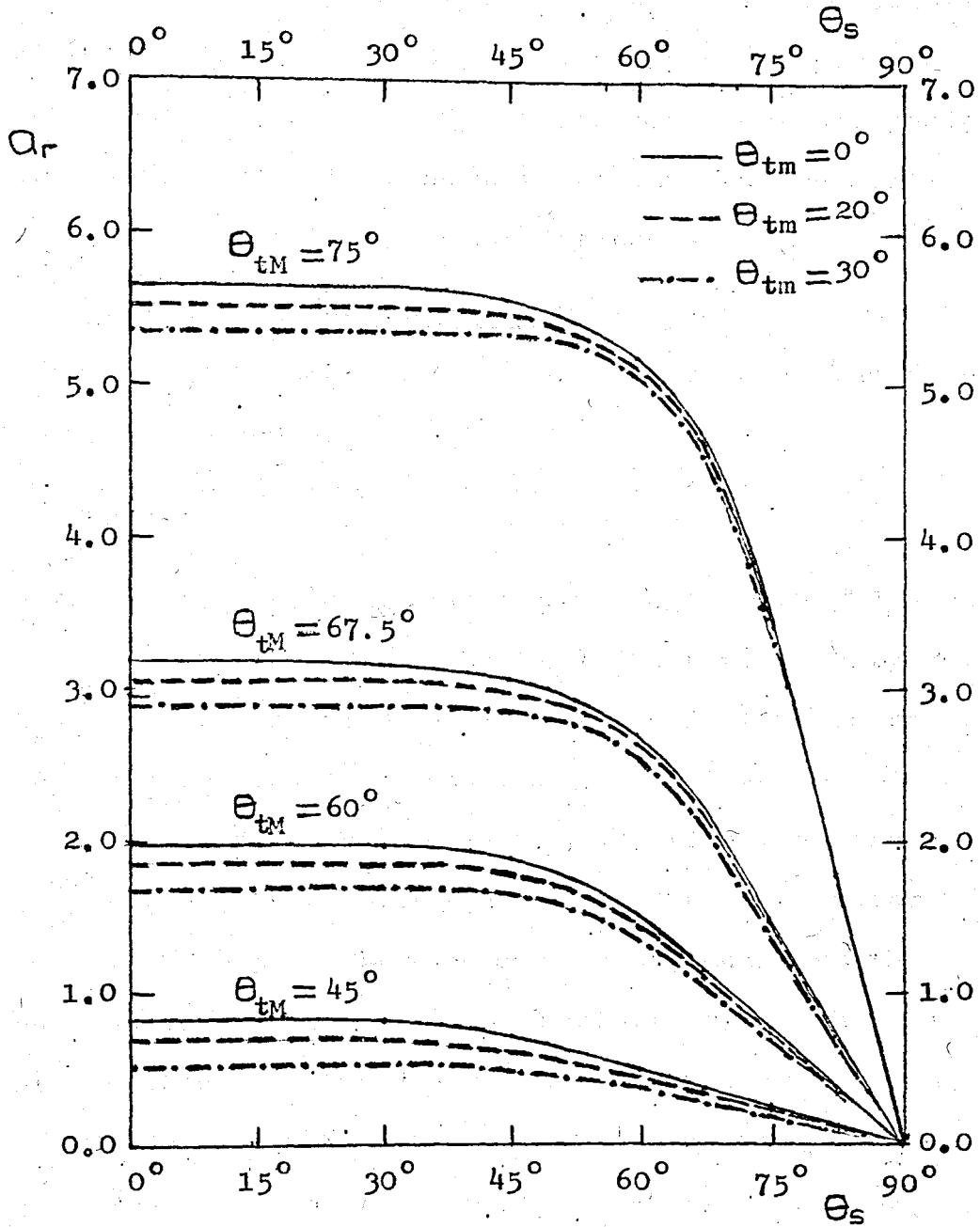
Fig. 3.11 Effective concentrator area characteristics.

Chapter IV

DESIGN OF A 150kw SOLAR POWER PLANT IN CIHANBEYLI

The overall analysis of the continuum field model of ideal heliostat arrays in the previous chapters provides the necessary background for a representative practical design. But in order to perform all necessary calculations we still need to employ some simplifying prescribtions.

4.1 A General Study of the Power Factors:

The power available from solar radiation at the receiver is simply expressed by

$$P = k_d . \bar{A}_r . \bar{I}^{(x)} \tag{4.1}$$

in which k_d is a derating factor standing for the product of a resultant steering-shadow factor k and a reflectivity factor k_r, $\bar{A}_r$ is a certain value of the total effective concentrator area A_r (i.e., corresponding to some special values of angles $\Theta_s, \Theta_{tm}, \Theta_{tM}$), and $\bar{I}$ is that of solar radiation I at any instant of the day. Then, it is obvious that the derating factor k_d includes all kinds of effects from very beginning of the steering action resulting in reduction in performance of the system except the abssorbtivity losses at the receiver.

A_r, being a product of dimensionless area a_r and dafined circular area ΠH^2, is governed by time-varying position of the sun, i.e., Θ_s and rim angles Θ_{tm} and Θ_{tM}. H is left as the variable to be determined last, once the others are assigned.

Theorethical expressions for solar radiation and their corrolation by experimental results are recently studied. Based

---

(x) A 'bar' (—) above symbols will stand for special evaluated values of functions represented by these symbols.

on these studies, solar radiation maps of lands or graphs are prepared. These are major sources of inputs for calculation. [2, 3, 12, 14.]

Since reflectivity is a material and production dependent property, the factor k_r is kept out of the discussion and as-signed arbitrarily throughout the calculations.

4.1.1 Effective Concentrator Area:

It is clear from Fig. 3.11 that maximum concentrator effec-tive per-unit area, thus the total effective concentrator area can be utilized in the range $\Theta_s \leqslant \Theta_{tM}$. Since for any site, rela-tively close to the equator, maximum concentrator area utiliza-tion and maximum solar radiation is attained almost at the same instant of the day, other factors being fixed, we obtain maximum power at that instant of the day. Furthermore, sharp decreases in dimensionless area curves are due to Θ_s values at which solar radiation is reletively ineffective so that for a given value of concentrator outer rim angle Θ_{tM} maximum value of a_r could be taken as the value used in the calculations. Of course this would be a special approach to the problem in which design is based on maximum available power.(x) However it should be guar-teed that Θ_{tM} is equal or greater than minimum sun zenith angle Θ_{smin} at solar noon of the characteristic day which is consid-ered in design. For Cihanbeyli $(\Theta_{smin})_{noon} = 61.92°$ (Dec. 22). Fig. 3.11 also shows that even small increaments in Θ_{tM} result in very appreciable increaments in dimensionless concentrator area for higher values of outer rim angle Θ_{tM} and these increaments are even measured by folds of its original value (i.e., of a_r)

_____

(x) This is not the approach utilized in this thesis.

as getting close to $90°$.Therefore we may think that we should
keep Θ_{tM} as large as possible.However,large values of Θ_{tM} also
means very large ground area required.Also,as a contradictory
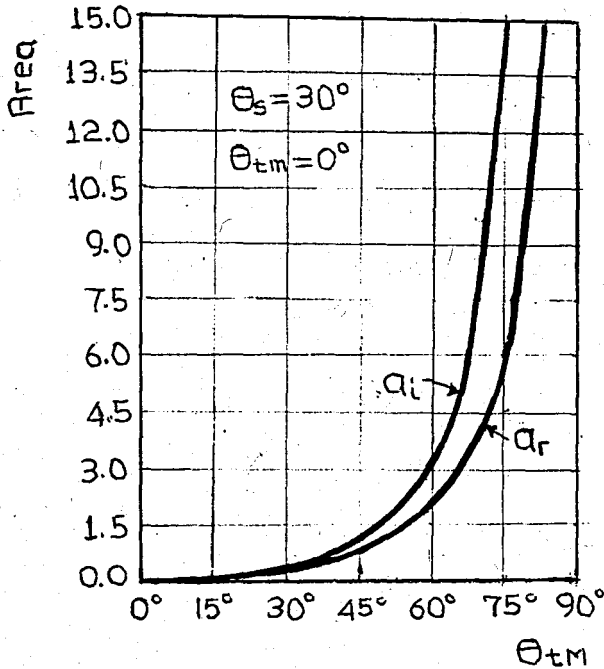effect to increasing concentrator effective per-unit area a_r,

Fig.4.1 Variations of per-
unit effective concentrator
area a_r and per-unit ground
area a_i with field size.

efficiency curves exhibit sharper drops for larger values of
Θ_{tM}.A comparison of the concentrator effective per-unit area a_r
with the ground per-unit area $a_i= A_i/\Pi H^2$ is shown in Fig.4.1.Thus
three important problems come into feature from point of view
 of total effective concentrator area;cost,efficiency and
availability of ground area.

   Cost is rather considered to be a problem of economy and
technology and,therefore,kept out of discussion.

   Once some difficulties and cost problems are avoided and
solar power plants become compatible with hydrolic and nuclear
plants,efficiency should not be a major factor to be thought
about since the equivalent of solar energy is nothing except

runing costs.Even though it is so,an improvement in concentrator effective area would be preferredrather than an improvement in efficiency.This idea can be supported by the following example:

Let's take $\Theta_{tm}=0$ .An increament in Θ_{tM} from 75° to 80° causes a drop of eleven percent (from 41% to 30%) for sun zenith angles $\Theta_{s}=0^{\circ}-30^{\circ}$ and a drop of only three percent (from 26% to 23%) for $\Theta_{s}=75^{\circ}$ in efficiency.We can assume a daily avarage drop of 8percent.However,increament in concentrator per -unit area resulting from the same increament in Θ_{tM} is more than the original value of it.On the other hand,ground area requirement is 1.3 times more than that of the original value, (i.e.,it is 2.3 times the original value.) Therefore cost and availability of ground area are more important design factors than efficiency to be considered against increaments in outer rim angle Θ_{tM}.

All main dimensions of a 150kw (thermal) power plant can be calculated by reasonable assumptions for Θ_{tM},k_{d} and I. Of course for such a small power plant the required ground area A_{i} would be small and available always.However our design should be completely representative for a megawatt based power plant so that we should not take ground area as large as we want.Calculations under different radiation values indicate areas of 1.5 to 5.0 square kilometers [1,5] which impose a strong restriction in selection of Θ_{tM}.For a constant value of the ground area A_{i} we can increase the efficiency by increasing the tower, but then Θ_{tM} thus a_{r} would decrease in turn.

4.1.2 Solar Radiation:

Besides its expected dependence on days of the year and time of the day, solar radiation also depends on atmospheric changes which can not be ruled. For this reason there are considerable variations in daily, monthly and even yearly avarage experimental values of solar radiation. In order to get reliable

SUN-EFFECTIVE TIME PERIOD, SETP (hour)					
	MAY	JUNE	JULY	AUGUST	SEPT.
1969	11.00	12.24	14.12	13.18	11.48
1970	10.36	12.12	13.30	12.42	10.06
1971	10.06	12.06	13.36	11.12	10.48
1972	10.00	10.42	12.36	11.36	9.36
1973	10.18	11.48	13.06	12.48	11.24
1974	9.54	13.06	13.30	11.24	10.12
1975	8.24	11.06	12.48	12.18	11.00
Avg. SETP	9.91	11.78	13.14	12.00	10.53
Max. SETP	14.113	14.658	14.401	13.459	12.214
SOLAR RADIATION, SR (MJ/M^2.DAY)					
	MAY	JUNE	JULY	AUGUST	SEPT.
1969	18.790	20.738	22.140	20.613	16.558
1970	18.369	21.046	17.401	19.859	15.496
1971	17.960	18.853	21.062	18.144	15.551
1972	18.153	19.144	19.341	18.306	14.631
1973	17.886	19.466	19.529	19.271	15.294
1974	16.932	19.665	20.136	17.901	14.044
1975	15.878	18.496	19.030	18.254	14.821
Avg. SR.	17.709	19.630	19.806	18.907	15.199
SROA$^{(x)}$	18.603	20.317	20.663	18.489	15.129

Table 4.1.

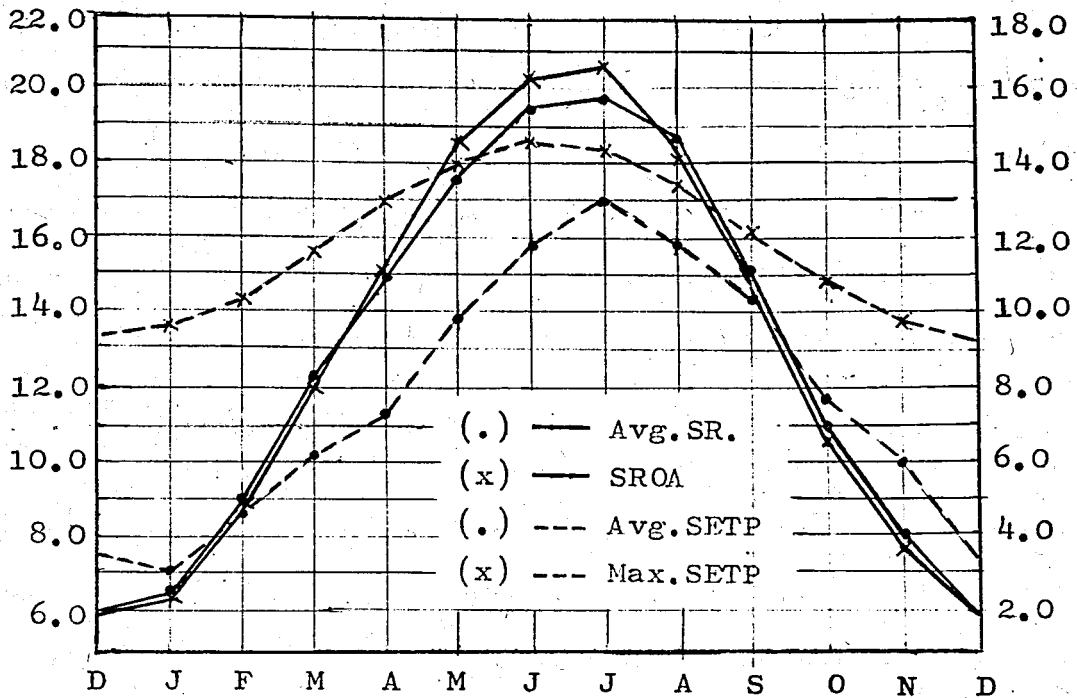$^{(x)}$ SROA, solar radiation outside the atmosphere

Fig. 4.2 Monthly diztribution of SR and SETP.

results in calculations, experiments must be reliable. Certainly

in order to get more stable avarage values greater must be the

number of years subject to observations.

Experimental solar radiation maps or graphs are exten-

sively available for some countries but, unfortunately, not so

much for Turkey. Our design will base on the experimental

results given for five months of the indicated years (for Cihan-

beyli) in Table 4.1. Among these months one is expected to have

maximum avarage radiation and one maximum sun-effective time

period, SETP. As seen from Table 4.1., July is the month satis-

fying the both expectations. Experimental values for all months

of the year are plotted in Fig. 4.2.

The most charasteristic variation of solarradiation is

observed during a day. Variation of diffuse solar radiation

from a clear sky incident upon various surfaces are plotted

in many references [2,3].We should reasonably choose south

faced vertical or horizontal surfaces.Such plots in literature

show that daily variation of diffuse solar radiation may be

approximated by a sine or parabolic curve.But since we don't

have enough experimental data for Cihanbeyli to prefer a sine

or a parabolic curve,we arbitrarilly decided to use a sine

curve for our design.

The variables,tried to be discussed above,indicate the

fact that once the desired power output (thermal or solar) is

given there are many constraints to deal with.We will just

come out with the results introducing these constraints.Some

restrictions still stand without being dealt such as the ones

related to mirror dimensions,inner rim angle t_m and receiver

size.These will be discussed during the design procedure.

4.2 Design Procedure:

Any design may be based on various criterion from point of view of available power. As known well the power factors $a_r(t)$ (or $a_r(\Theta_s)$) and $I(t)$ (or $I(\Theta_s)$) are functions taking values between zero and each its own maximum depending upon value of argument t(time). The function $a_r(t)$ has only theoretical limits so that once the outer rim angle Θ_{tM} is given it shows a certain curve for a given location. $I(t)$ is however governed by atmospheric changes as much as the theoretical expectations, as mentioned before. Therefore, although we decided to express $I(t)$ by a sine curve, in order to determine the exact form of the function, we should develop a certain criterion.

4.2.1 Estimation of Daily Solar Radiation Curve:

In our analysis the following criterion is utilized:

a) The month of the year with maximum experimental daily avarage solar radiation is considered. This month is July for Cihanbeyli and experimental solar radiation result in a total energy of 19.806 MJ/m^2.day.

b) Avarage experimental SETP for July is used as the day length. It is noted to be 14.401 hr.

c) Daily solar radiation curve is considered to be a sine curve.

This last assumption is checked by the results of experiments performed on various locations on the earth in cloudless days. This means that, although we will use experimental values, these will be adopted as values observed in a characteristic cloudless day. Then the exact form of the function $I(t)$ for this
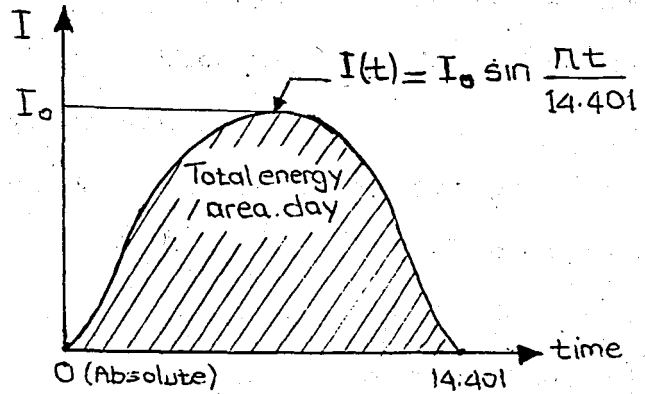
characteristic day is determined as follows:

Fig. 4.3 Representative daily time-variation of solar radiation.

The shaded area under the curve in Fig. 4.3 represents the total radiation energy per day which is equal to the time integration of the solar radiation function $I(t)$. In its most general form $I(t)$ can be written as

$$I(t) = I_o \sin \frac{\pi t}{T}$$

in which T is time equal to the length of the characteristic day, i.e., sun-effective time period. Then

$$19.806 = \int_{t_1}^{t_2} I(t).dt = \int_{0}^{14.401} I_o \sin \frac{\pi t}{14.401}.dt$$

$$= -I_o \cdot \frac{14.401}{\pi}(-1-1) = I_o \frac{28.802}{\pi}$$

$$I_o = 2.16035 \text{ MJ/m}^2.\text{hr}$$

Hence the variation of diffuse solar radiation is expressed by

$$I(t) = 2.16035 \sin \frac{\pi t}{14.401} \tag{4.2}$$

Klain suggests that [13] 198th day of the year is the characteristic day for July. For Cihanbeyli ($L = 38.67^\circ$) length of the 198th day is 14.409 hours which well confirms our experimental value of SETP, 14.401 hours.

Determination of the characteristic day above permits us also to calculate $\Theta^{(x)}_{smin}$ (i.e., $(\Theta_s)_{noon}$) and thus to determine the maximum value of a_r. Since the functions $a_r(t)$ and (I) are symmetric about constant Θ_{smin} lines we can utilize half of the curves throughout the calculations.

4.2.2 Combined Area-Radiation Factor:

Daily time-variations of concentrator effective per-unit area and solar radiation are determined and given by the equations (3.45) and (4.2) respectively. But since power is an instantaneous property, in order to determine main dimensions and final properties of the plant we should use some instantaneous values of these functions, namely $\bar{a}_r$ and $\bar{I}$, in Eq.(4.1). We can utilize several approaches to assign such values for them. The attention, however, shold be paid to the question; how realistic is the approach from point of view of availability of the assigned power most of the time and daily total energy? Three such approaches are introduced and briefly discussed below.

a) We can use maximum $\bar{a}_r$ and $\bar{I}$ values whuch are attained at solar noon of the characteristic day. Pay attention that when we speak about maximum $\bar{I}$ we mean the maximum value obtained from Eq.(4.2) which is 2.16035 MJ/m^2.hr. Since we used experimental values in determination of this equation it is possible to exceed this value. But of course power is below the

assigned value most of the time. For this reason this approach is not a reliable one.

b) Design may base on daily avarage values of the functions $a_r(t)$ and $I(t)$. We can calculate avarage values seperately in the given time interval, between solar noon and sunset, or in the corresponding angular interval, $\theta_{smin} < \theta_s < 90$ and insert these values into Eq(4.1.) For 198th day of the year $\theta_{smin} = 17.5°$ ($7\pi/72$ radians.) This explanation may be illustrated by the following integral calculations:

$$\overline{(a_r)}_{avg.} = \frac{1}{\Delta\theta_s}\left[\int_{\theta_s=\frac{7\pi}{72}}^{\theta_{tm}} a_r^{(a)} \cdot d\theta_s + \int_{\theta_{tm}}^{\theta_{tM}} a_r^{(b)} \cdot d\theta_s + \int_{\theta_{tM}}^{\frac{\pi}{2}} a_r^{(c)} \cdot d\theta_s\right]$$

$$(4.3)$$

in which, obviously, $\Delta\theta_s = (\pi/2 - 7\pi/72) = t_4 - t_1$ and,

$$\overline{(I_{avg.})} = \frac{1}{\Delta t}\int_{t=t_1}^{t_4} 2.16035 \sin\frac{\pi t}{14.401}$$

$$\overline{(I_{avg.})} = 1.3753 \text{ MJ/m}^2.\text{hr.} = 382.027 \text{ W/m}^2 \qquad (4.4)$$

This approach is much more reliable than the first one since it avoids the disadvantages stated for the first approach. Most of the time power output is above the value calculated by this approach. Therefore energy output calculated by using the assigned power output is always available.
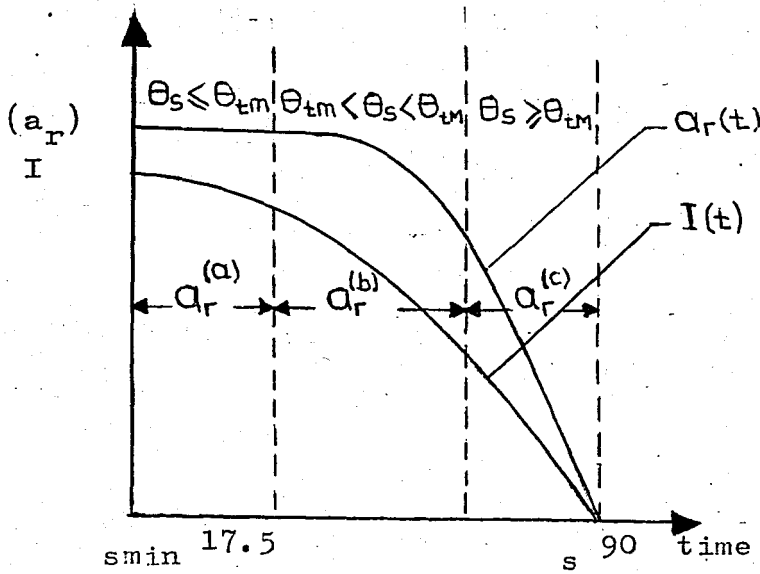
Fig.4.4 Illustration of the numerical approach to the problem of effective concentrator area and solar radiation values.

c) As a third approach we can multiply the two functions $a_r(t)$ and $I(t)$ in the given interval and then calculate time avarage of the product. Since effective concentrator area and solar radiation cannot be isolated from each other at any instant of the day, this approach is preferred rather than the second one. The product $a_r(t).I(t)$ is named as "combined area-radiation factor" and its time avarage is calculated by the following integral due to the piecewise continious function given by Eq.(3.45) and Fig.4.4:

$$\overline{(a_r.I)}_{avg.} = \frac{1}{\Delta t} \int_{t=t_1}^{t_4} a_r(t).I(t).dt = \frac{1}{\Delta t}\left[\int_{t=t_1\left(\frac{7}{72}\right)}^{t_2(\theta_{tm})} a_r^a(t).I(t).dt\right.$$

$$+ \int_{t_2}^{t_3(\theta_{tM})} a_r^b(t).I(t).dt + \left.\int_{t_3}^{t_4\left(\frac{\pi}{2}\right)} a_r^c(t).I(t).dt\right]$$

$$(4.5)$$

The number given by Eq.(4.4) is the daily total radiation value incident to a surface perpendicular to sun rays for July which is the month with maximum avarage radiation for Cihanbeyli.

The last two approaches differs from each other due to the following inequality

$$\overline{(a_r)_{avg.}} \cdot \overline{(I_{avg.})} < \overline{(a_r \cdot I)_{avg.}}$$

in which a_r and I are time dependent functions as known well.

We utilized these two approaches got results which well confirms the ideas expressed in previous paragraphs. Only 9-16 % differences are observed in the values in favour of the last approach.

4.2.3 Determination of Field Properties:

The analyses made so far may be summarized by the following results and assumptions:

a) The design point is defined by a power level $P = 150$ kw (solar) to be achieved as a mean value of the combined area-radiation function on 198th day of the year for a site (Cihanbeyli) located at $L = 38.67°$.

b) A derating factor of $k_d = .72$ is assumed to account for loss of mirror area coverage (or resultant steering-shadow factor) of $k = .85$ and for a mirror reflectivity of $k_r = .85$.

c) In connection with the explanation in Section 4.1.1 $\theta_{tM} = 75°$ is considered to be a reasonable assumption and also let θ_{tm} be equal to $15°$ (Section 4.2.4 is illustrative for the selection of θ_{tm} greater than $0°$.)

d) The value of solar insolation is taken as $I_{avg.} = 382.0$ when required.

Nothing thet $\bar{A}_r = \Pi H^2 \cdot \bar{a}_r$, by Eq. (4.1) and Table 5.2 the tower height is found to be equal to

$$H = \left[\frac{P}{k_d \Pi \cdot (a_r \cdot I)_{avg.}} \right]^{1/2} = \left[\frac{150 \times 10^3}{.72 . \Pi . 2038.8} \right]^{1/2} = 5.70m$$

H is calculated by utilizing second and third approaches for many combinations of rim angles and results are given in Table 4.2. Once we know the tower height, we can easily calculate required ground and total effective concentrator mirror areas.

Ground area:

$$A_i = \Pi H^2 (\tan^2 \theta_{tM} - \tan^2 \theta_{tm})$$

$$= \Pi (5.70)^2 (\tan^2 75 - \tan^2 15)$$

$$= 1414.3 \ m^2$$

$$A_i = 1415 \ m^2.$$

Total effective concentrator mirror area:

$$\bar{A}_r = \Pi H^2 \cdot \bar{a}_r . 0.85$$

in which .85 is reflectivity factor, k_r. But, since we have utilized third approach in calculations above, there has been no isolated value to substitute for $\bar{a}_r$. Therefore, it would be the best approach to use instantaneous values for $\bar{a}_r$ and $\bar{I}$ which would result in a product of 2038.8 at that instant when required. For the given rim angles, these values are approximately 5.37 and 379.7 W/m^2 respectively. Thus,

(x)

θ_{tM} \ θ_{tm}	0° (W/m2) – (m)	10° (W/m2) – (m)	15° (W/m2) – (m)	20° (W/m2) – (m)	25° (W/m2) – (m)	30° (W/m2) – (m)
65°	942.7 – 8.4 796.3 – 9.2	933.9 – 8.5 789.3 – 9.2	922.5 – 8.5 780.0 – 9.3	905.4 – 8.6 766.3 – 9.3	881.6 – 8.7 747.0 – 9.5	849.7 – 8.9 721.4 – 8.6
70°	1355.1 – 7.0 1162.7 – 7.6	1346.3 – 7.1 1155.6 – 7.6	1334.9 – 7.1 1146.4 – 7.6	1317.8 – 7.1 1132.7 – 7.7	1294.0 – 7.2 1113.5 – 7.8	1262.1 – 7.3 1087.7 – 7.8
75°	2059.1 – 5.7 1802.1 – 6.1	2050.3 – 5.7 1795.0 – 6.1	2038.8 – 5.7 1785.8 – 6.1	2021.8 – 5.8 1772.0 – 6.2	1998.0 – 5.8 1752.9 – 6.2	1966.1 – 5.8 1727.1 – 6.2
80°	3492.3 – 4.4 3136.9 – 4.6	3483.6 – 4.4 3129.9 – 4.6	3472.1 – 4.4 3120.6 – 4.6	3455.1 – 4.4 3106.9 – 4.6	3431.3 – 4.4 3087.8 – 4.6	3399.4 – 4.5 3062.0 – 4.7

Table 4.2. Calculated values of $(a_r \cdot I)_{avg.}$, and those of products of $(a_r)_{avg.}$ and $(I)_{avg.}$ together with the corresponding tower heights.

(x) Values in first rows correspond to $(a_r \cdot I)_{avg.}$.

$$\overline{A}_r = (5.70)^2 (5.37)(.85)$$

$$= 465.90 \ m^2$$

$$\overline{A}_r \simeq 466 \ m^2.$$

By definition efficiency

$$\eta = \overline{A}_r / A_i = 465.9/1414.3$$

$$\simeq .329$$

$$\eta \simeq .33.$$

The results obtained above can easily be checked. That is,

$$P \simeq .85 \cdot 466m^2 \cdot 379.7W/m^2 \simeq 150.4 \ kw$$

In this case .85 stands for resultant steering-shadow factor k and the error of .4 kw should be attributed to the assumption made for isolated values of $\overline{a}_r$ and $\overline{I}$.

4.2.4 Mirror and Receiver Sizes:

Determination of mirror and receiver dimensions is of special importance. Although we have determined the required mirror area it is still questionable whether we are going to use 466 mirrors of $1m^2$ or 932 mirrors of $0.5m^2$ or what so ever, since because limits for receiver dimensions are put by mirror dimensions. That is for a full utilization of effective concentrator mirror area, any reflected ray must not miss the receiver. This makes an analysis of mirror and receiver dimensions primarily important.

Fig. 4.5 illustrates the physics of the problem schematically. In the side view we see the height of an imaginative plane which is completely targeted by one of the heliostats closest to the tower. By simple geometry, imaginary height W_i is
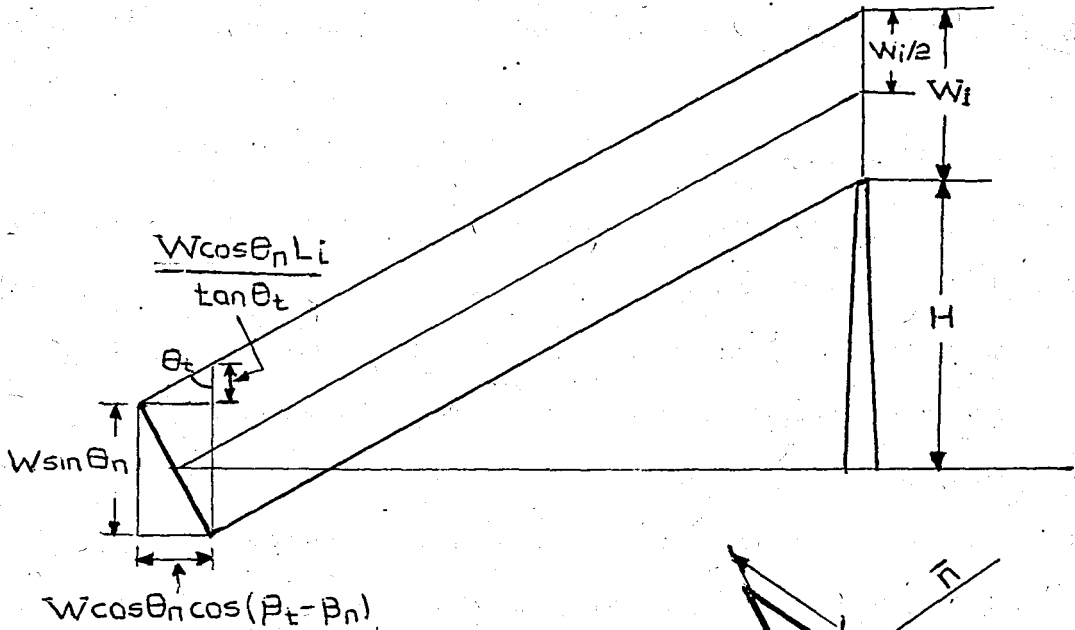
Fig. 4.5 Reflected mirror dimensions at receiver.
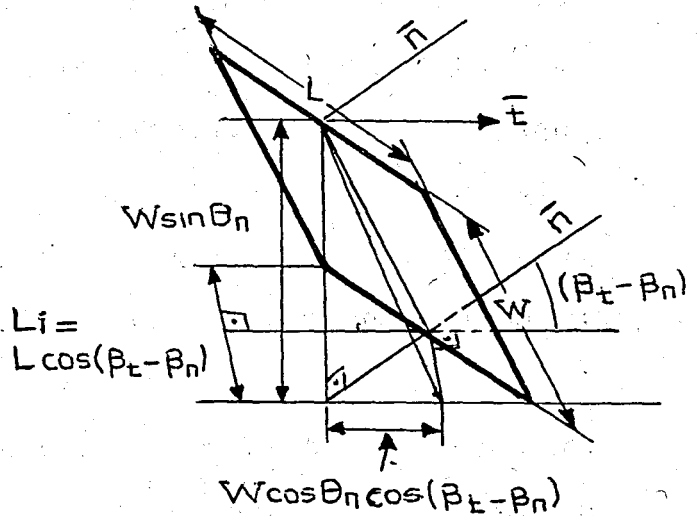
calculated as

$$W_i = W(\sin\theta_n + \frac{\cos\theta_n \cos(\beta_t - \beta_n)}{\tan\theta_t})$$ (4.6)

From plan view, on the other hand, the horizontal side of the imaginary plane is expressed by

$$L_i = L\cos(\beta_t - \beta_n)$$ (4.7)

As easily seen from Eq. (4.6) imaginary height W_i is very sensitive to the variations in radial distance, i.e., in θ_t for

small values of it.Therefore it is reasonable to use Θ_{tm} values

greater than zero.That is why we have chosen $\Theta_{tm} = 15^{\circ}$ in Sec-

tion 4.2.3.

It is clear from Eq.(4.7) that $(L_i)_{max} = L$. For $\Theta_{tm} = 15^{\circ}$

however,theoretical upper limit for W_i,i.e.,$(W_i)_{max}$ is 3.862W

which is the value for a mirror located at an azimuthal loca-

tion $\beta_t = 0^{\circ}$ at solar noon of June 22 $(\Theta_n = 15.0^{\circ})$.This mean for

rectangular mirrors with sides L and W of unity we need a cyl-

indirical (for example) receiver of length 3.9m and radius 0.5m.

But it is unreasonable to use such a big receiver with a tower

of length about 6m.Therefore we have to use heliostats of

smaller size and/or a receiver of different shape. Design

technique of receiver is itself a special topic to be studied.

This is not aimed.However we could say that it is reasonable

to have receiver length (height) l_R below 1m. in comparison with

a tower of 6m high.

Let the mirrors be 0.8 m square
ones.If we like the receiver to be a
straight half cone-shaped one,then
from the positions of the closest and
farest mirrors,it has to have a length
of $l_R = .67$m in order to catch all the
reflected rays.This is a reasonably
good size for the receiver.Referring
to intersection points of extreme rays the
surface inclination angle is calcula-
ted to be $M = 45^{\circ}$. Fig.4.6 depicts the
situation for such a pair of rays.

Fig 4.6 Receiver size
and shape requirements
for 1m x 1m square
mirrors.

Thus the assigned values of $\Theta_{tm} = 15°$ and $\Theta_{tM} = 75°$ would give reasonable results for mirror and receiver dimensions.

Although the calculated mirror and receiver dimensions are said to be reasonable, this reasonableness is concluded referring to relative dimensions of the system elements only. For a more realistic comparison or design criteria of dimensions all technical and economical details should be included. As a matter of fact, what we aimed by this analysis is to indicate the strict and important relation between mirror and receiver dimensions. Once we know the technical and economical restrictions we should be able to make most favorable changes in the analysis at this point.

4.3 Results:

The overall results may be listed as follows:

Power level $P = 150$ kw

Tower height $H = 5.7$ m

Required ground area $A_i = 1415$ m^2 $(R_M = 21.27$ m

$R_m = 1.53$ m$)$

Total effectve concentrator

mirror area $\overline{A}_r = 466$ m^2

Efficiency $\eta = .33$

Receiver main dimensions $l_R = .67$ m

$r_R = .40$ m

Number of .64 m^2 (.8x.8)

mirrors   728

Receiver surface

inclinetion angle $M = 45°$

DISCUSSION

A fundamental theory of solar concentrators for central receiver power plants has been formulated in terms of ideal heliostat arrays. The principal results deduced during various steps of the analysis of ideal solar concentrators can be outlined as follows:

1- Postulating an ideal heliostat field model: A continuum field model of ideal haliostat arrays is postulated. The idea under this postulate is that a continious circular field of reflection formed by closed-packed heliostat arrays of certain width between . given limits of rim angles constitute the system, such that the performance analysis of the system may base on relative positions of these arrays. Some advantages and consequences of this postulate are explained below.

a) Since some analytic expressions of the shadow analysis (such as the one for Y) are complex, it is very difficult to use a numerical approach for an actual system composed of thousadns of mirrors and for so many possibilities of mirror distribution. However the analytic results derived from this ideal model are inherently simple and, more importantly, provide the physical basis underlying the central receiver concept of solar power concentration.

b) Performance of ideal heliostat arrays field depends on only two factors; the sun zenith angle Θ_s (i.e., the time of day) and the size of concentrator (limited by Θ_{tM} and Θ_{tm}). Since heliostat arrays are of closed-packed form, azimuthal orientation is not effective on performance.

c) Solar flux density at a given time is uniformly distri-
buted around the receiver. This is a direct conclusion from the
expression of resultant steering-shadow factor k, namely

$$k = \begin{cases} \cos\theta_s & \text{for } \theta_t < \theta_s \\ \cos\theta_t & \text{for } \theta_t < \theta_s \end{cases}$$

(This would not be the case had shadowing effects being ignored).

The differences between an ideal system and a realistic
system have been indicated already. We have also stated the neces-
sity of expecting azimuthal variation of field performance in
the case of shadowing effects being considered. But our analysis
doesn't permit us to show such a variation graphically.

Although we didn't try to estimate the feature of azimuthal
variation of field performance, by a crude assumption of it we
are able to make a graphical proof of the last conclusion above.
That is, we can prove that as a realistic system is idealized,
plots of field performance tend to be circles (i.e., independent
of azimuthal orientation).

Now assume that such an azimuthal variation can be charac-
terized by a certain proportion of shaded heliostat area (which
we are not sure that it can be). Then this variation can graphi-
cally be shown. But since the ideal analysis considers azimuthal
independence, as the assumed proportion closes to zero plots
should tend to be circles. This idea is well confirmed by exam-
ining two different cases; for one percent and for ten percent
of shaded area. The situation is illustrated in Fig. D.1. In the
first case plots of iso-energy lines (of the same performance)
tend to be circles for smaller values.
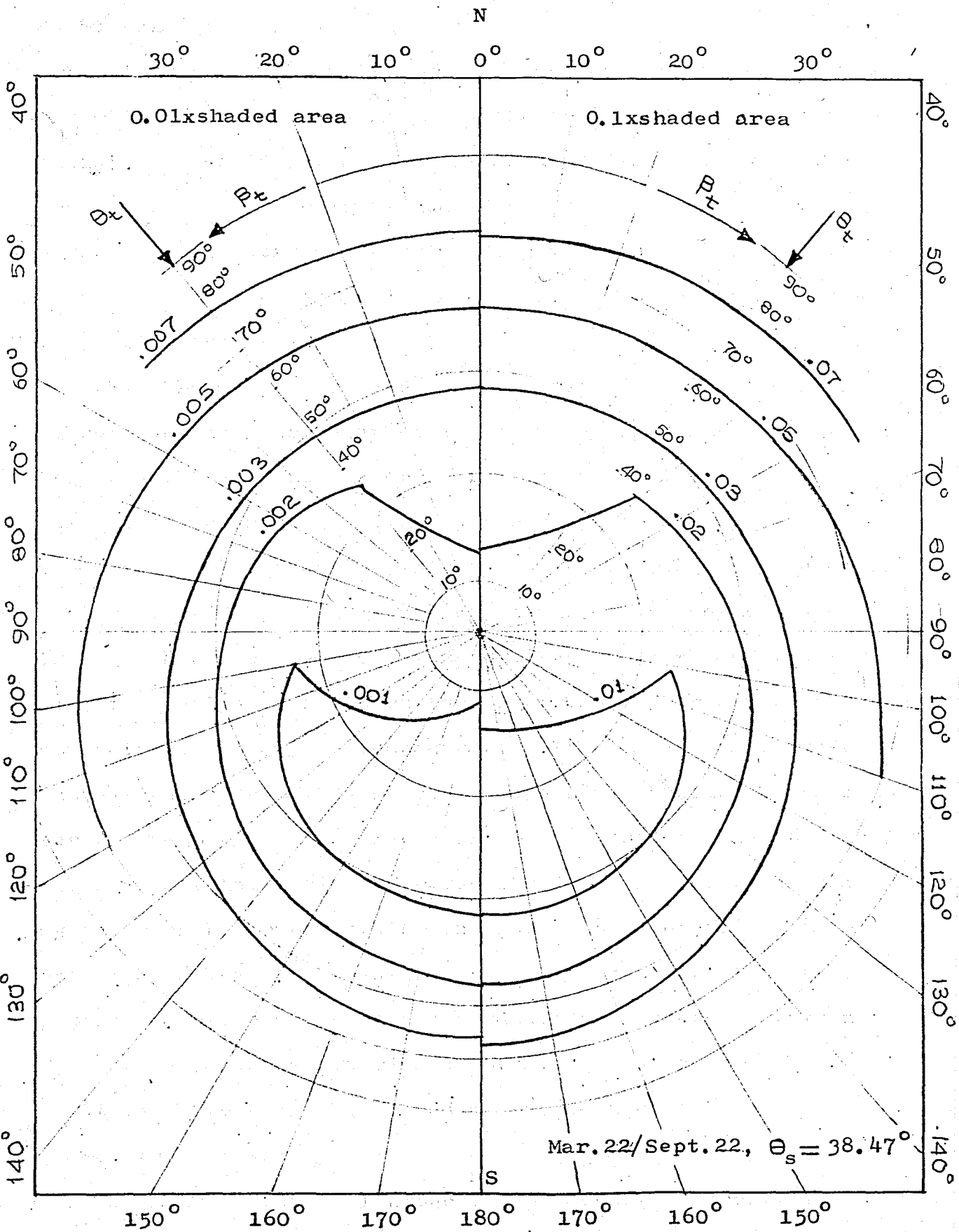
Fig.D.1 Iso-energy profiles of mirror
field distribution at solar noon. L=38.67°.

2- Steering Relations:

a) A steering analysis has yielded the space-time charac-
teristics of heliostat arrays in the form of field mappings
exhibiting iso-tilt lines and iso-azimuth lines and of time
profiles of mirror orientations.The notion of NODE for the
mirror field distribution coinciding with the sun's hourly
path is extremely useful in describing the properties of he-
liostat arrays.

b) A shadow analysis has been performed for rctangular
mirrors showing the relationship between sun shading and tower
screening.Two key parameters defining the utilization factors,
$\cos_s$ for sun shading and $\cos_t$ for tower screening express
the local effectiveness of mirrors in reflecting solar energy.

c) The ideal global characteristics of circular concen-
trators have been derived from the preceeding shadow and
steering analyses as closed-form expressions for effective
concentrator areas and concentrator efficiencies.From these
expressions dimensionless curves have been obtained to charac-
terize the behaviour of large-area concentrators and to estab-
lish theoretical limits of performance against which actual
systems can be compared.With the ideal model providing a best
performance level,the base design of solar power.plant can
proceed with the introduction of derating factors accounting
for such effects as steering errors,mirror size and reflec-
tivity,area coverage,solar radiation,cloud cover exc...

3- Design Factors:

a) Mean of integral product of effective concentrator
per-unit area function $a_r(t)$ and solar radiation function $I(t)$

is referred to as the resultant solar utilization factor upon which power level of the plant is based.In determination of solar irradiance constant the month with maximum experimentally determined irradiance is taken into account.A sine curve is fitted to avarage of these yearly values to obtain the daily variation of solar radiation.However such a curve defines a completely different characteristic cloudless day rather than a day with a certain amount of cloud uniformly distrubuted during the day.

b) Its contradictory effects on area requirement make an efficiency improvement almost impossible.Therefore area improvement is of major preference and this have been discussed in a certain limit.Appreciable increaments in area,on the other hand,take us away from applicability of the theory.

c) Receiver dimensions and shape are arising as important design considerations for the reason that it must receive all reflected rays with a minimum incidence loss.

REFERENCES

1 - Hildebrandt,A.F. and Vant-Hull,L.L., "Science,Power with
    Heliostats";Reprint Series,16 September 1977.Volume 198,
    pp. 1139-1146.

2 - Sayigh,A.A.M.,"Solar Energy Engineering"; Academic Press,
    New York, San Francisco, London,1977, pp. 5-47.

3 - Threlkeld,J.L., "Thermal Environmental Engineering"; Sec-
    ond Edition, Prentice-Hall Inc., Englewood Cliffs, New
    Jersey, pp. 279-303.

4 - Deriş,N.,"Sıcak Su İle Isıtma Tekniği"; Sermet Matbaası,
    İstanbul,1979, pp. 12-45,

5 - Riaz,M., "A Theory of Concentrators of Solar Energy on a
    Central Receiver for Electric Power Generation"; ASME
    paper,Pap. n75-WA/SOL.1, For meeting, Nov.30-Dec.5,1975
    pp. 1-10.

6 - Curtner,K.L., Fourakis,E.M. and Mitchell,P.D., "Conceptual
    Heliostat Field Design for the ERDA 5MW Solar Thermal
    Test Facility at Sandia,Albuquerque"; Honeywell,Energy
    Resources Center, 2600 Ridgway Parkway,Minneapolis,MN
    55413, April 26-27,1976, pp.636-640.

7 - Knasel,T.M.,Liner,R.T.,Simons,J. and Higgins,R., "The
    Tower Reflector as an Alternate to the Tower Boiler Con-
    cept for a Central Receiver Solar Thermal Electric Con-
    version Plant"; SPIE Semin.Proc.,V.68,1975; Opt.in Solar
    Energy Util.,for meeting, San Diego, Calif.,Aug.1975,
    pp. 85-96.

8 - Jarvinen,P.O., "Solar-Heated Air Turbine Generating Sys-
   tems"; prep. for 10th Intersociety Energy Conversion and
   Engineering Conference of Delaware,Newark,Delaware,Aug.
   17-22,1975.

9 - Jarvinen,P.O., "Windowed Versus Windowless Solar Energy
   Cavity Receivers"; prep. for 11th Intersociety Energy
   Conversion and Engineering Conference,Lake Tahoe,Nevada,
   Sept. 12-17,1976.

10- Kılıç,A. and Öztürk,A., "Solar Maps Related With the Me-
   teorological Data for Turkey"; İ.T.Ü. Maçka Makina Fakül-
   tesi,İstanbul,Turkey.

11- Blanco,V.M. and McCuskey,S.W., "Basic Physics of the Solar
   System"; Addison-Wesley Puplishing Company, Inc. Reading,
   Massachusetts,U.S.A.,London,England.

12- Öztürk,A. and Kılıç,A., "Türkiye için Güneş Işınımı Dağı-
   lımı"; İ.T.Ü.,İstanbul,Turkey.

13- Klein,S.A., "Calculation of Monthly Avarage Insolation on
   Tilted Surfaces"; Sharing the Sun, Joint Conf.,ISES and
   SESC,1976, v.1, pp. 376-389.

14- Duffie,J.A., and Beckman,W.A., "Solar Energy Thermal Pro-
   cesses"; J.Wiley and Sons,New York,1974

APPENDIX
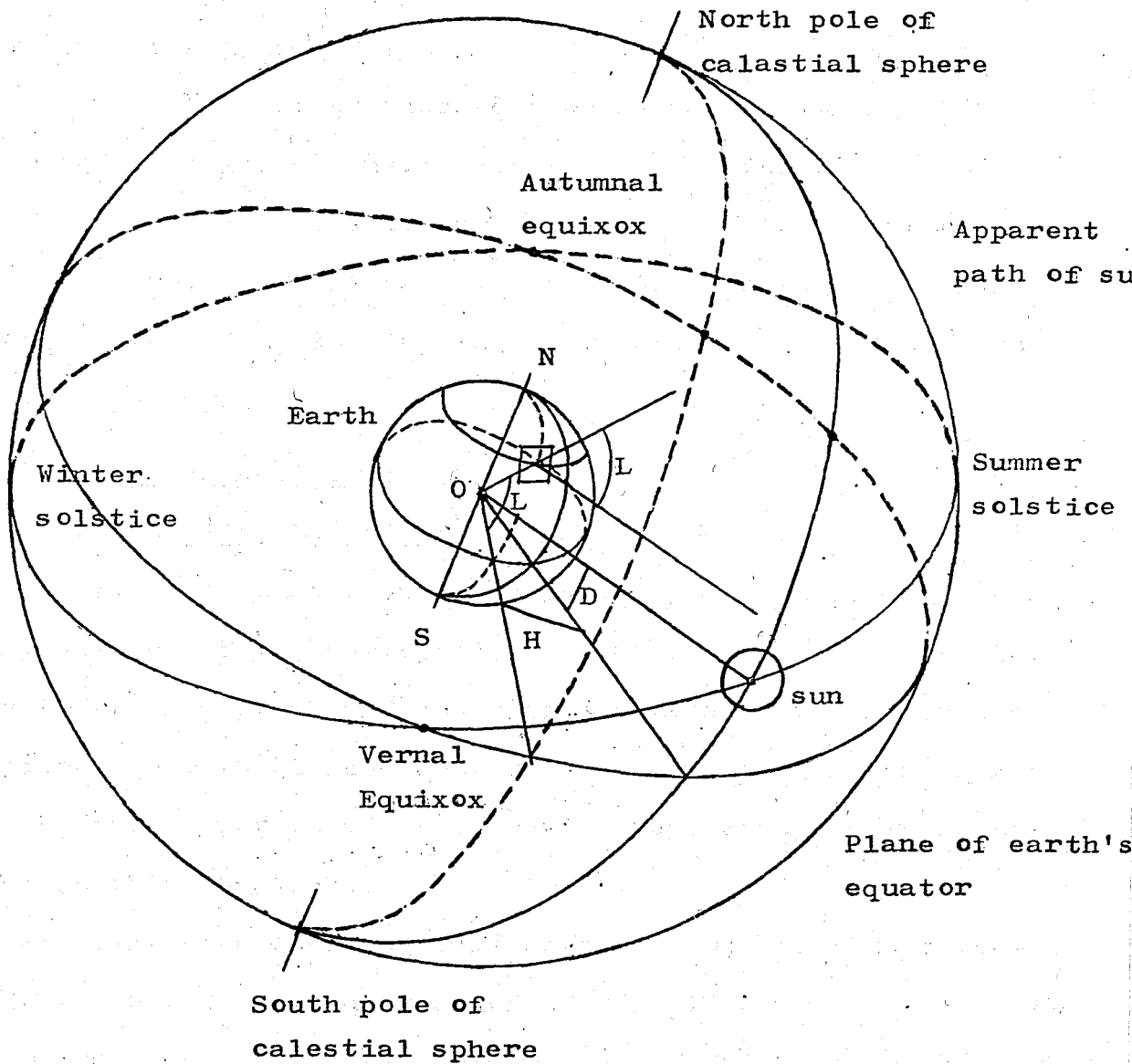
Fig.A.1 Schematic calestial sphere showing apparent path
of sun and sun's declination angle.

Fig.A.1. on the previous page, shows a very general view of the solar system. As a difference from the realistic system however, in this figure the sun's and earth's positions are interchanged, since it provides easeness in visualizing the system and in calculations. It should be easy for the reader to define ecliptic, calestial equator and the four solstices from the figure. We will deal with only the derived and defined sun angles here. Some special angles related to tilted surfaces are studied also.

A.1 Basic Solar Angles:

A.1.1 Defined Earth-Sun Angles:

The position of a point P on the earth's surface is known at any instant of the day, specified by the hour angle H, if the latitude L for this point and sun's declination D at that instant are given. These three fundamental angles are also shown in Fig. A.1. We should note that point P will represent any location on the Northern Hemisphere.

At solar noon the hour angle is zero. One hour of time corresponds to 360/24 or 15 degrees of hour angle.

For Cihanbeyli, the site under consideration, L= 38.67°.

In our calculations we willnot use instantaneous values of declination; instead we will use representative daily values which are calculated by the following equation as usual:

$$D = 23.45 \sin\left(360 \ \frac{284 + N}{365}\right)$$

by which declination angle for N^{th} day of the year is to be calculated.

A.1.2 Derived Earth Sun Angles:

Besides the three basic solar properties (angles);hour angle,latitude and sun's declination,several (other) angles are useful in solar energy calculations.Such angles include the sun's zenith angle Θ_s,altitude angle α and azimuth angle β_s.Fig.A.2 schematically shows an apparent solar path and depicts the positions of these angles which are not independent angles and expressed in terms of the three fundamental angles.Furthermore the sun's zenith angle Θ_s and altitude angle α are not independent of each other,that is $\alpha - \Theta_s = 90°$.
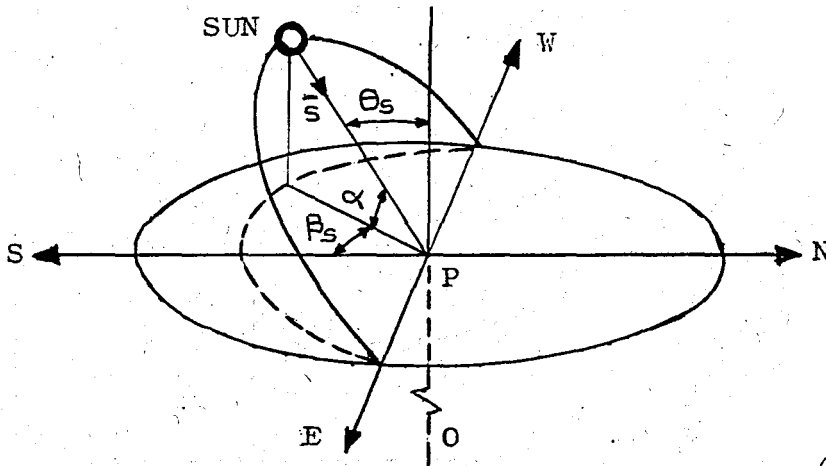
Fig.A.2 Definitions of sun's zenith,altitude
and azimuth angles.

Fig.A.3. shows a coordinate system with the z axis coincident with the earth's axis of rotation.The xy plane coincides with the earth's equatorial plane.The line $\overline{PN}$,pointing North from point P,is perpendicular to $\overline{OP}$ and lies in the plane containing the line $\overline{OP}$ and z axis.

In Fig.A.3. let a_1,b_1 and c_1 be the direction cosines of $\overline{OP}$ and a_2,b_2 and c_2 be those of the unit sun vector $\overline{s}$. with

respect to x,y and z axes.Thus,

$$a_1 = \cos L \cos H \qquad\qquad a_2 = \cos D$$

$$b_1 = \cos L \sin H \qquad\qquad b_2 = 0$$

$$c_1 = \sin L \qquad\qquad\qquad c_2 = \sin D$$

Since the sun's zenith angle Θ_s is the angle between $\overline{OP}$ and $\overline{s}$, by a common equation from analytic geometry we have

$$\cos\Theta_s = a_1 a_2 + b_1 b_2 + c_1 c_2$$

Thus

$$\cos\Theta_s = \cos L \cos H \cos D + \sin L \sin D \qquad\qquad (A.1.1)$$
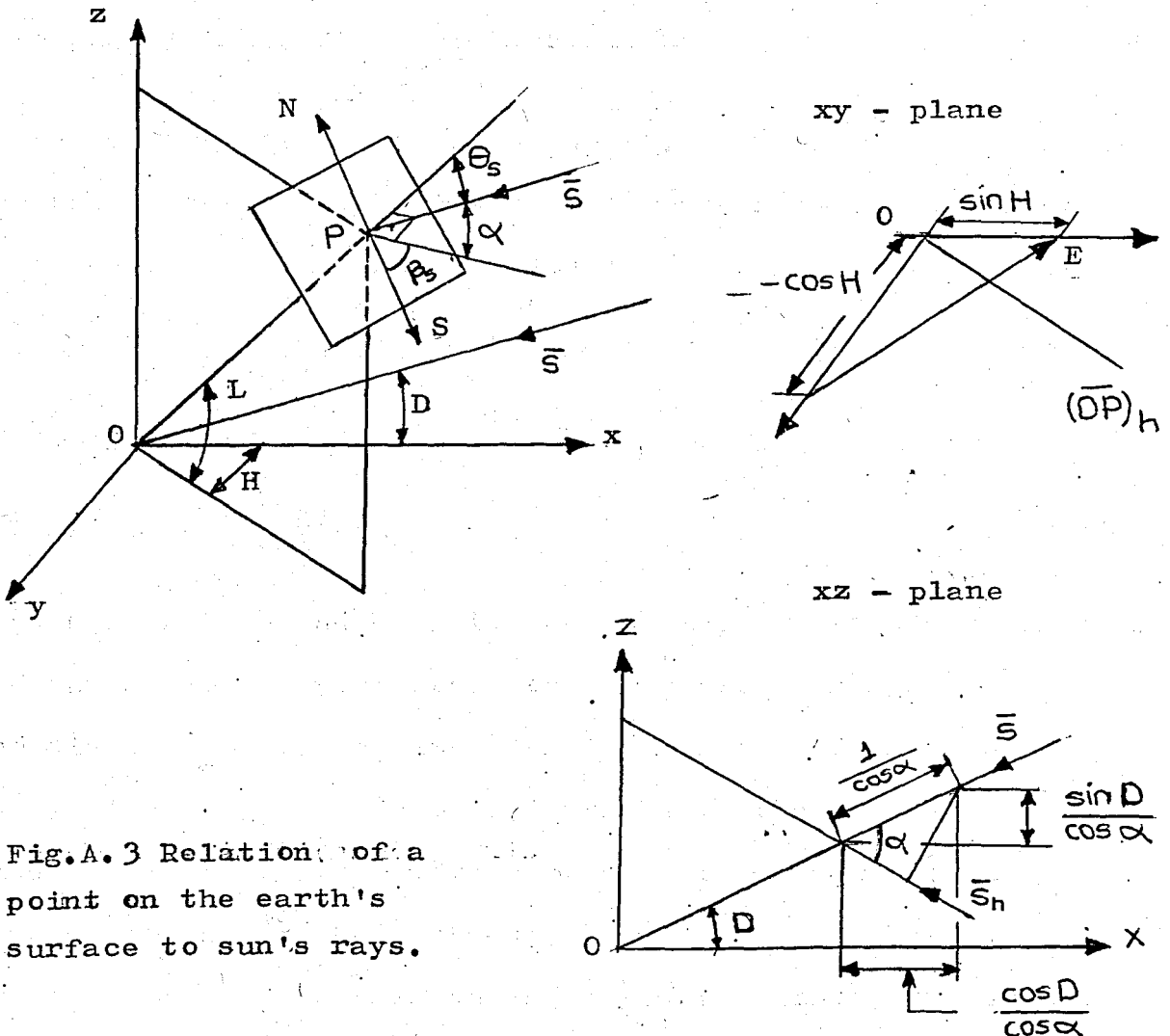
Fig.A.3 Relation of a point on the earth's surface to sun's rays.

Since $\alpha = 90° - \theta_s$, we may write

$$\sin\alpha = \cos L \cos H \cos D + \sin L \sin D \qquad (A.1.2)$$

Similarly direction cosines of a vector directed to south and those of the horizontal component of the unit vector $\bar{s}$, namely $\bar{s}_h$, are.

$$a_3 = \sin L \cos H \qquad a_4 = -\cos D / \cos\alpha$$
$$b_3 = \sin L \sin H \qquad b_4 = 0$$
$$c_3 = -\cos L \qquad c_4 = -\sin D / \cos\alpha$$

respectively. It follows that

$$\cos\beta_s = \frac{\cos L \sin D - \cos H \cos D \sin L}{\cos\alpha} \qquad (A.1.3)$$

By the squares of Eqs. (A.1.2) and (A.1.3), and with the trigonometric identity $\cos^2 x + \sin^2 x = 1$ (here x is a general notation) we may obtain the relation

$$\sin\beta_s = \frac{\cos D \sin H}{\cos\alpha} \qquad (A.1.4a)$$

or equivalently

$$\sin\beta_s = \frac{\cos D \sin H}{\cos\theta_s} \qquad (A.1.4b)$$

Eqs. (A.1.3) and (A.1.4) make us capable of demonstrating the sun's time-varying position graphically in a quasi-polar coordinate system. The situation is illustrated in Figs.A.4. and A.5. for 22th days of all months of the year at a latitude $38.67°$ North. The plots are completely symmetric with respect to the North-South axis. The length of any curve gives the length of the corresponding day. For example, for June 22th sunset occurs 7 hours 21 minutes 15:09 seconds after noon. Thus

Fig.A.4 Polar plots of sun's hourly position for Çihanbeyli, L = 38.
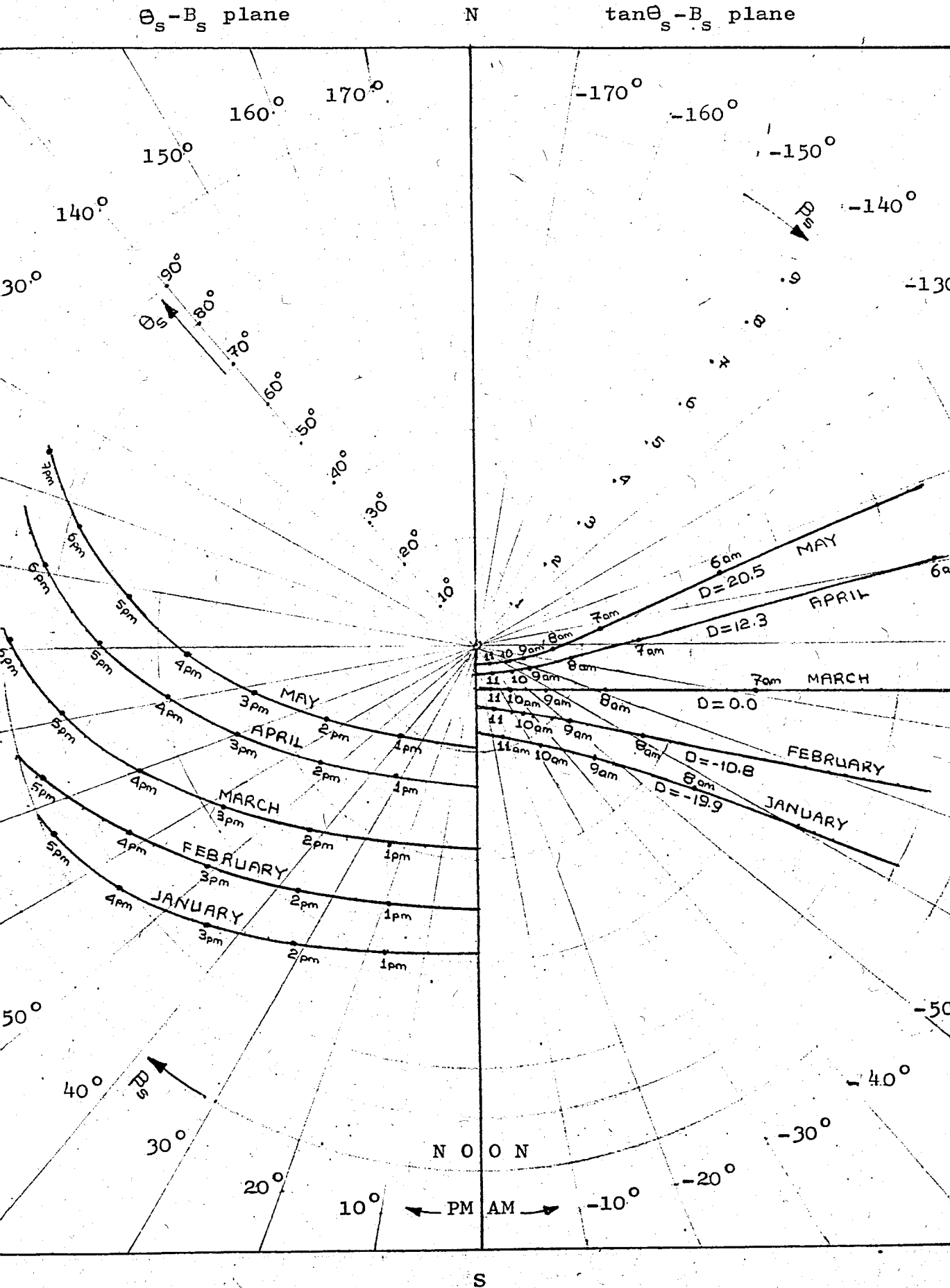
Fig.A.5 Polar plots of sun's hourly position for Cihanbeyli,L= 38.67
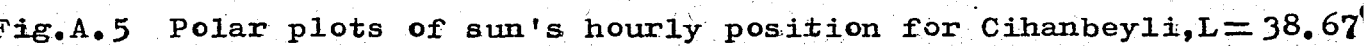
the length of the day is 2(07hr. 21min. 15.09s.) or 14hr. 42min. 30.18s..

The explanations up to this point may be interpreted in the following results:

a) At equator $L = 0^{\circ}$.

b) At the two equinoxes $D = 0^{\circ}$.

c) At solar noon $H = 0^{\circ}$.

By the last interpretation above, and Eqs.(A.1.3) and (A.1.4)

d) At solar noon $\beta_s = 0^{\circ}$ if $L \succeq D$ and $\beta_s = 180^{\circ}$ if $L \preceq D$. β_s is undefined if $L = D$.

e) At sunrise and sunset $\theta_s = 90^{\circ}$.

f) $\alpha_{noon} = 90^{\circ} - |L-D|$.

The interpretation 'd' is worth to be illuminated a little more.

Fig.A.6. below is a special form of Fig.A.3. in which the hour angle $H = 0^{\circ}$. In this case all the existing solar angles can be shown in xz plane.

Fig.A.6 Schematic illustration of solar angles at solar noon.
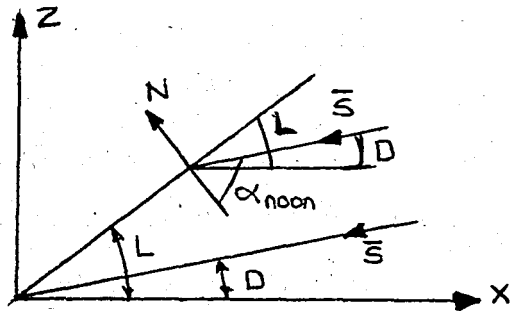
For $H = 0^{\circ}$, $\sin\beta_s = 0$ by Eq.(A.1.4). Thus $\beta_s = 0^{\circ}$ or 180°. The value of β_s can be decided by the sign of $\cos\beta_s$. From Eq. (A.1.3), then,

$$\cos\beta_s = \frac{\sin(D-L)}{\cos\alpha}$$

Since α takes values between $0°$ and $90°$, $\cos\alpha$ is always posi-
tive.Therefore when $L < D$, $\cos\beta_s$ is positive and thus $\beta_s = 0°$.
When $L > D$, opposite situation occurs and then $\beta_s = 180°$.

Eqs.(A.1.1)-(A.1.4) permit us to calculate the sun's
zenith (or altitude) and azimuth angles if the three basic
angles,hour angle,latitude and sun's declination are given.In
applying these equations,attention must be given to correct
signs for these basic angles.For Northern Hemisphere latitude
is taken to be positive and for Southern Hemisphere negative.
The sun's declination will be positive for the summer period
between the vernal equinox and autumnal equinoxes (March 22 to
September 22 approximately) and negative at other times.The
hour angle is measured on either side of solar noon.Thus H is
limited to values between $-90°$ and $90°$;negative before noon
and positive after noon.The azimuth angle is positive when it
is measured clockwise,and negative when it is measured counter-
clockwise from South.Thus the azimuth angle is limited to
values between $-180°$ and $180°$.

A.2 Tilted Surfaces:

Fig.A.7. shows the position of a rectangular plate as a
tilted surface on a horizon.The axes X and Y are pointing
East and North respectively,and x and y are coincident with
the projection of two adjacent sides of the plate (or mirror).
It should be made clear that all four axes are in horizon.Z
and z are the same coordinate axes pointing toward local ver-
tical,i.e.,perpendicular to horizon.The xyz coordinate system
is obtained by a clockwise rotation of the XYZ coordinate

system around Z (or z) axis by an azimuthal angle δ. Fig.A.8.
illustrates the situation better.
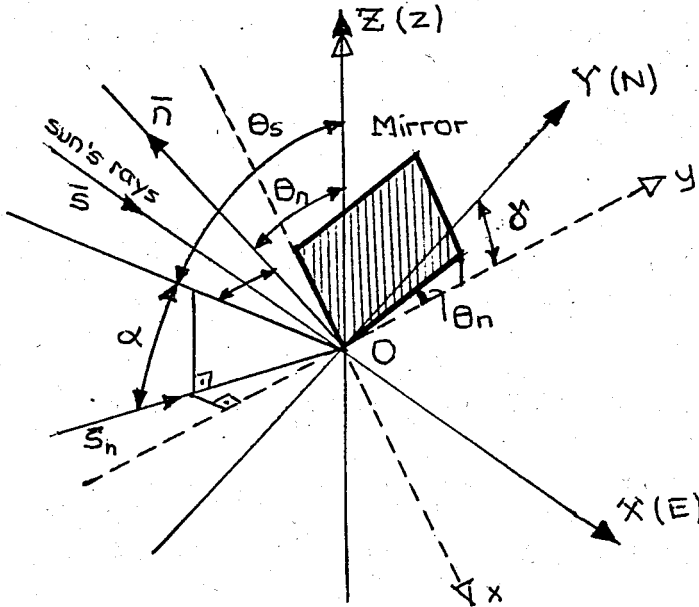
Fig.A.7 Definition of position
angles of a tilted surface.

Assume that the surface is tilted by an angle θ_n. Then from
Fig.A.7. direction cosines of the unit vectors $\bar{s}$ and $\bar{n}$ are
written as follows:
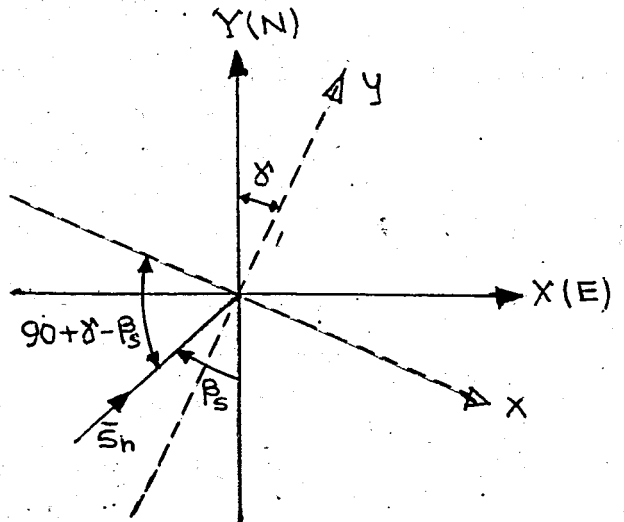
Fig.A 8 Azimuthal angles
in the horizontal plane.

$$a_s = \cos\alpha \cos(90 + \delta - \beta_s) \qquad\qquad a_n = 0$$
$$= \sin\theta_s \sin(\beta_s - \delta)$$

$$b_s = \cos\alpha \cos(\beta_s - \delta) \qquad\qquad b_n = -\cos(90-\theta_n)$$
$$= \sin\theta_s \cos(\beta_s - \delta) \qquad\qquad\qquad = -\sin\theta_n$$

$$c_s = \sin\alpha \qquad\qquad\qquad\qquad c_n = \cos\theta_n$$
$$= \cos\theta_s$$

Thus the incidence angle ϕ for tilted surfaces may be expressed by the following relation

$$\cos\phi = -\sin\theta_n \sin\theta_s \cos(\beta_s - \delta) + \cos\theta_n \cos\theta_s \qquad (A.2.1)$$

Don't worry about the sense of the sun's vector $\bar{s}$ in Fig.A.7. and be careful that the incidence angle ϕ and the tilt angle θ_n are not measured in the same plane.

Writing Eq.(A.2.1) in its open form and substituting $\cos\theta_s$, $\cos\beta_s \sin\theta_s$ ($=\cos\beta_s \cos\alpha$) and $\sin\beta_s \sin\theta_s$ from Eqs.(A.1.1) (A.1.3) and (A.1.4b) respectively, in this new form of the equation we can obtain a relation for the incidence angle ϕ which is expressed in terms of the three basic solar angles L, D and H and position angles δ and θ_n of the tilted surface. That is,

$$\cos\phi = -\sin\theta_n \sin D \cos\delta \cos L + \sin\theta_n \sin L \cos\delta \cos D \cos H$$

$$+ \sin\theta_n \sin\theta_s \sin\beta_s \sin\delta + \cos\theta_n \sin D \sin L$$

$$+ \cos\theta_n \cos D \cos L \cos H \qquad (A.2.2)$$

For a south-facing tilted surface $\delta = 0°$. Then we can write Eq.(A.2.2) as

$$\cos\phi = \cos D \cos H \cos(L-\theta_n) + \sin D \sin(L-\theta_n) \qquad (A.2.3)$$

It is obvious from Fig.A.6. that for $\theta_n = 0°$ $\phi = \theta_s$. Thus,

$$\cos\Theta_s = \cos D \cos H \cos L + \sin D \sin L$$

which is nothing than Eq. (A.1.1).

For a south-facing vertical plate $\Theta_n = 90°$. Then by Eq. (A.2.3)

$$\cos\emptyset = \cos D \cos H \sin L - \sin D \cos L \qquad (A.2.4)$$

Since flat-faced mirrors are especially south-facing for Northern Hemisphere, it is useful to express the incidence angle in terms of the derived earth-sun angles α and β_s. Writing the open form of Eq. (A.2.3) and substituting Eq. (A.1.2) and (A.1.3) in the new form we obtain

$$\cos\emptyset = \cos\Theta_n \sin\alpha - \sin\Theta_n \cos\beta_s \cos\alpha \qquad (A.2.5)$$

A.3

$$\bar{s} = \sin\Theta_s \sin\beta_s \; \bar{i} - \sin\Theta_s \cos B_s + \cos\Theta_s$$

$$\bar{s} \times \bar{k} = \begin{vmatrix} \bar{i} & \bar{j} & \bar{k} \\ \sin\Theta_s \sin\beta_s & -\sin\Theta_s \cos\beta_s & \cos\Theta_s \\ 0 & 0 & 1 \end{vmatrix}$$

$$= -\sin\Theta_s \cos\beta_s \; \bar{i} - \sin\Theta_s \sin\beta_s \; \bar{j}$$

Similarly

$$\bar{t} = -\sin\Theta_t \sin\beta_t \; \bar{i} - \sin\Theta_t \cos\beta_t \; \bar{j} + \cos\Theta_t \; \bar{k}$$

and

$$\bar{t} \times \bar{k} = -\sin\Theta_t \sin\beta_t \; \bar{i} - \sin\Theta_t \sin\beta_t \; \bar{j} \; .$$

Then,

$$|\bar{s} x \bar{k} + \bar{t} x \bar{k}| = \left[(-\sin\theta_s \cos\beta_s - \sin\theta_t \cos\beta_t)^2 \right.$$
$$\left. + (-\sin\theta_s \sin\beta_s + \sin\theta_t \sin\beta_t)^2 \right]^{1/2}$$

Performing some necessary simplifications we get

$$|\bar{s} x \bar{k} + \bar{t} x \bar{k}| = \left[\sin^2\theta_s + \sin^2\theta_t + 2\sin\theta_s \sin\theta_t \cos(\beta_t - \beta_s) \right]^{1/2}.$$

Thus,

$$\sin\theta_n = \frac{1}{|\bar{N}|} (\bar{s} x \bar{k} + \bar{t} x \bar{k})$$

$$= \frac{1}{|\bar{N}|} \left[\sin^2\theta_s + \sin^2\theta_t + 2\sin\theta_s \sin\theta_t \cos(\beta_t - \beta_s) \right]^{1/2}.$$

$$(3.6)$$

A.4

The vectors $\bar{s}$ and $\bar{t}$ are as given in A.3. Additionally

$$\bar{n} = -\sin\theta_n \sin\beta_n \ \bar{i} - \sin\theta_n \cos\beta_n \ \bar{j} + \cos\theta_n \ \bar{k}$$

It follows that in the horizontal plane

$$\bar{s}_h + \bar{t}_h = \bar{N}_h = |\bar{N}_h| \ \bar{n}_h$$

$$(-\bar{k}) \cdot (\bar{s}_h + \bar{t}_h) = |\bar{N}_h| \ \bar{n}_h \cdot (-\bar{k})$$

$$\sin\theta_s \cos\beta_s + \sin\theta_t \cos\beta_t = |\bar{N}_h| \sin\theta_n \cos\beta_n$$

$$\cos\beta_n = \frac{1}{|\bar{N}_h|} \ \frac{\sin\theta_s \cos\beta_s + \sin\theta_t \cos\beta_t}{\sin\theta_n} \qquad (A.4.1)$$

and,

$$|(-\bar{k}) x (\bar{s}_h + \bar{t}_h)| = |\bar{N}_h| \ |(-\bar{k}) x (\bar{n}_h)|$$

$$(\sin\theta_s \sin\beta_s + \sin\theta_t \sin\beta_t) \ \bar{k} = |\bar{N}_h| \sin\theta_n \sin\beta_n \ \bar{k}$$

$$\sin\beta_n = \frac{1}{|\bar{N}_h|} \frac{\sin\theta_s \sin\beta_s + \sin\theta_t \sin\beta_t}{\sin\theta_n} \qquad (A.4.2)$$

Thus,

$$\tan\beta_n = \frac{\sin\theta_s \sin\beta_s + \sin\theta_t \sin\beta_t}{\sin\theta_s \cos\beta_s + \sin\theta_t \cos\beta_t} \qquad (3.8)$$

A.5

Let the diad of unit vectors $\bar{i}_1$ and $\bar{j}_1$ define the components of a coordinate system whose axes x and y are along the horizontal projection of the mirrors normal, and those of $\bar{i}_2$ and $\bar{j}_2$ define the components of the East-South coordinate system, x' y', which is obtained by a counterclockwise rotation of the first by an angle B_n. These two coordinate systems are shown in Fig.3.4. seperately. Then,

$$\bar{i}_2 = T_{11}\bar{i}_1 + T_{21}\bar{j}_1 = \sin\beta_n \ \bar{i}_1 + \cos\beta_n \ \bar{j}_1$$

$$\bar{j}_2 = T_{12}\bar{i}_1 + T_{22}\bar{j}_1 = -\cos\beta_n \ \bar{i}_1 + \sin\beta_n \ \bar{j}_1,$$

from which the transformation tensor $\underline{\underline{T}}$ is obtained as

$$[\underline{\underline{T}}] = \begin{bmatrix} \sin\beta_n & -\cos\beta_n \\ \cos\beta_n & \sin\beta_n \end{bmatrix} \qquad (A.5.1)$$

Thus, the vector components of one longitudinal side of the sun shade in the new coordinate system, namely X'_{ms} and Y'_{ms}, may be obtained from the following matrix equation

$$\begin{bmatrix} X'_{ms} \\ Y'_{ms} \end{bmatrix} = \begin{bmatrix} \sin\beta_n & -\cos\beta_n \\ \cos\beta_n & \sin\beta_n \end{bmatrix} \begin{bmatrix} X_{ms} \\ Y_{ms} \end{bmatrix}$$

as

$$X'_{ms} = \sin\beta_n \ X_{ms} - \cos\beta_n \ Y_{ms}$$

(A.5.2)

$$Y'_{ms} = \cos\beta_n \ X_{ms} + \sin\beta_n \ Y_{ms}$$

in which X_{ms} and Y_{ms} are the components in xy coordinate system. Substituting the expressions for X_{ms} and Y_{ms}, i.e., Eqs. (3.19a) and (3.21) in the above equation we obtain

$$X'_{ms} = \cos\theta_n \sin\beta_n + \sin\theta_n \tan\theta_s \sin\beta_s$$

(3.22a)

$$Y'_{ms} = \cos\theta_n \cos\beta_n + \sin\theta_n \tan\theta_s \cos\beta_s$$

(3.22b)

A.6

By Eq. (3.31) the angles between the vectors $\bar{s}_s$ and $\bar{n}_h$, and $\bar{t}_s$ and $\bar{n}_h$. However we can not establish the same relation between the unit vectors $\bar{s}_h, \bar{t}_h$ and $\bar{n}_h$ (i.e., $\bar{n}_h \cdot \bar{s}_h = \bar{n}_h \cdot \bar{t}_h$ is not correct. This is obvious from the following calculations:

By Eq. (3.3)

$$\bar{n}_h \cdot \bar{s}_h = -\sin\theta_n \sin\beta_n \sin\theta_s \sin\beta_s + \sin\theta_n \cos\beta_n \sin\theta_s \cos\beta_s$$

$$= \sin\theta_n \sin\theta_s (\cos\beta_n \cos\beta_s - \sin\beta_n \sin\beta_s)$$

$$= \sin\theta_n \sin\theta_s \cos(\beta_n + \beta_s)$$

Similarly

$$\bar{n}_h \cdot \bar{t}_h = \sin\theta_n \sin\theta_t \cos(\beta_n - \beta_t)$$

It is not difficult to see that the equality

$$\sin\theta_s \cos(\beta_n + \beta_s) = \sin\theta_t \cos(\beta_n - \beta_t)$$

is not identicelly correct.

A.7
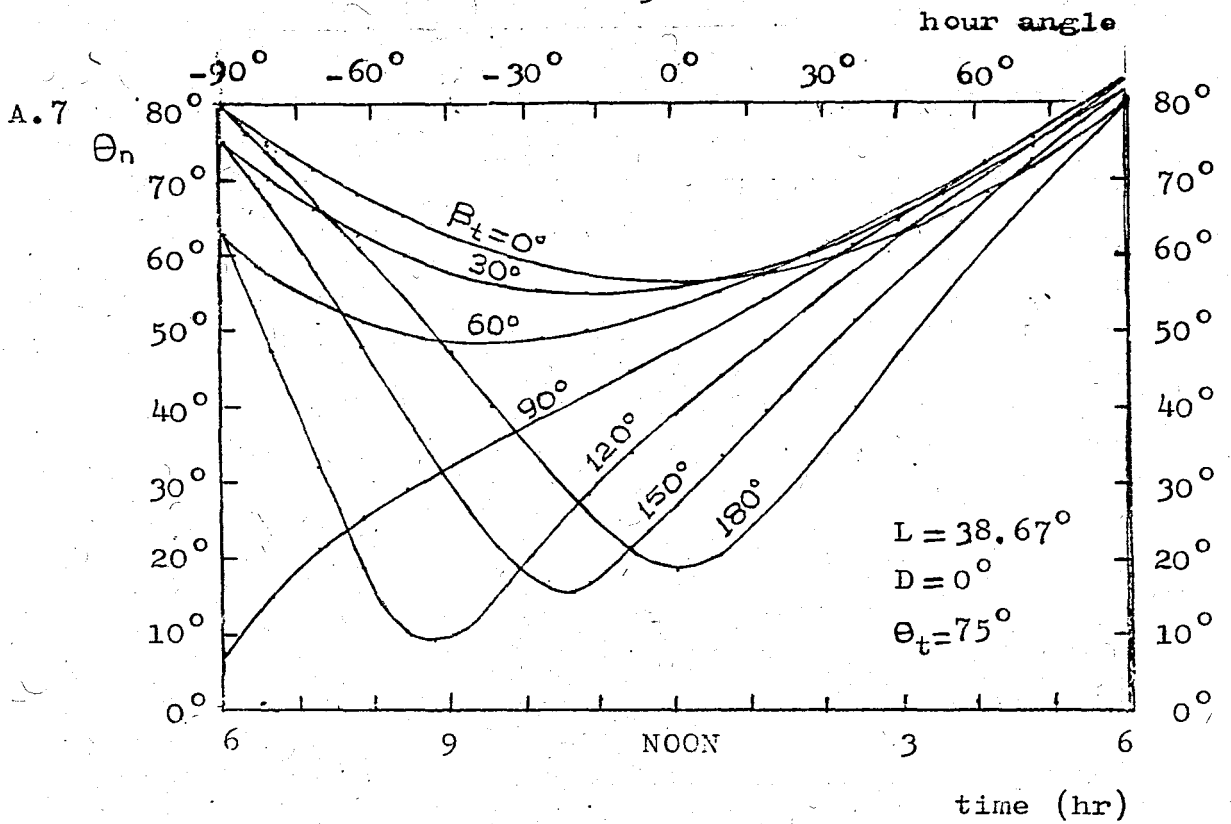
Fig.A.9 Time profiles of mirror position angles.
(Mar.22, Sept.22)
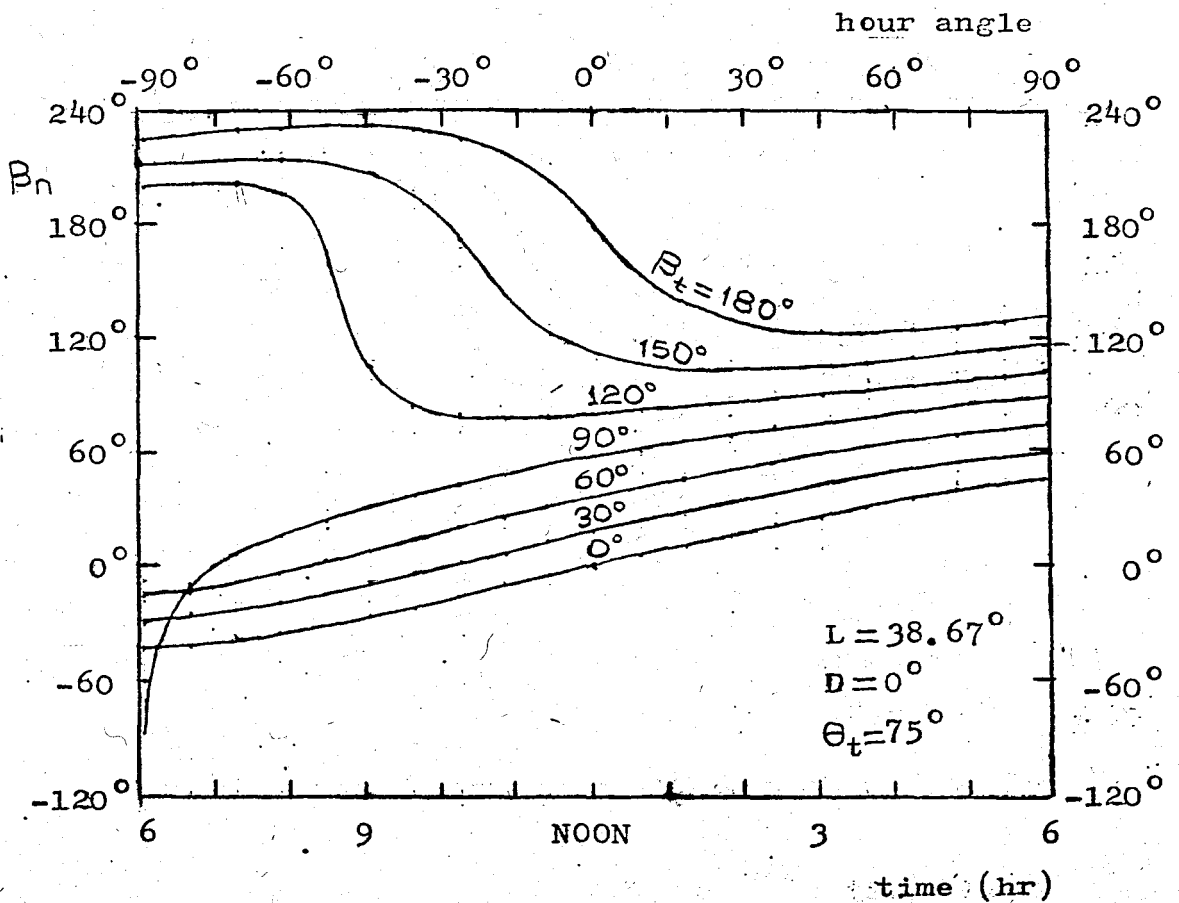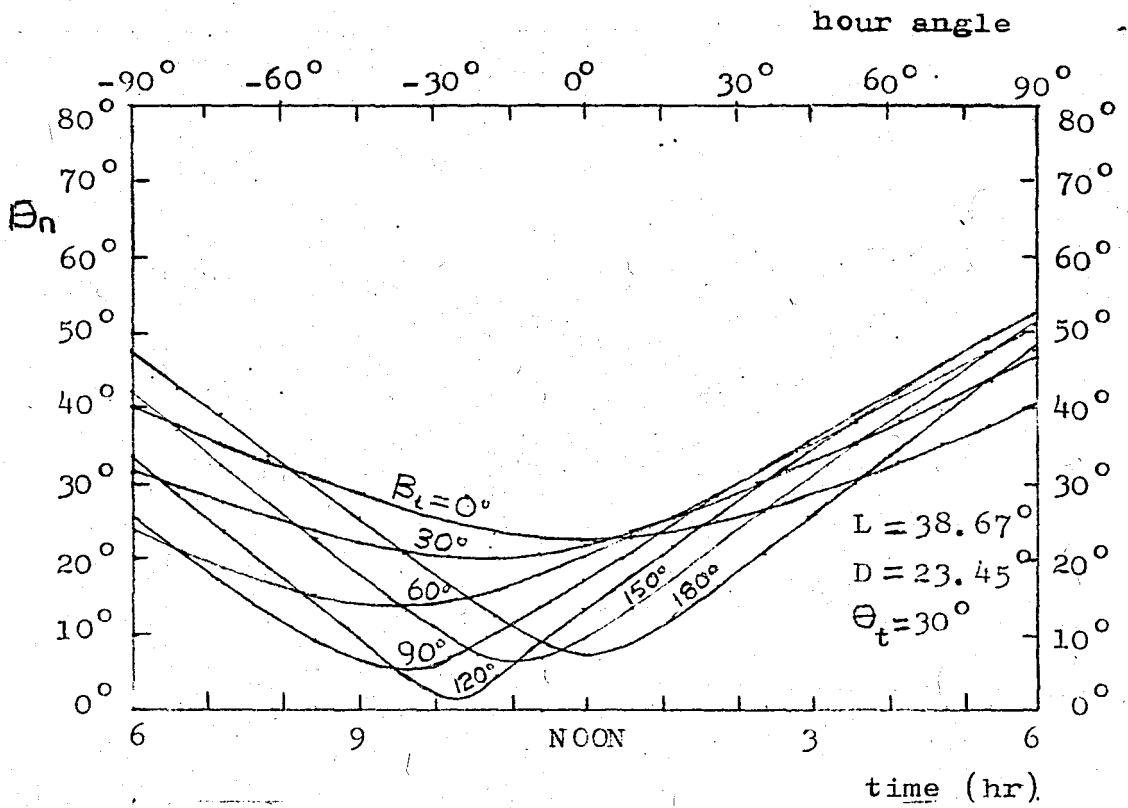
Fig.A.10 Time profiles of mirror position angles.
(June 22)
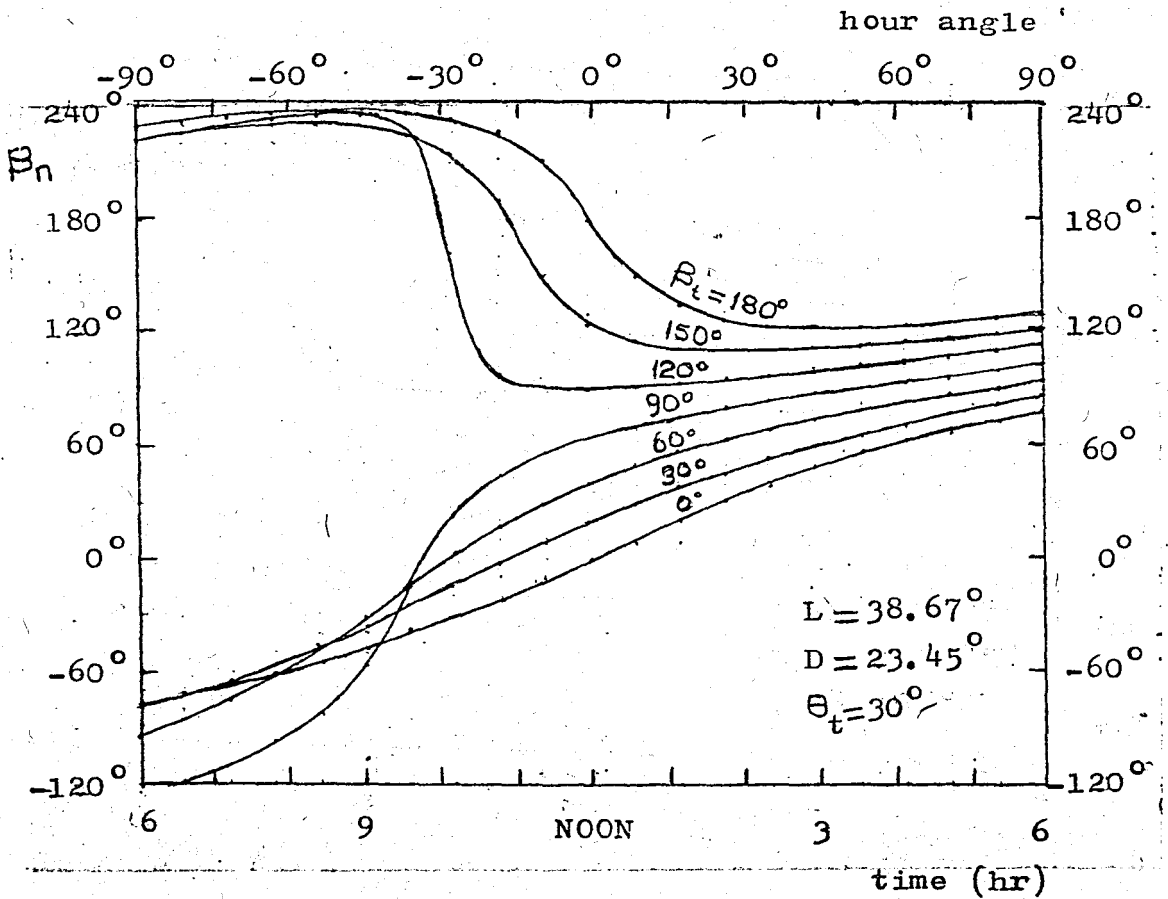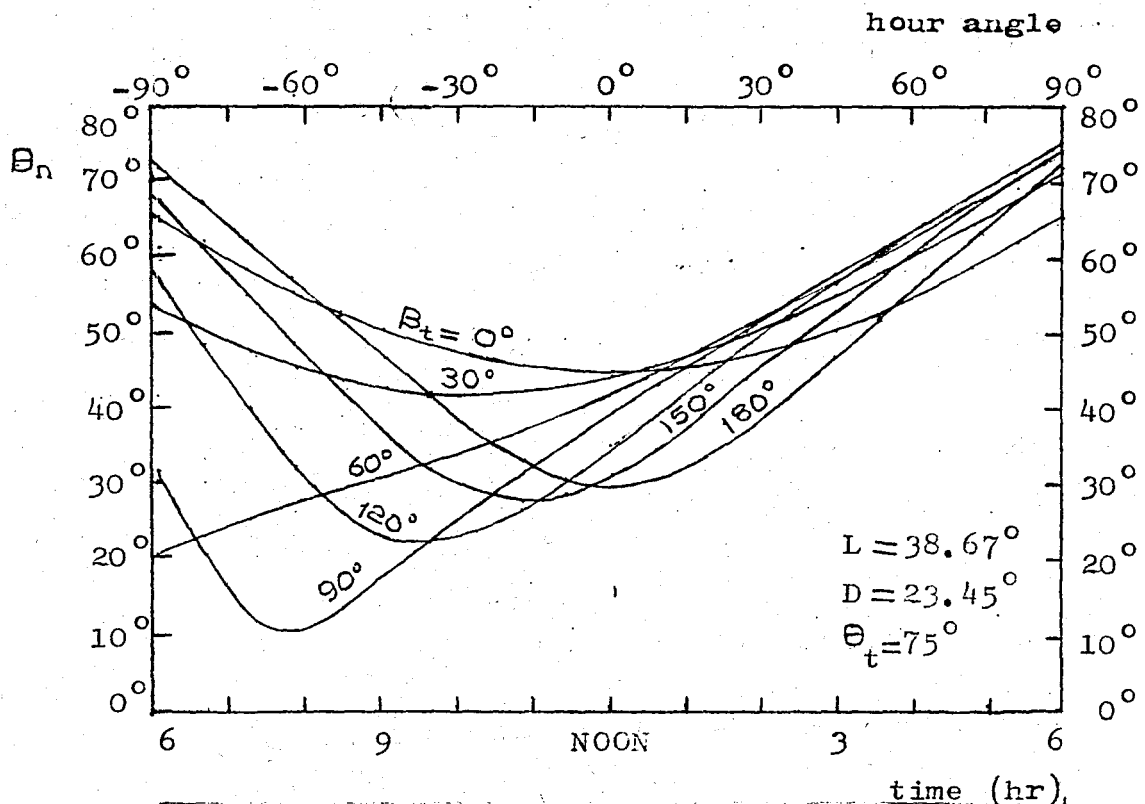
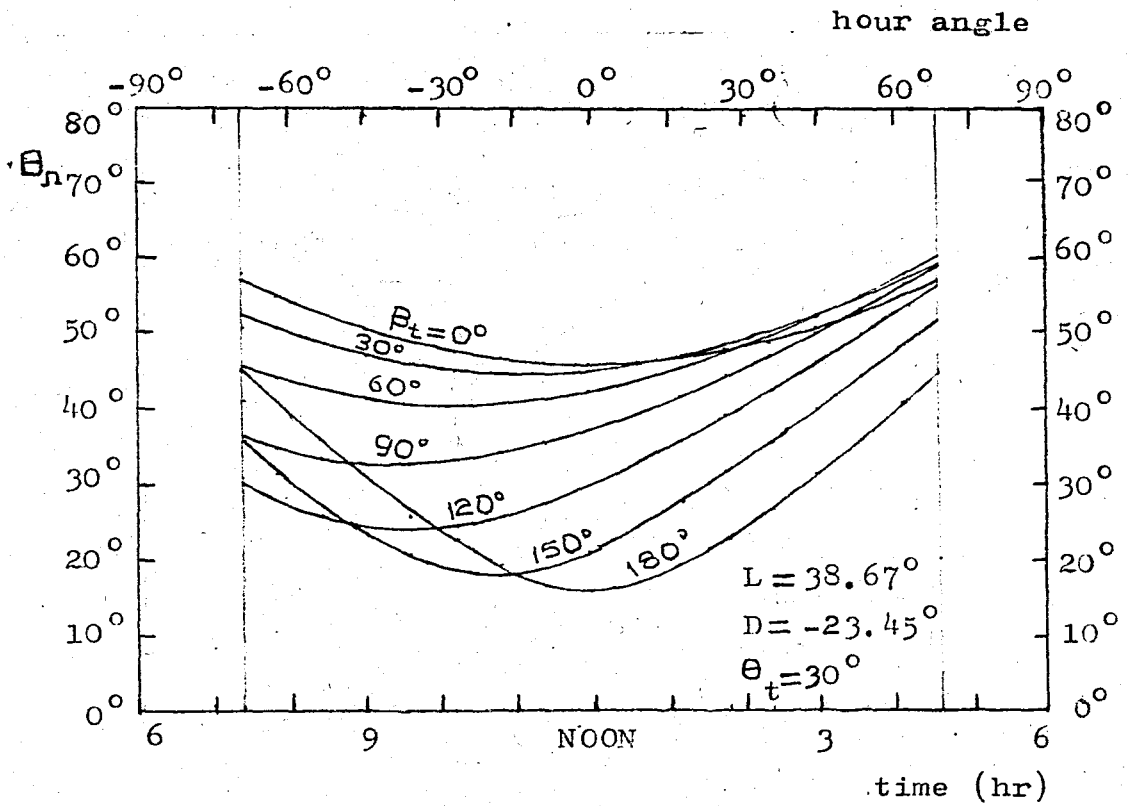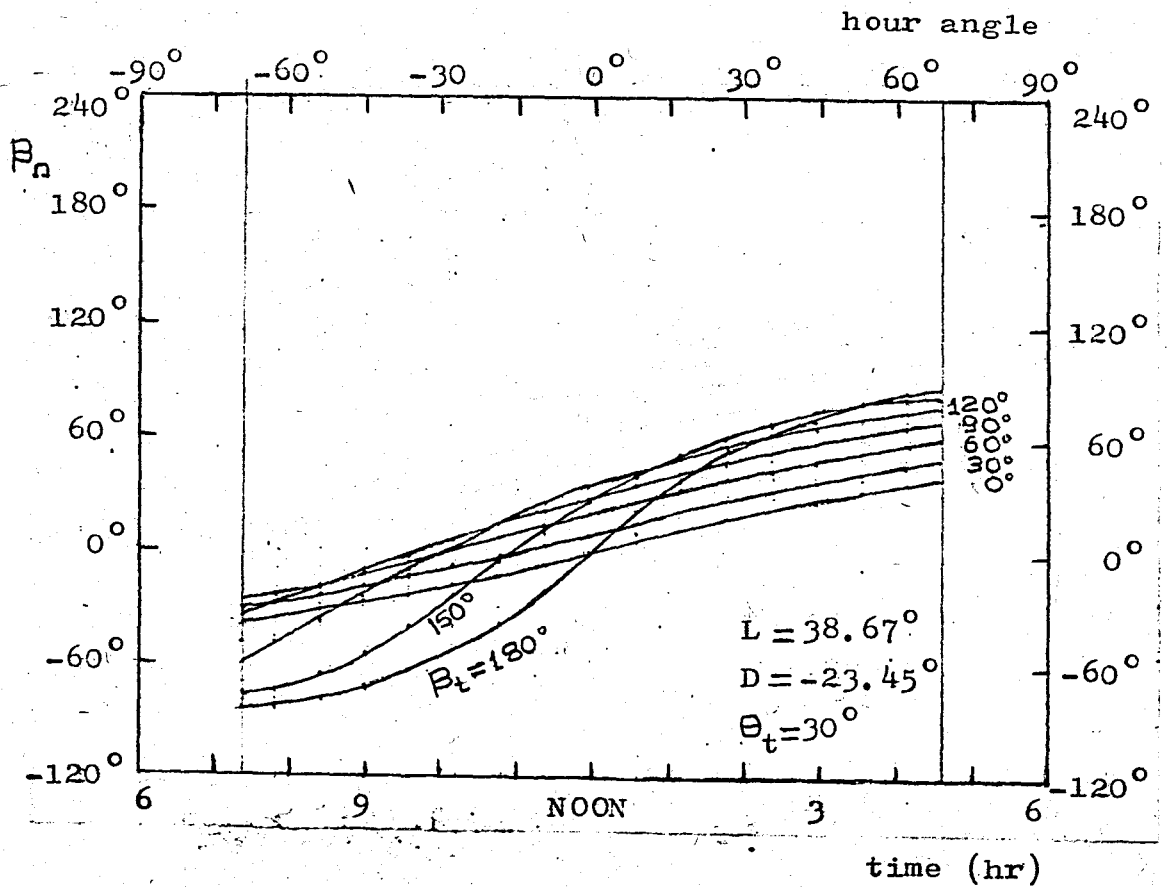Fig.A.11 Time profiles of mirror position angles.
(June 22)
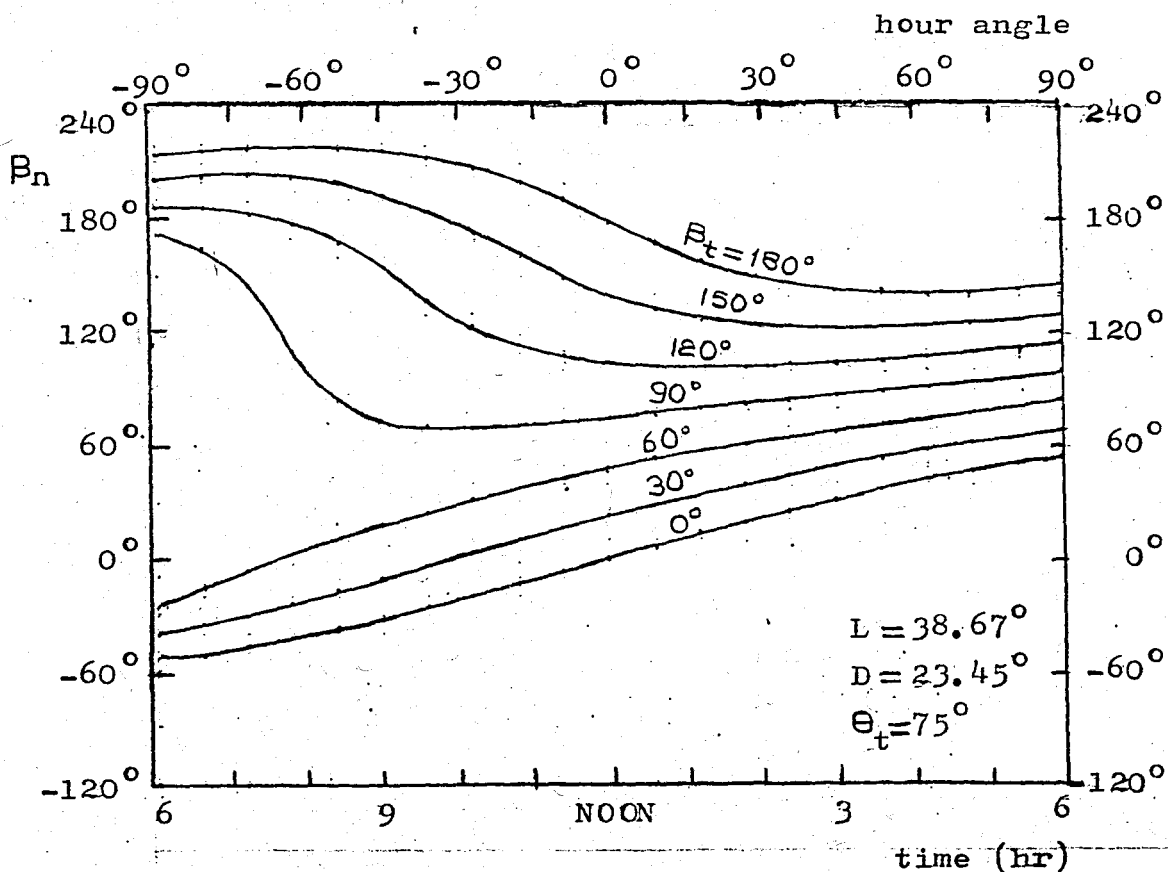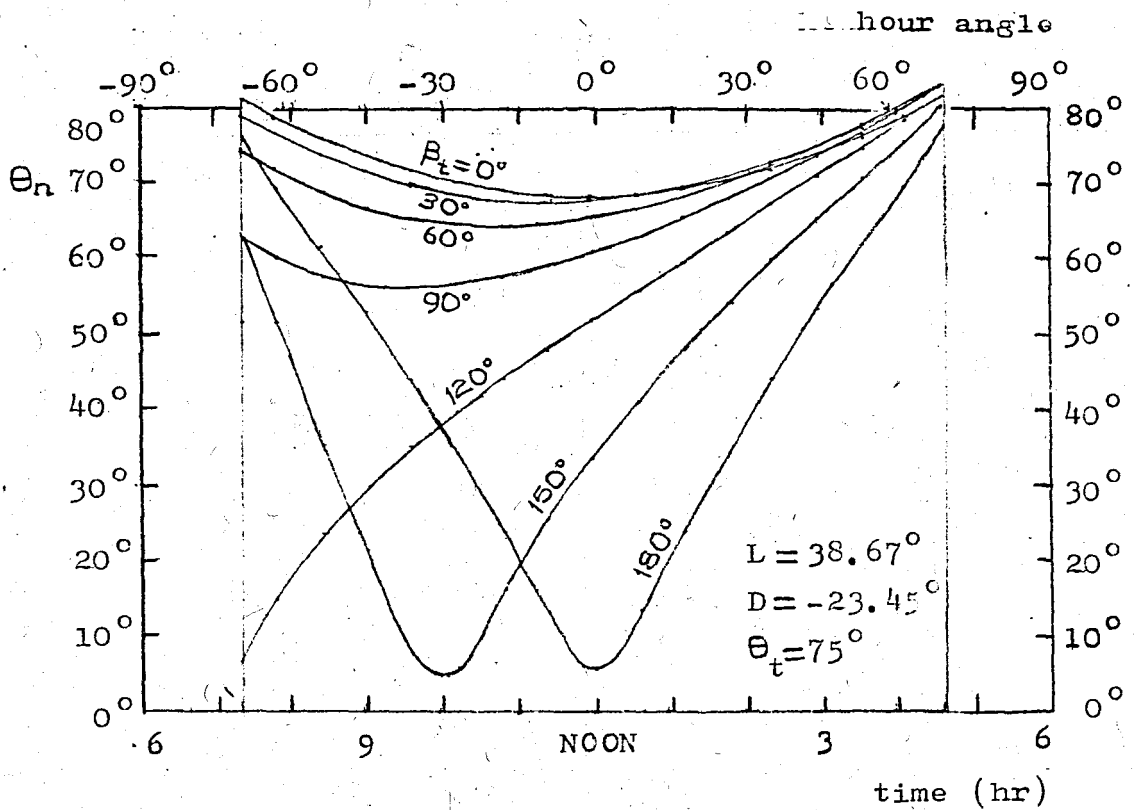
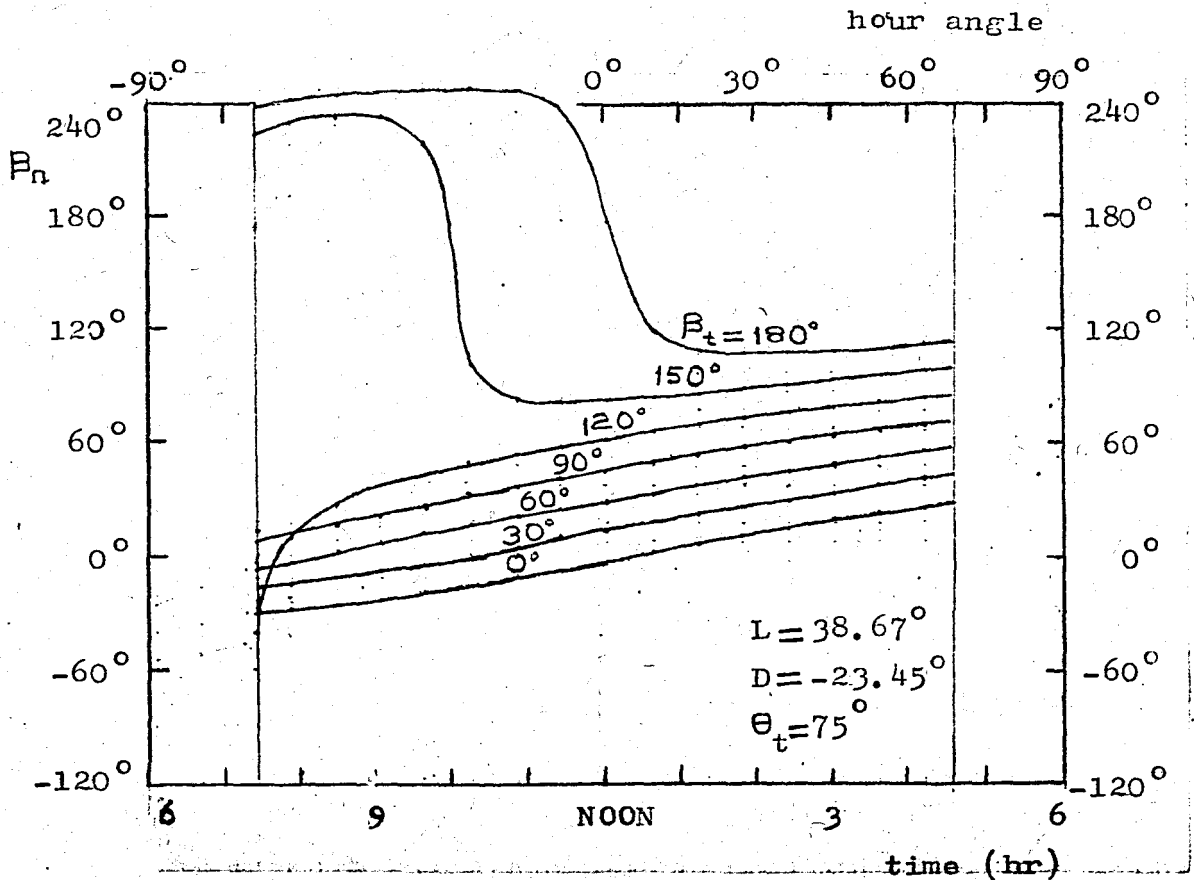Fig.A.12 Time profiles of mirror position angles.
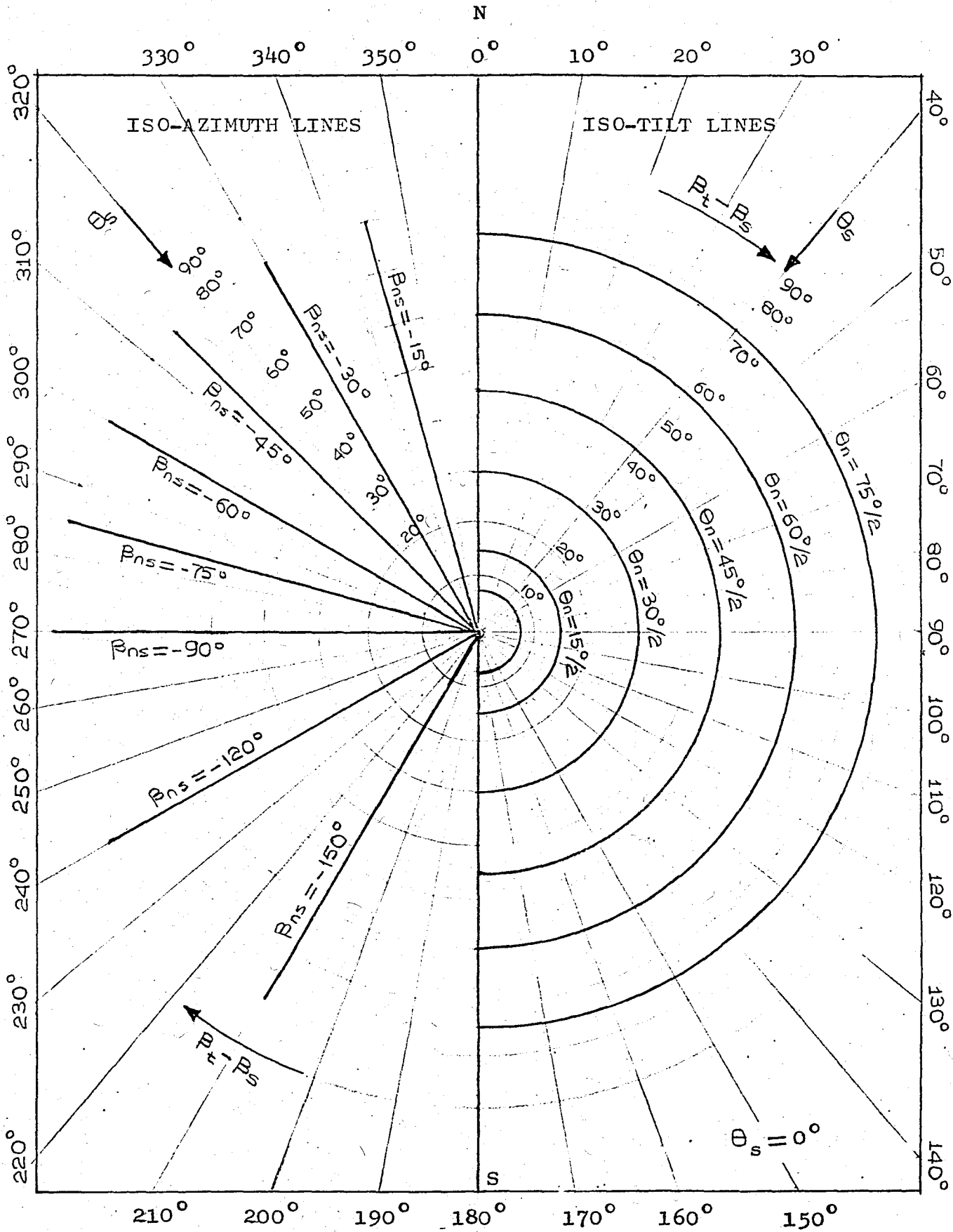(Dec. 22)

Fig.A.13 Time profiles of mirror position angles.
(Dec. 22)

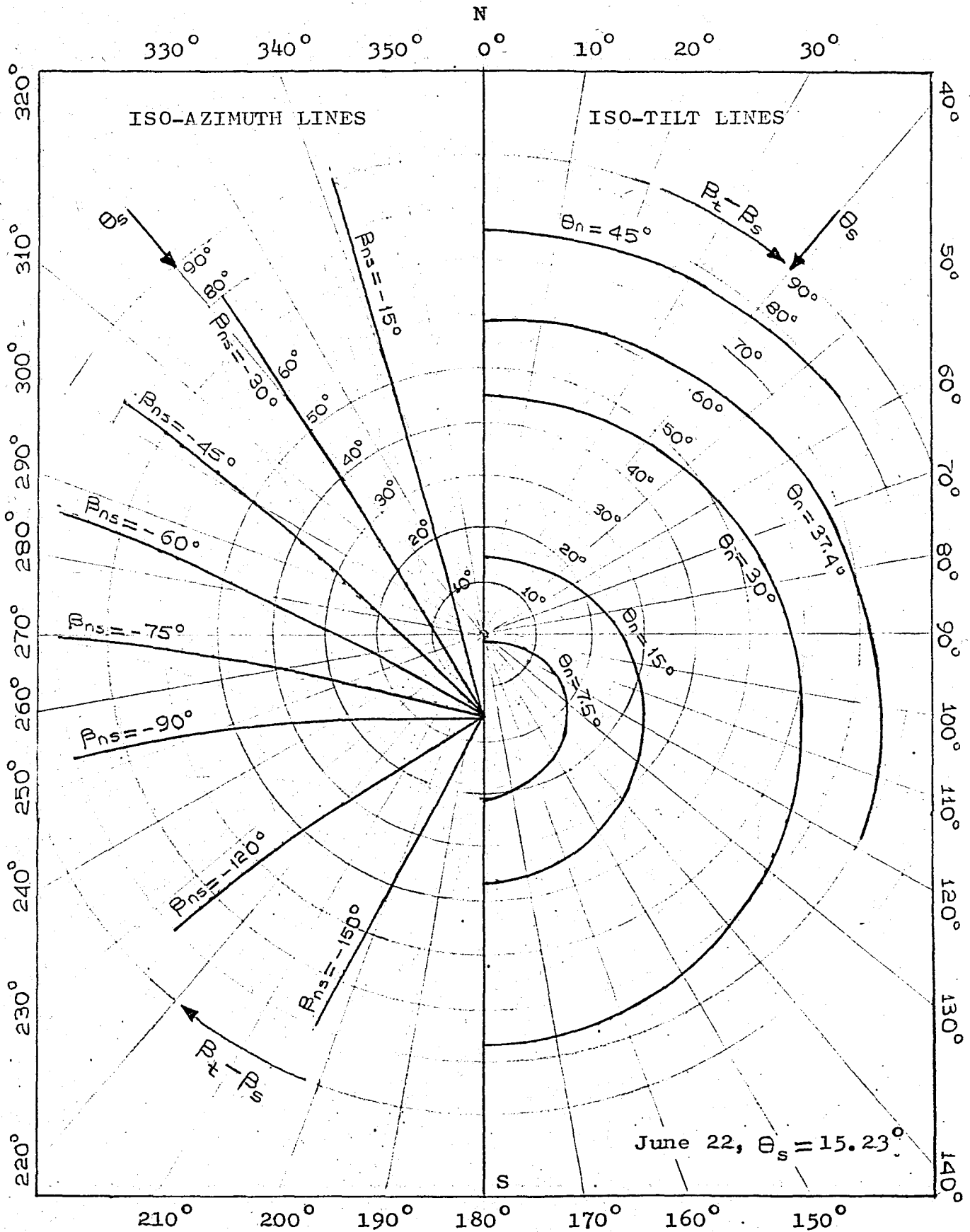Fig.A.14 Mirror field distribution.

Special case. $\beta_s = 0°$.

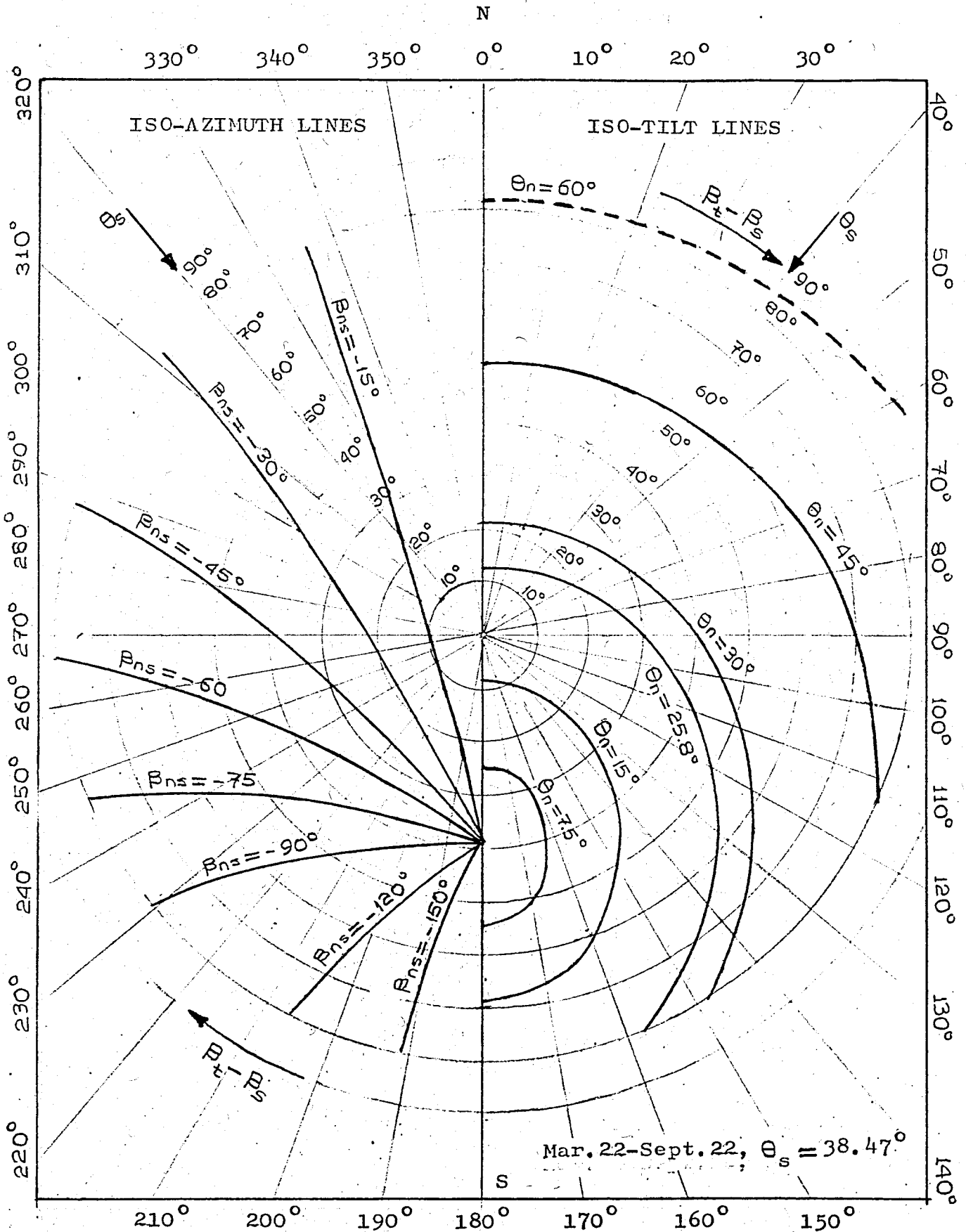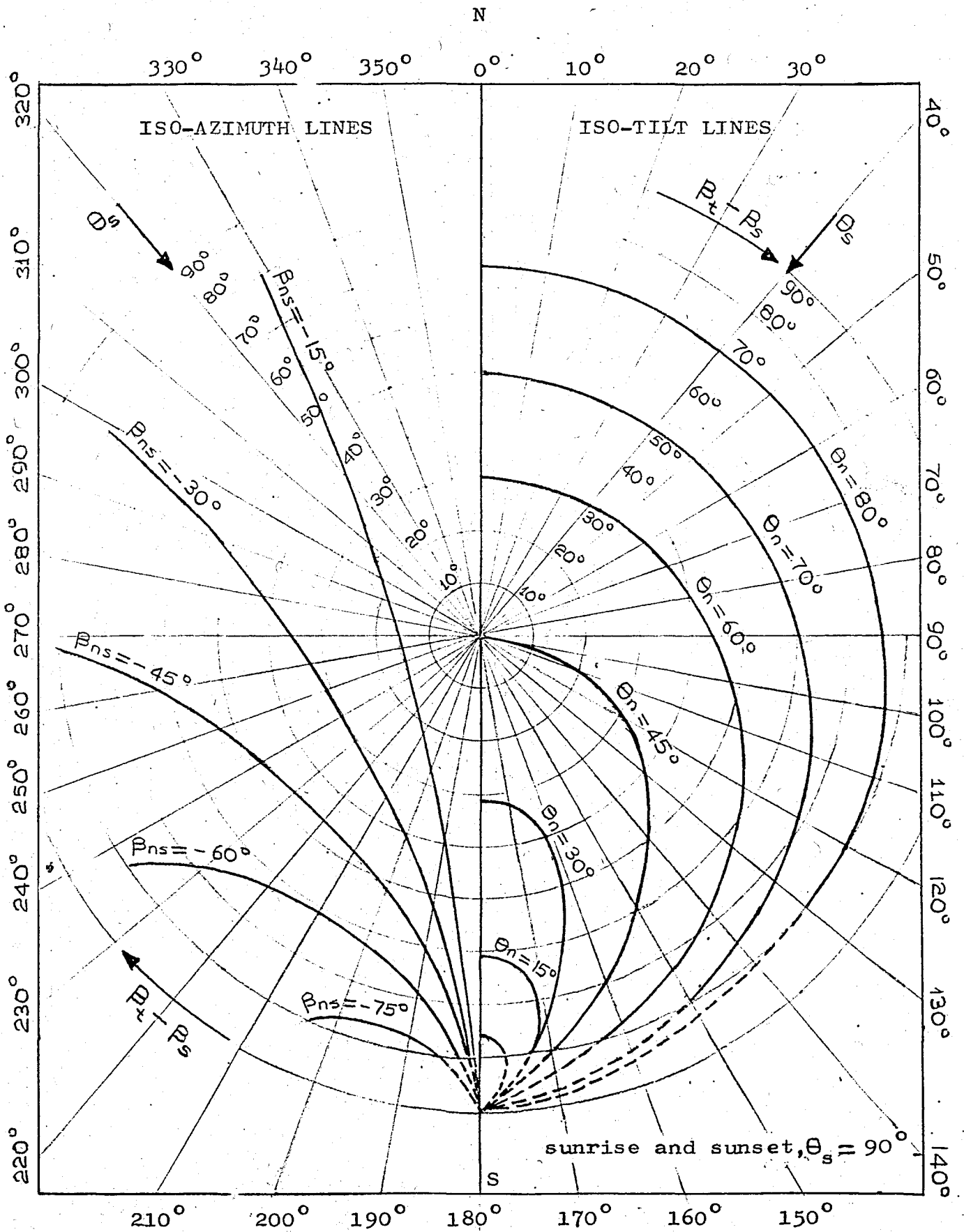Fig. A.15 Mirror field distribution

for Cihanbeyli (L = 38.67°). $\beta_s = 0°$.

Fig. A.16 Mirror field distribution

for Cihanbeyli (L=38.67°). $\beta_s = 0°$.
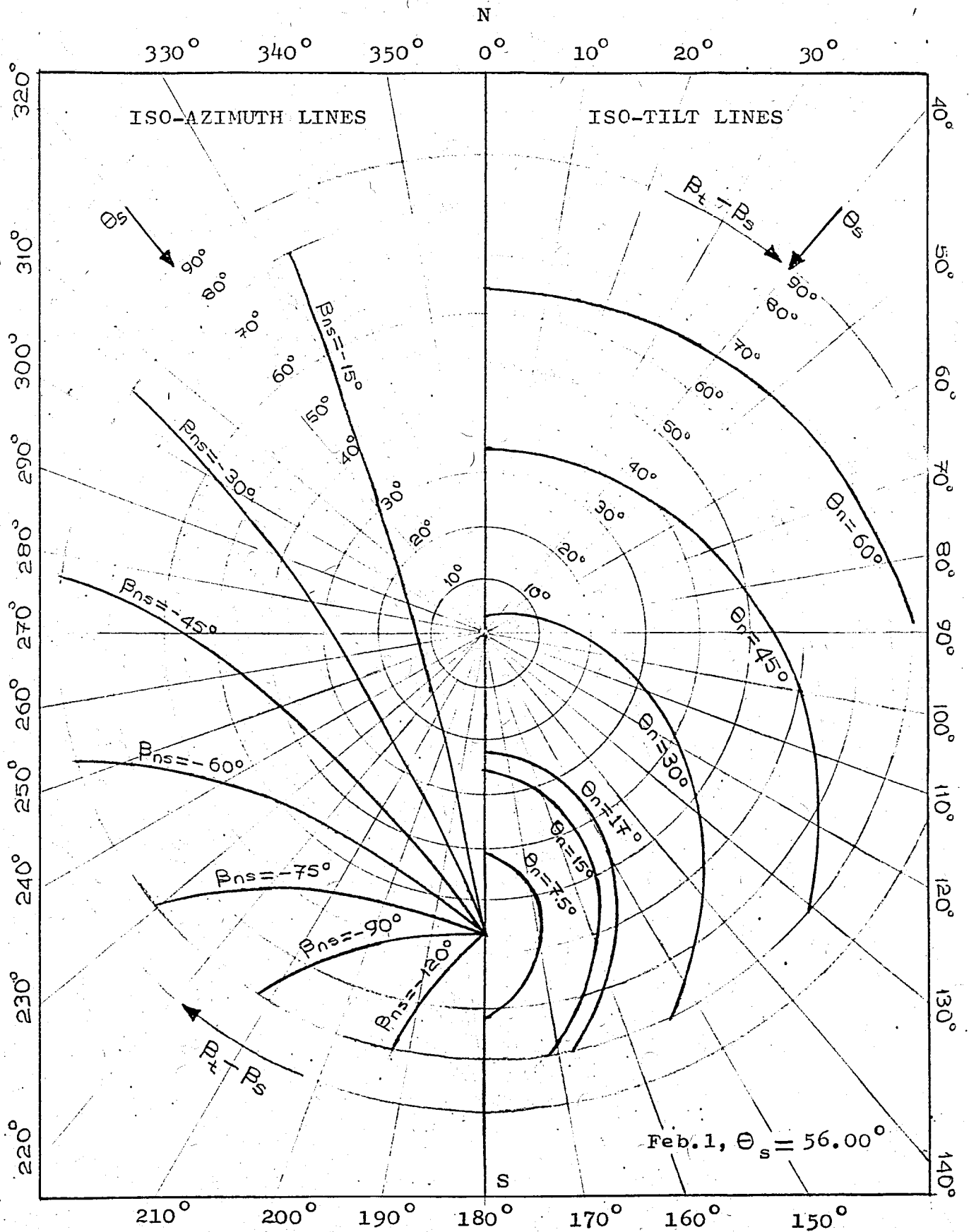
Fig.A.17 Mirror field distribution

for Cihanbeyli (L=38.67°). $\beta_s = 0°$.

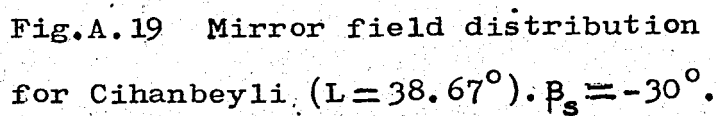Fig.A.18   Mirror field distribution.

Special case. $\beta_s = 0°$.

Fig.A.19   Mirror field distribution

for Cihanbeyli (L = 38.67°). $\beta_s = -30°$.